Supporting Information

Coordination of $Al(C_6F_5)_3$ vs $B(C_6F_5)_3$ on Group 6 End-On Dinitrogen Complexes: Chemical and Structural Divergences.

Léon Escomel[a], Frederico Martins[b], Laure Vendier[a], Anaïs Coffinet[a], Nicolas Queyriaux[a], Vera Krewald[b] and Antoine Simonneau[a]*

[a] LCC-CNRS, Université de Toulouse, CNRS, UPS, 205 route de Narbonne, BP44099, F-31077 Toulouse cedex 4, France.
[b] Technical University of Darmstadt: Department of Chemistry, Theoretical Chemistry,L202 444, Peter-Grünberg-Str. 464287 Darmstadt.

Content

1 Experimental Section....3
1.1 General considerations....3
1.2 Synthesis....3
1.2.1 *Trans*-$[Cr(dmpe)_2(N_2)_2]$, modified procedure of Salt and Girolami[11] 3
1.2.2 Synthesis of 1_{Al} – *trans*-$[W(depe)_2(N_2)(\mu\text{-}N_2)Al(C_6F_5)_3]$ 4
1.2.3 Reaction of 1_B with $Al(C_6F_5)_3(tol)$ forming 1_{Al}....4
1.2.4 Synthesis of 2_{Al} – *trans*-$[Mo(depe)_2(N_2)(\mu\text{-}N_2)Al(C_6F_5)_3]$ 4
1.2.5 Formation of 4_{Al} – *trans*-$[Mo(dppe)_2(\mu\text{-}N_2)Al(C_6F_5)_3]$ 5
1.2.6 Synthesis of 5_{Al} – *trans*-$[W(dppe)_2(N_2)(\mu\text{-}N_2)Al(C_6F_5)_3]$ 5
1.2.7 Synthesis of 6_{Al} – *trans*-$[Mo(dppe)_2(N_2)(\mu\text{-}N_2)Al(C_6F_5)_3]$ 5
1.2.8 NMR-scale reaction of *trans*-$[W(dppe)_2(\mu\text{-}N_2)B(C_6F_5)_3]$ + $Al(C_6F_5)_3(tol)$ 6
1.2.9 NMR-scale reaction of *trans*-$[Mo(dppe)_2(\mu\text{-}N_2)B(C_6F_5)_3]$ + $Al(C_6F_5)_3(tol)$ 6
1.2.10 NMR monitoring of the reaction of *trans*-$[W(dppe)_2(N_2)_2]$ + $B(C_6F_5)_3$ under N_2 6
1.2.11 Synthesis of 7_{Al} – *trans*-$[Cr(dmpe)_2(N_2)(\mu\text{-}N_2)Al(C_6F_5)_3]$ 7
1.2.12 Reaction of $B(C_6F_5)_3$ (1 eq. or excess) with $[Cr(dmpe)_2(N_2)_2]$ 7
1.2.13 Synthesis of 8_{Al} – *trans*-$[W(depe)_2\{(\mu\text{-}N_2\text{-}Al(C_6F_5)_3\}_2]$ 7
1.2.14 Synthesis of 11_{Al} – *cis*-$[W(depe)_2\{(\mu\text{-}N_2\text{-}Al(C_6F_5)_3\}_2]$ 7
1.2.15 Synthesis of 12_{Al} – *cis*-$[Mo(depe)_2\{(\mu\text{-}N_2\text{-}Al(C_6F_5)_3\}_2]$ 8
1.2.16 NMR monitoring of $[Mo(depe)_2(N_2)_2]$ + 2 eq. of $Al(C_6F_5)_3$ (in toluene-d_8) 8

1.2.17 Reaction of $M(depe)_2(N_2)_2$ with two equivalents or an excess (10 eq.) of $B(C_6F_5)_3$ 8

1.2.18 Synthesis of 13_{Al} – *cis*-$[Cr(dmpe)_2\{\mu\text{-}N_2\text{-}Al(C_6F_5)_3\}_2]$. 8

1.2.19 Synthesis of 15_{Al} – *cis*-$[W(PMe_2Ph)_4(N_2)\{\mu\text{-}N_2\text{-}Al(C_6F_5)_3\}]$.....9

1.2.20 Synthesis of 16_{Al} – *cis*-$[W(PMe_2Ph)_4\{\mu\text{-}N_2\text{-}Al(C_6F_5)_3\}_2]$.....9

1.2.21 Reaction of *cis*-$[W(PMe_2Ph)_4(N_2)_2$ with $B(C_6F_5)_3$.....9

2 NMR spectroscopic data.....10

3 IR spectroscopic data.....43

4 UV-vis spectroscopic data 49

5 Crystallographic data.....55

5.1 Data collection and refinement.....55

5.2 XRD data 55

6 DFT calculations.....60

6.1 Computational details 60

6.2 Computational model assessment 60

6.3 Molecular Orbital diagrams.....63

6.4 Electronic excitations.....65

7 References.....68

1 Experimental Section

1.1 General considerations

All reactions were performed in flame- or oven-dried glassware with rigorous exclusion of air and moisture, using Schlenk lines technics or Jacomex glove boxes (O_2 < 1.0 ppm, H_2O < 1 ppm). An important part of the experiments were carried out under a dinitrogen atmosphere. If not, we clearly indicated in the figure labels or in the synthetic procedures when the experiments were performed under an argon atmosphere. Solvents used were pre-dried (*n*-pentane and tetrahydrofuran by passing through a Puresolv MD 7 solvent purification machine; benzene, fluorobenzene, hexamethyldisiloxane (HMDSO) and tetrahydropyran by distillation over CaH_2), degassed by freeze-pump-thaw cycles, dried over molecular sieves and stored in the glove box. C_6D_6, C_6D_5Cl and THF-d_8 (purchased from Eurisotop) were degassed by freeze-pump-thaw cycles, dried over molecular sieves and stored in the glove box. The M-dinitrogen (M = Mo, W, Cr) complexes[1–12] and $Al(C_6F_5)_3(tol)$[13] were prepared according to reported procedures from unpurified commercially available chemicals and stored in the glove box. ^1H, ^{13}C, ^{19}F and ^{31}P NMR spectra were recorded using NMR tubes equipped with J. Young valves on a Bruker Avance III 400 spectrometer. Chemical shifts are reported in parts per million (ppm) downfield from tetramethylsilane and are referenced to the most upfield residual solvent resonance as the internal standard in ^1H NMR (C_6HD_5: δ reported = 7.16 ppm, C_6HD_4Cl: δ reported = 6.96 ppm, THF-d_8: δ reported = 1.72 ppm). ^{11}B, ^{15}N, ^{19}F and ^{31}P NMR spectra were calibrated according to the IUPAC recommendation using a unified chemical shift scale based on the proton resonance of tetramethylsilane as primary reference.[14] ^1H and ^{13}C NMR assignments were confirmed by ^1H–^1H COSY and ^1H–^{13}C HSQC and HMBC experiment. Data are reported as follows: chemical shift, multiplicity (b = broad, s = singlet, d = doublet, t = triplet, q = quartet, quint = quintet, sex = sextet, hept = heptet, m = multiplet), coupling constant (Hz), and integration. Infrared (IR) spectra were recorded in the glove box (O_2 < 1.0 ppm, H_2O < 1 ppm) on an Agilent Cary 630 FT-IR spectrophotometer equipped with ATR or transmission modules and are reported in wavenumbers (cm^{-1}) with (s), (m), (w) indicating strong, medium, and weak absorption respectively. UV-Vis spectra were recorded on a PerkinElmer LAMBDA 950 uv/vis spectrophotometer equipped with a dual-beam setup. The UV cells (quartz cells equipped with air-tight Teflon caps) were prepared under inert atmosphere of dinitrogen in dried benzene at a concentration of 30 µmol/L for diluted samples and 1000 µmol/L for concentrated samples. Elemental analyses were performed on samples sealed in tin capsules under Ar or N_2 by the Analytical Service of the Laboratoire de Chimie de Coordination; results are the average of two independent measurements.

1.2 Synthesis

1.2.1 *Trans*-[Cr(dmpe)$_2$(N$_2$)$_2$], modified procedure of Salt and Girolami[11]

Trans-[Cr(dmpe)$_2$Cl$_2$] (500 mg, 1.18 mmol, 1.0 eq.) was progressively added into a 100 mL THF mixture of lithium (41 mg, 5.90 mmol, 5 eq.). The resulting green suspension was left stirred overnight under a nitrogen flux which produced a red/orange mixture. The solids were filtered off and THF volatiles of the filtrate were removed *in vacuo*. The resulting solid residue was dissolved in the minimum amount of toluene and filtered (to get rid of salt impurities) yielding a dark red/brown solution. Volatiles of the latter were removed *in vacuo* yielding *trans*-[Cr(dmpe)$_2$(N$_2$)$_2$] as a dark red/brown powder with acceptable purity (350 mg, 73% yield but some paramagnetic and *cis*-compounds are noticed in minor

amounts). Washing the solid with a minimal amount of benzene afforded to get *trans*-[Cr(dmpe)$_2$(N$_2$)$_2$] as a pure light red powder.

1.2.2 Synthesis of $\mathbf{1_{Al}}$ – *trans*-[W(depe)$_2$(N$_2$)(μ-N$_2$)Al(C$_6$F$_5$)$_3$]

A 1.5 mL colorless toluene solution of Al(C$_6$F$_5$)$_3$(tol) (59 mg, 0.10 mmol, 1.0 eq.) was added dropwise into a 0.5 mL red toluene solution of *trans*-[W(depe)$_2$(N$_2$)$_2$] (62.7 mg, 0.096 mmol, 1.00 eq.). Instantly, the solution turned deep purple. The latter was stirred at room temperature for 5 minutes. Then, *n*-pentane (ca. 12 mL) was added into the resulting solution which did not trigger precipitation of solids. Therefore, the solution was put at T = -40 °C for 18 hours yielding deep purple-yellowish platelets-like crystals that were recovered by filtration and dried *in vacuo* for 2 hours (100 mg, 89% yield). The ^{15}N-labelled analogue – **^{15}N-1$_{Al}$** – was obtained similarly starting from [W(depe)$_2$(^{15}N$_2$)$_2$] and one equivalent of Al(C$_6$F$_5$)$_3$(tol) but the resulting ^{15}N-NMR signals are not enough resolved to assign them (see Figure S7 page 13) Note that repeating the same experiment at NMR-scales under an argon atmosphere did not change the reactivity. **^{1}H NMR** (400 MHz, C$_6$D$_6$, 298 K) δ 1.79 (m, 4H, CH$_{2\text{-terminal}}$), 1.56 (m, 8H, CH$_{2\text{-terminal}}$), 1.43 (m, 4H, CH$_{2\text{-terminal}}$), 1.27 (m, 4H, CH$_{2\text{-bridging}}$), 1.08 (m, 4H, CH$_{2\text{-bridging}}$), 0.87 (m, 12H, CH$_3$), 0.76 (m, 12H, CH$_3$). **^{13}C{^{1}H} NMR** (100 MHz, C$_6$D$_6$, 298 K) δ 24.3 (m, CH$_{2\text{-bridging}}$), 19.5 (b, CH$_{2\text{-terminal}}$), 8.5 (b, CH$_3$). **^{19}F NMR** (376.2 MHz, C$_6$D$_6$, 298 K) δ -122.1 (dd, $^3J_{F\text{-}F}$=28 Hz & 11 Hz, 6F, CF$_{ortho}$), -154.9 (t, $^3J_{F\text{-}F}$=20 Hz, 3F, CF$_{para}$), -162.5 (m, 6F, CF$_{meta}$). **^{31}P{^{1}H} NMR** (163.2 MHz, C$_6$D$_6$, 298 K) δ 34.6 (t, $^1J_{P\text{-}W}$=146 Hz, 4P). **IR-ATR** (293 K, cm^{-1}) σ 2962 (m, *ν*C-H), 2937 (m, *ν*C-H), 2902 (m, *ν*C-H), 2876 (m, *ν*C-H), 2088 (m, *ν*N≡N), 1778 (s, *ν*(μ-N≡N)), 1636 (m), 1506 (s), 1436 (s). **Elemental analysis** calcd (%) for C$_{38}$H$_{48}$AlF$_{15}$N$_4$P$_4$W: C 38.66, H 4.10, N 4.75. Found: C 38.86, H 3.97, N 4.84.

1.2.3 Reaction of $\mathbf{1_B}$ with Al(C$_6$F$_5$)$_3$(tol) forming $\mathbf{1_{Al}}$

A 0.5 mL colourless C$_6$D$_6$ solution of **BCF** (7.9 mg, 15.4 μmol, 1.0 eq.) was added into a 0.1 mL red C$_6$D$_6$ solution of *trans*-[W(depe)$_2$(N$_2$)$_2$] (9.8 mg, 15.0 μmol, 1.0 eq.). The resulting crimson solution, which relates to *in situ* formation of adduct **1_B** - *trans*-[W(depe)$_2$(N$_2$)(μ-N$_2$)Al(C$_6$F$_5$)$_3$] – was left standing for 2 minutes - solution A. Then, a 0.4 mL colourless C$_6$D$_6$ solution of Al(C$_6$F$_5$)$_3$(tol) (9.7 mg, 15.6 μmol, 1.0 eq.) was added into solution A which instantly trigger a colour change to deep purple, typical of **1_{Al}**. The resulting solution was sealed in a J-Young NMR tube and analysed over time by NMR spectroscopy revealing the formation of **1_{Al}** + free **BCF** with a NMR yield higher than 90%. This equilibrium did not evolve over time (see Figure S8 page 13 and Figure S9 page 14).

1.2.4 Synthesis of $\mathbf{2_{Al}}$ – *trans*-[Mo(depe)$_2$(N$_2$)(μ-N$_2$)Al(C$_6$F$_5$)$_3$]

A 2.0 mL colourless toluene solution of Al(C$_6$F$_5$)$_3$(tol) (66.0 mg, 0.106 mmol, 1.00 eq.) was added dropwise into a 1.0 mL red/orange toluene solution of *trans*-[Mo(depe)$_2$(N$_2$)$_2$] (59.4 mg, 0.105 mmol, 1.00 eq.). Instantly, the solution turned deep burgundy and was stirred at room temperature for 5 minutes. Then, *n*-pentane (ca. 16 mL) was added into the resulting solution which did not trigger precipitation of solids even at cold temperature (T = -40 °C). Thereof, volatiles were removed *in vacuo* to yield an oil. The latter was dissolved to saturation in a mixture of toluene/*n*-pentane – 1 mL/15 mL – filtered, and put at T = -40 °C for 5 days, which triggered the growth of purple microcrystals that were recovered by filtration and dried *in vacuo* for 2 hours (119 mg, 100% yield). **^{1}H NMR** (400 MHz, C$_6$D$_6$, 298 K) δ 1.53 (m, 16H, CH$_{2\text{-terminal}}$), 1.23 (m, 8H, CH$_{2\text{-bridging}}$), 0.86 (m, 24H, CH$_3$). **^{13}C{^{1}H} NMR** (100 MHz, C$_6$D$_6$, 298 K) δ 22.5 (m, CH$_{2\text{-bridging}}$), 19.4 (b, CH$_{2\text{-terminal}}$), 8.3 (b, CH$_3$). **^{19}F NMR** (376.2 MHz, C$_6$D$_6$, 298 K) δ -122.0 (dd, $^3J_{F\text{-}F}$=29 Hz & 11 Hz, 6F, CF$_{ortho}$), -154.8 (t, $^3J_{F\text{-}F}$=19 Hz, 3F, CF$_{para}$), -162.4 (m, 6F, CF$_{meta}$). **^{31}P{^{1}H} NMR** (163.2 MHz, C$_6$D$_6$, 298 K) δ 52.6 (s, 4P). **IR-ATR** (293 K, cm^{-1}) σ 2947 (m, *ν*C-H), 2932 (m, *ν*C-H), 2906 (m, *ν*C-H), 2876 (m, *ν*C-H), 2137 (m, *ν*N≡N), 1790 (s, *ν*(μ-N≡N)), 1634 (m), 1506 (s), 1441 (s). **Elemental analysis** calcd (%) for C$_{38}$H$_{48}$AlF$_{15}$N$_4$P$_4$Mo: C 41.77, H 4.43, N 5.13. Found: C 41.90, H 4.28, N 4.49.

1.2.5 Formation of 4_{Al} – *trans*-[Mo(dppe)$_2$(μ-N$_2$)Al(C$_6$F$_5$)$_3$]

In an argon filled-glovebox, a 0.5 mL colourless C_6D_6 solution of $Al(C_6F_5)_3$(tol) (8.0 mg, 13 μmol, 1.0 eq.) was added dropwise into a 0.3 mL orange C_6D_6 suspension of *trans*-[Mo(dppe)$_2$(N$_2$)$_2$] (11.8 mg, 12.4 μmol, 1.00 eq.). Instantly, the solution turned dark red/wine and bubbling was noticed (N_2 gas evolution) upon mixing. The latter was sealed in a J-Young NMR tube and left at room temperature for 24 hours. NMR analysis of the solution revealed an equilibrium between adduct **4_{Al}** (73% NMR yield) and **6_{Al}** (27% NMR yield). Single-crystals of sufficient quality to proof the atom connectivity of **4_{Al}** were grown by cold diffusion of *n*-pentane into a saturated toluene solution of crude **4_{Al}**. **^{1}H NMR** (400 MHz, C_6D_6, 298 K) δ 7.4-5.8 (40H, CH_{Ph}), 2.6-2.3 (8H, $CH_{2\text{-bridging}}$). **^{19}F NMR** (376.2 MHz, C_6D_6, 298 K) δ -121.2 (b, 6F, CF_{ortho}), -155.9 (b, 3F, CF_{para}), -162.6 (b, 6F, CF_{meta}). **^{31}P{^{1}H} NMR** (163.2 MHz, C_6D_6, 298 K) δ 70.9 (b, 4P).

1.2.6 Synthesis of 5_{Al} – *trans*-[W(dppe)$_2$(N$_2$)(μ-N$_2$)Al(C$_6$F$_5$)$_3$]

A 2.5 mL colourless toluene solution of $Al(C_6F_5)_3$(tol) (61 mg, 0.10 mmol, 1.0 eq.) was added dropwise into a 0.5 mL orange toluene suspension of *trans*-[W(dppe)$_2$(N$_2$)$_2$] (104 mg, 0.100 mmol, 1.00 eq.). Instantly, the solution turned deep reddish/brownish and was stirred at room temperature for 6 hours. Then, *n*-pentane (ca. 10 mL) was added into the resulting solution which triggered precipitation of orange solids that were filtered off (ca. 60 mg). The deep red supernatant was filtered, put at T = -40 °C for 5 days which triggered precipitation of product **5** along with small amounts of $Al(C_6F_5)_3$(THF) adduct (likely due to the presence of THF molecules in the W starting materials) as red/brown solids that were recovered by filtration and dried *in vacuo* for 2 hours (80 mg, 51% yield). Note that repeating the same reaction at NMR-scales under an argon atmosphere (argon-filled glovebox or freeze-pump thaw/argon cycles using Schlenck lines) did not change the reactivity. **^{1}H NMR** (400 MHz, C_6D_6, 298 K) δ 7.55 (b, 8H, CH_{Ph}), 7.06-6.95 (m, 8H, CH_{Ph}), 6.86 (t, $^3J_{H\text{-}H}$=7.1 Hz, 8H; CH_{Ph}), 6.45 (b, 8H; CH_{Ph}), 6.41 (b, 8H, CH_{Ph}), 2.23 (b, 8H, $CH_{2\text{-bridging}}$). **^{13}C{^{1}H} NMR** (100 MHz, C_6D_6, 298 K) δ 134.0(CH_{Ph}), 132.1 (CH_{Ph}), 130.3 (CH_{Ph}), 129.3 (CH_{Ph}), 129.0 (CH_{Ph}), 128.6 (CH_{Ph}), 31.2 (m, $CH_{2\text{-bridging}}$). **^{19}F NMR** (376.2 MHz, C_6D_6, 298 K) δ -120.8 (dd, $^3J_{F\text{-}F}$=30 Hz & 12 Hz, 6F, CF_{ortho}), -154.8 (t, $^3J_{F\text{-}F}$=20 Hz, 3F, CF_{para}), -162.0 (m, 6F, CF_{meta}). **^{31}P{^{1}H} NMR** (163.2 MHz, C_6D_6, 298 K) δ 45.4 (t, $^1J_{P\text{-}W}$=152 Hz, 4P). **IR-ATR** (293 K, cm^{-1}) σ 3048 (w, *ν*C-H), 2905 (w, *ν*C-H), 2121 (m, *ν*N≡N), 1947 (w), 1773 (s, *ν*(μ-N≡N)), 1634 (m), 1507 (s), 1432 (s).

1.2.7 Synthesis of 6_{Al} – *trans*-[Mo(dppe)$_2$(N$_2$)(μ-N$_2$)Al(C$_6$F$_5$)$_3$]

A 4.0 mL colourless toluene solution of $Al(C_6F_5)_3$(tol) (80.5 mg, 0.130 mmol, 1.00 eq.) was added dropwise into a 3.0 mL orange toluene suspension of *trans*-[Mo(dppe)$_2$(N$_2$)$_2$] (122 mg, 0.105 mmol, 1.00 eq.). Instantly, the solution turned deep redish/brownish and was stirred at room temperature for 5 minutes. Then, *n*-pentane (ca. 14 mL) was added into the resulting solution which did not trigger precipitation of solids even at cold temperature (T = -40 °C). Therefore, the solution was concentrated until a volume of toluene of about 3.0 mL and then saturated with 6.0 mL of *n*-pentane. The latter was filtered and put at T = -40 °C for 5 days which triggered the growing of dark orange/brown single-crystals relating to product **6_{Al}** along with small amounts (≈10% by NMR) of unreacted *trans*-[Mo(dppe)$_2$(N$_2$)$_2$] and $Al(C_6F_5)_3$(THF) adduct (likely due to the presence of THF molecules in the Mo starting materials). These solids were recovered by filtration and dried *in vacuo* for 2 hours (172 mg, 81% yield for product **6_{Al}**). **^{1}H NMR** (400 MHz, C_6D_6, 298 K) δ 7.55 (b, 8H, CH_{Ph}), 7.07-6.99 (m, 12H, CH_{Ph}), 6.87 (t, $^3J_{H\text{-}H}$=7.4 Hz, 4H; CH_{Ph}), 6.74 (t, $^3J_{H\text{-}H}$=7.4 Hz, 8H; CH_{Ph}), 6.41 (b, 8H, CH_{Ph}), 2.29 (b, 8H, $CH_{2\text{-bridging}}$). **^{13}C{^{1}H}** NMR (100 MHz, C_6D_6, 298 K) δ 133.8 (CH_{Ph}), 132.0 (CH_{Ph}), 130.1 (CH_{Ph}), 129.3 (CH_{Ph}), 128.9 (CH_{Ph}), 128.6 (CH_{Ph}), 28.8 (m, $CH_{2\text{-bridging}}$). **^{19}F NMR** (376.2 MHz, C_6D_6, 298 K) δ -120.8 (d, 6F, CF_{ortho}),

-154.7 (b, 3F, CF_{para}), -162.0 (b, 6F, CF_{meta}). **$^{31}P\{^1H\}$ NMR** (163.2 MHz, C_6D_6, 298 K) δ 63.1 (b, 4P). **IR-ATR** (293 K, cm^{-1}) σ 3048 (w, *ν*C-H), 2905 (w, *ν*C-H), 2161 (m, *ν*N≡N), 1975 (m), 1786 (s, *ν*(μ-N≡N)), 1635 (m), 1455 (s), 1431 (s).

1.2.8 NMR-scale reaction of *trans*-[W(dppe)$_2$(μ-N$_2$)B(C$_6$F$_5$)$_3$] + Al(C$_6$F$_5$)$_3$(tol)

In an argon-filled glovebox, a 0.4 mL colourless C_6D_6 solution of $B(C_6F_5)_3$ (6.9 mg, 14 μmol, 1.0 eq.) was added into a 0.2 mL orange C_6D_6 suspension of *trans*-$[W(dppe)_2(N_2)_2]$. (14 mg, 14 μmol, 1.0 eq.). The resulting dark green solution (relating to *in situ* formation of adduct **3$_B$** – *trans*-$[W(dppe)_2(\mu\text{-}N_2)B(C_6F_5)_3]$ – note that N_2 gas evolution was noticed) was kept at room temperature for 5 minutes – solution A. Next, a 0.5 mL colourless solution of $Al(C_6F_5)_3$(tol) (8.4 mg, 13.5 μmol, 1.0 eq.) was added dropwise into solution A that instantly triggered a colour change from dark green to deep brown. The latter was sealed in a J-Young NMR tube and analysed by NMR spectroscopy revealing the predominant formation of product **5$_{Al}$** - *trans*-$[W(dppe)_2(N_2)(\mu\text{-}N_2)Al(C_6F_5)_3]$ (>95%) - along with free BCF (see **Figure S28** page 23).

1.2.9 NMR-scale reaction of *trans*-[Mo(dppe)$_2$(μ-N$_2$)B(C$_6$F$_5$)$_3$] + Al(C$_6$F$_5$)$_3$(tol)

In a dinitrogen atmosphere. In a dinitrogen-filled glovebox, a 0.5 mL colourless C_6D_6 solution of $B(C_6F_5)_3$ (6.6 mg, 13 μmol, 1.0 eq.) was added into a 0.2 mL orange C_6D_6 suspension of *trans*-$[Mo(dppe)_2(N_2)_2]$. (12.0 mg, 12.6 μmol, 1.00 eq.). The resulting dark green brown solution (relating to *in situ* formation of adduct **4$_B$** – *trans*-$[Mo(dppe)_2(\mu\text{-}N_2)B(C_6F_5)_3]$ – note that N_2 gas evolution was noticed) was kept at room temperature for 10 minutes – solution A. Next, a 0.5 mL colourless solution of $Al(C_6F_5)_3$(tol) (8.2 mg, 13 μmol, 1.0 eq.) was added dropwise into solution A that instantly triggered a colour change from dark green to deep blood-red. The latter was sealed in a J-Young NMR tube and analysed by NMR spectroscopy revealing the quantitative formation of product **6$_{Al}$** - *trans*-$[Mo(dppe)_2(N_2)(\mu\text{-}N_2)Al(C_6F_5)_3]$ along with free BCF (see **Figure S29** page 24).

In an argon atmosphere. In an argon-filled glovebox, a 0.5 mL colourless C_6D_6 solution of $B(C_6F_5)_3$ (6.5 mg, 13 μmol, 1.0 eq.) was added into a 0.2 mL orange C_6D_6 suspension of *trans*-$[Mo(dppe)_2(N_2)_2]$. (11.9 mg, 12.5 μmol, 1.00 eq.). The resulting dark green/brown solution (relating to *in situ* formation of adduct **4$_B$** – *trans*-$[Mo(dppe)_2(\mu\text{-}N_2)B(C_6F_5)_3]$ – note that N_2 gas evolution was noticed) was kept at room temperature for a few minutes – solution A. Next, a 0.5 mL colourless solution of $Al(C_6F_5)_3$(tol) (7.8 mg, 13 μmol, 1.0 eq.) was added dropwise into solution A, which instantly triggered a colour change from dark green to dark crimson/wine (some bubbling noticed). The latter was sealed in a J-Young NMR tube and analysed by NMR spectroscopy revealing the predominant formation of product **4$_{Al}$** (*ca.* 72%) - *trans*-$[Mo(dppe)_2(\mu\text{-}N_2)Al(C_6F_5)_3]$ –along with free BCF and minor amounts of products **6$_{Al}$** (*ca.* 23%) and **4$_B$** (*ca.* 5%) (see **Figure S30** & **Figure S31** page 24).

1.2.10 NMR monitoring of the reaction of *trans*-[W(dppe)$_2$(N$_2$)$_2$] + B(C$_6$F$_5$)$_3$ under N$_2$

In a dinitrogen-filled glovebox, *trans*-$[W(dppe)_2(N_2)_2]$ (20.7 mg, 20.0 μmol, 1.00 eq.) and $B(C_6F_5)_3$ (10.2 mg, 20.0 μmol, 1.00 eq.) were dissolved in 0.7 mL of toluene-d_8. The resulting solution turned orange-brownish (unlike under argon where the solution turned dark green due to the formation of $[W(dppe)_2(\mu\text{-}N_2\text{-BCF})]$ – species **3$_B$**) and was sealed in a J-Young NMR tube. ^{31}P-NMR analyses of the solution were regularly recorded to follow the kinetics of the formation of the putative product **5$_B$** $[W(dppe)_2(N_2)(\mu\text{-}N_2\text{-BCF})]$ emerging at δ = 65.5 ppm *vs* adduct **3$_B$** emerging at a chemical shift of 69.0 ppm. After one night, the solution reached an equilibrium of **5$_B$/3$_B$ =** 69/31 (see **Figure S32** page 25)**.**

1.2.11 Synthesis of 7_{Al} – *trans*-[Cr(dmpe)$_2$(N$_2$)(μ-N$_2$)Al(C$_6$F$_5$)$_3$]

A 1.5 mL colourless toluene solution of Al(C$_6$F$_5$)$_3$(tol) (38.0 mg, 61.3 μmol, 1.00 eq.) was added dropwise into a 1.0 mL red toluene solution of *trans*-[Cr(dmpe)$_2$(N$_2$)$_2$] (24.9 mg, 61.0 μmol, 1.00 eq.). The resulting deep wine/brown solution was left standing at room temperature for 15 minutes. Then, this was layered with *n*-pentane (*c.a.* 2.5 mL) and put T = -40 °C for 7 days yielding **7_{Al}** as dark platelets-like crystals that were recovered by filtration and dried *in vacuo* for one hour (45 mg, 79% yield). **^{1}H NMR** (400 MHz, C$_6$D$_6$, 298 K) δ 1.13-1.08 (b, 32H, CH$_{2\text{-ethyl}}$ & CH$_{3\text{-methyl}}$). **^{19}F NMR** (376.2 MHz, C$_6$D$_6$, 298 K) δ -122.0 (b, 6F, CF$_{ortho}$), -154.8 (b, 3F, CF$_{para}$), -162.4 (b, 6F, CF$_{meta}$). **^{31}P{^{1}H} NMR** (163.2 MHz, C$_6$D$_6$, 298 K) δ 62.3 (s, 4P). **IR-ATR** (293 K, cm^{-1}) σ 2975 (w, *ν*C-H), 2911 (w, *ν*C-H), 2122 (m, *ν*N≡N), 1802 (s, *ν*(μ-N≡N)), 1637 (m), 1507 (s), 1439 (s). Elemental analysis calculated (%) for C$_{30}$H$_{32}$AlF$_{15}$N$_4$P$_4$Cr: C 38.48, H 3.44, N 5.98. Found: C 38.93, H 2.86, N 3.45.

1.2.12 Reaction of B(C$_6$F$_5$)$_3$ (1 eq. or excess) with [Cr(dmpe)$_2$(N$_2$)$_2$]

B(C$_6$F$_5$)$_3$ (15.4 mg, 30.0 μmol, 1.00 eq.) and *trans*-[Cr(dmpe)$_2$(N$_2$)$_2$] (12.2 mg, 30.0 μmol, 1.00 eq.) were dissolved in 0.6 mL of C$_6$D$_6$ which triggered an immediate colour change to a dark solution with precipitation of a blackish oil. The latter was sealed in a J-Young NMR tube and left at room temperature for a few hours. NMR analysis of the solution revealed a complex mixture of species (at least 3, see spectra page 27&29) where the starting Cr material was identified (δ ^{31}P = 68.8 ppm). The oil was partly dissolved in dichlorobenzene-d_4 which revealed low signal-to-noise ratio. Repeating the same experiment in toluene-d_8 at lower temperature (T = -40 °C) did not change the NMR spectra.
Using two equivalents of BCF (31 mg, 60 μmol, 2.0 eq.) on *trans*-[Cr(dmpe)$_2$(N$_2$)$_2$] (12.2 mg, 30.0 μmol, 1.00 eq.) led to a decomposition reaction (dark mixture with no NMR signature).

1.2.13 Synthesis of 8_{Al} – *trans*-[W(depe)$_2${(μ-N$_2$-Al(C$_6$F$_5$)$_3$}$_2$]

A 0.7 mL colourless benzene solution of Al(C$_6$F$_5$)$_3$(tol) (30.0 mg, 48.4 μmol, 2.00 eq.) was added into a 0.3 mL red benzene solution of *trans*-[W(depe)$_2$(N$_2$)$_2$] (15.6 mg, 23.9 μmol, 1.00 eq.). Then, volatiles of the resulting blue azure solution were removed *in vacuo* for 30 minutes yielding **7_{Al}** as a cyan powder (40 mg, 96% yield). Green plate single crystals suitable for XRD studies were grown from a cold toluene/*n*-pentane solution of **7_{Al}**. **^{1}H NMR** (400 MHz, C$_6$D$_6$, 298 K) δ 1.44 (m, 16H, CH$_{2\text{-terminal}}$), 1.13 (m, 8H, CH$_{2\text{-bridging}}$), 1.08 (m, 4H, CH$_{2\text{-bridging}}$), 0.68 (m, 12H, CH$_3$). **^{19}F NMR** (376.2 MHz, C$_6$D$_6$, 298 K) δ -122.1 (dd, $^3J_{F\text{-}F}$=28 Hz & 16 Hz, 12F, CF$_{ortho}$), -151.6 (t, $^3J_{F\text{-}F}$=20 Hz, 6F, CF$_{para}$), -161.0 (m, 12F, CF$_{meta}$). **^{31}P{^{1}H}** NMR (163.2 MHz, C$_6$D$_6$, 298 K) δ 31.0 (t, $^1J_{P\text{-}W}$=141 Hz, 4P). **IR-ATR** (293 K, cm^{-1}) σ 2977 (w, *ν*C-H), 2942 (w, *ν*C-H), 2919 (w, *ν*C-H), 2885 (w, *ν*C-H), 1808 (s, *ν*(μ-N≡N)), 1640 (m), 1509 (s), 1439 (s). **Elemental analysis** calculated (%) for C$_{56}$H$_{48}$Al$_2$F$_{30}$N$_4$P$_4$W: C 39.36, H 2.83, N 3.28. Found: C 39.63, H 2.70, N 2.90.

1.2.14 Synthesis of 11_{Al} – *cis*-[W(depe)$_2${(μ-N$_2$-Al(C$_6$F$_5$)$_3$}$_2$]

A 0.7 mL colourless C$_6$D$_6$ solution of Al(C$_6$F$_5$)$_3$(tol) (30.1 mg, 48.5 μmol, 2.00 eq.) was added into a 0.2 mL red C$_6$D$_6$ solution of *trans*-[W(depe)$_2$(N$_2$)$_2$] (15.6 mg, 23.9 μmol, 1.00 eq.). Instantly, the solution turned into a blue-azure colour (corresponding to the formation of intermediate **8_{Al}**). The latter was sealed in a J-Young NMR tube and kinetics of the reaction was regularly monitored by NMR spectroscopy. After 3 hours, the solution turned into a deep green/brown colour and product **11_{Al}** is predominant in the mixture. After 6 hours, some light/brown plate single crystals started to grow in the tube. After 24 hours, the solution turned into a brown colour and further crystals were observed on the walls of the tube. NMR analysis indicated completion of the reaction (residues of **11_{Al}** are almost exclusive in solution) and that a big part of **11_{Al}** came out of the solution (significant decrease of the signal intensity relating to **11_{Al}** in solution). The brown crystals of **11_{Al}** were extracted with *n*-pentane (*c.a.* 3 mL) and were dried *in vacuo* for one hour (32 mg, 77%yield). The ^{15}N-labelled analogue – **^{15}N-**

11_{Al} – was obtained similarly starting from $[W(depe)_2(^{15}N_2)_2]$ and two equivalents of $Al(C_6F_5)_3(tol)$. **^{1}H NMR** (400 MHz, C_6D_6, 298 K) δ 1.82-0.34 (b&m, 48H). **^{19}F NMR** (376.2 MHz, C_6D_6, 298 K) δ -121.8 (dd, $^3J_{F\text{-}F}$=28 Hz & 16 Hz, 12F, CF_{ortho}), -152.9 (t, $^3J_{F\text{-}F}$=19 Hz, 6F, CF_{para}), -161.8 (m, 12F, CF_{meta}). **^{31}P{^{1}H} NMR** (163.2 MHz, C_6D_6, 298 K) δ 28.6 (t, $^1J_{P\text{-}W}$=141 Hz & $^2J_{P\text{-}H}$=6 Hz, 2P), 16.6 (t, $^1J_{P\text{-}W}$=106 Hz & $^2J_{P\text{-}H}$=6Hz, 2P). **^{15}N{^{1}H} NMR** (40.5 MHz, C_6D_6, 298 K) δ -26.6 (ddt, $^1J_{N\text{-}N}$=8.9 Hz, $^2J_{P\text{-}P}$=6.21, 3.04, 2.88 Hz, N_α-W), -61.6 (d, $^1J_{N\text{-}N}$=8.9 Hz, N_β-Al). **IR-ATR** (293 K, cm^{-1}) σ 2974 (w, *v*C-H), 2945 (w, *v*C-H), 2912 (w, *v*C-H), 2885 (w, *v*C-H), 1903 (s, *v*(μ-N≡N)), 1802 (s, *v*(μ-N≡N)), 1638 (m), 1507 (s), 1438 (s). **Elemental analysis** calculated (%) for $C_{56}H_{48}Al_2F_{30}N_4P_4W$: C 39.36, H 2.83, N 3.28. Found: C 39.51, H 2.62, N 2.86.

1.2.15 Synthesis of 12_{Al} – *cis*-$[Mo(depe)_2\{(\mu\text{-}N_2\text{-}Al(C_6F_5)_3\}_2]$

A 0.5 mL colourless C_6D_6 solution of $Al(C_6F_5)_3(tol)$ (21.0 mg, 33.9 μmol, 2.00 eq.) was added into a 0.3 mL red/orange C_6D_6 solution of *trans*-$[Mo(depe)_2(N_2)_2]$ (9.2 mg, 16 μmol, 1.0 eq.). Instantly, the resulting solution coloured into a green/blue. The latter was sealed in a J-Young NMR tube and was left standing at room temperature. After 90 minutes, the solution turned into a brown colour and some orange/brown plate single crystals were formed on the walls of the tube. NMR analysis of the solution at that time revealed the quantitative formation of product **12_{Al}**. The tube was further left at room temperature for 24 hours, which triggered the growing of further crystals of **12_{Al}**. The latter were extracted with toluene (*c.a.* 3 mL) into a vial. Then, volatiles were removed *in vacuo* yielding, after trituration with *n*-pentane and drying under vacuum for 1 hour, a light brown powder relating to **12_{Al}** (25 mg, 94% yield). **^{1}H NMR** (400 MHz, C_6D_6, 298 K) δ 1.79-0.43 (b&m, 48H). **^{19}F NMR** (376.2 MHz, C_6D_6, 298 K) δ -121.7 (dd, $^3J_{F\text{-}F}$=28 Hz & 16 Hz, 12F, CF_{ortho}), -152.8 (t, $^3J_{F\text{-}F}$=19 Hz, 6F, CF_{para}), -161.8 (m, 12F, CF_{meta}). **^{31}P{^{1}H} NMR** (163.2 MHz, C_6D_6, 298 K) δ 44.4 (t, $^2J_{P\text{-}P}$ = 14 Hz, 2P), 29.2 (t, $^2J_{P\text{-}P}$= 14Hz, 2P). ATR (293 K, cm^{-1}) σ 2977 (w, *v*C-H), 2942 (w, *v*C-H), 2912 (w, *v*C-H), 2885 (w, *v*C-H), 1927 (s, *v*(μ-N≡N)), 1821 (s, *v*(μ-N≡N)), 1640 (m), 1509 (s), 1441 (s).

1.2.16 NMR monitoring of $[Mo(depe)_2(N_2)_2]$ + 2 eq. of $Al(C_6F_5)_3$ (in toluene-d_8)

A 0.6 ml colourless toluene-d_8 solution of $Al(C_6F_5)_3(tol)$ (21.7 mg, 35.0 μmol, 2.00 eq.) was added into a 0.3 ml orange/reddish toluene-d_8 solution of *trans*-$[Mo(depe)_2(N_2)_2]$ (9.8 mg, 17 μmol, 1.0 eq.). The resulting light green solution (relating to the presence of $\mathbf{9}_{Al}$) was sealed in a J-Young NMR tube. The latter was left standing at room temperature and was analysed by NMR after 15 minutes and 90 minutes. Note that after 30 minutes the solution turned into a brown colour (relating to the presence of $\mathbf{12}_{Al}$).

1.2.17 Reaction of $M(depe)_2(N_2)_2$ with two equivalents or an excess (10 eq.) of $B(C_6F_5)_3$

A 0.3 mL colourless toluene-d_8 solution of $B(C_6F_5)_3$ (30.7 mg, 60.0 μmol, 2.00 eq.) was added into a 0.3 mL red toluene-d_8 solution of *trans*-$[W(depe)_2(N_2)_2]$ (19.5 mg, 29.9 μmol, 1.00 eq.). The resulting purple solution was sealed in a J-Young NMR tube for Variable Temperature NMR studies. The latter revealed the formation of the monoadduct **1_B** – *trans*-$[W(depe)_2(N_2)(\mu\text{-}N_2)\{B(C_6F_5)_3\}]$ – in equilibrium with free **BCF** and a putative double adduct (see spectra page 38). Repeating the same reaction using 10 equivalents of BCF led also to the same species with some other side-products. Repeating a similar experiment using $[Mo(depe)_2(N_2)_2]$ precursor led to a similar conclusion to that of tungsten.

1.2.18 Synthesis of 13_{Al} – *cis*-$[Cr(dmpe)_2\{\mu\text{-}N_2\text{-}Al(C_6F_5)_3\}_2]$.

A 4 mL colourless benzene solution of $Al(C_6F_5)_3(tol)$ (87 mg, 140 μmol, 2.1 eq.) was added dropwise into a 5 mL red benzene solution of *trans*-$[Cr(dmpe)_2(N_2)_2]$ (27 mg, 66 μmol, 1.0 eq.). Instantly, the

resulting solution turned into a green colour relating to *in situ* formation of *trans*-[Cr(dmpe)$_2${μ-N$_2$-Al(C$_6$F$_5$)$_3$}$_2$] species. The latter was left standing for 20 hours which progressively (within minutes) turned into a reddish solution and produced **13$_{Al}$** as redcrystalline blocks (75 mg, 77% yield) that were recovered by filtration and dried *in vacuo* for 2 hours. Insolubility of **13$_{Al}$** in non-polar and aromatic solvents (*n*-pentane, benzene, toluene, chlorobenzene, and dichlorobenzene) and its instability in more polar ones (THF, dichloromethane) precluded its analysis in solution. **IR-ATR** (293 K, cm^{-1}) σ 1948 (s, *ν*(μ-N≡N)), 1833 (s, *ν*(μ-N≡N)), 1640 (m), 1509 (s), 1442 (s). **Elemental analysis** calculated (%) for C$_{48}$H$_{32}$Al$_2$F$_{30}$N$_4$P$_4$Cr-0.5(C$_6$H$_6$): C 40.74, H 2.35, N 3.73. Found: C 40.89, H 2.23, N 3.02.

1.2.19 Synthesis of 15$_{Al}$ – *cis*-[W(PMe$_2$Ph)$_4$(N$_2$){μ-N$_2$-Al(C$_6$F$_5$)$_3$}]

A 0.6 mL colourless benzene solution of Al(C$_6$F$_5$)$_3$(tol) (47 mg, 76 μmol, 1.0 eq.) was added dropwise into a 0.2 mL yellow/orange benzene suspension of *cis*-[W(PMe$_2$Ph)$_4$(N$_2$)$_2$] (60 mg, 76 μmol, 1.0 eq.). The resulting deep blood-red solution was layered with *n*-pentane (*c.a.* 4 mL) and left standing at room temperature for two weeks then at T = -40 °C for one further week. This triggered precipitation of a reddish/brownish oil that was filtered-off (colourless supernatant was discarded) and dried *in vacuo* for 2 hours yielding **15$_{Al}$** as a light brown powder/foam (65 mg, 60% yield). Attempts to grow single-crystals of **15$_{Al}$** were unsuccessful. **^{1}H NMR** (400 MHz, C$_6$D$_6$, 298 K) δ 7.06-6.65 (m, 24H, CH$_{Ph}$), 1.24 (b, 6H, CH$_{3\text{-Me}}$), 0.82 (b, 6H, CH$_{3\text{-Me}}$). **^{19}F NMR** (376.2 MHz, C$_6$D$_6$, 298 K) δ -121.0 (dd, $^3J_{F\text{-}F}$=32 Hz & 16 Hz, 12F, CF$_{ortho}$), -152.5 (b, 6F, CF$_{para}$), -161.5 (b, 12F, CF$_{meta}$). **^{31}P{^{1}H} NMR** (163.2 MHz, C$_6$D$_6$, 298 K) δ -18.8 (b, 1P),-22.1 (q, $^1J_{W\text{-}P}$=148 Hz, 2P), -25.5 (b, 1P). **IR-ATR** (293 K, cm^{-1}) σ 3057 (w, *ν*C-H), 2928 (w, *ν*C-H), 2915 (w, *ν*C-H), 2037 (m, *ν*(N≡N)), 1776 (s, *ν*(μ-N≡N)), 1637 (m), 1506 (s), 1434 (s). **Elemental analysis** calculated (%) for C$_{50}$H$_{44}$AlF$_{15}$N$_4$P$_4$W. C 45.47, H 3.36, N 4.24. Found: C 45.06, H 3.28, N 3.23.

1.2.20 Synthesis of 16$_{Al}$ – *cis*-[W(PMe$_2$Ph)$_4${μ-N$_2$-Al(C$_6$F$_5$)$_3$}$_2$]

A 1.5 mL colourless toluene solution of Al(C$_6$F$_5$)$_3$(tol) (61.0 mg, 98.3 μmol, 2.00 eq.) was added dropwise into a 0.5 mL light orange toluene solution of *cis*-[W(PMe$_2$Ph)$_4$(N$_2$)$_2$] (38.2 mg, 48.2 μmol, 1.00 eq.). The resulting brown solution was layered with *n*-pentane (*c.a.* 3 mL) and put at T = -40 °C for seven days yielding plate-shaped brown/yellow singe-crystals that were dried *in vacuo* for 1 hour (81 mg, 91% yield). **^{1}H NMR** (400 MHz, C$_6$D$_6$, 298 K) δ 7.06-6.65 (m, 24H, CH$_{Ph}$), 1.24 (b, 6H, CH$_{3\text{-Me}}$), 0.82 (b, 6H, CH$_{3\text{-Me}}$). **^{19}F NMR** (376.2 MHz, C$_6$D$_6$, 298 K) δ -121.0 (dd, $^3J_{F\text{-}F}$=32 Hz & 16 Hz, 12F, CF$_{ortho}$), -152.5 (b, 6F, CF$_{para}$), -161.5 (b, 12F, CF$_{meta}$). **^{31}P{^{1}H}** NMR (163.2 MHz, C$_6$D$_6$, 298 K) δ -24.3 (b, 2P), -26.5 (b, 2P). **IR-ATR** (293 K, cm^{-1}) σ 3063 (w, *ν*C-H), 2925 (w, *ν*C-H), 2915 (w, *ν*C-H), 1901 (s, *ν*(μ-N≡N)), 1804 (s, *ν*(μ-N≡N)), 1640 (m), 1509 (s), 1442 (s). **Elemental analysis** calculated (%) for C$_{68}$H$_{44}$Al$_2$F$_{30}$N$_4$P$_4$W: C 44.18, H 2.40, N 3.03. Found: C 44.44, H 2.29, N 1.82.

1.2.21 Reaction of *cis*-[W(PMe$_2$Ph)$_4$(N$_2$)$_2$ with B(C$_6$F$_5$)$_3$

cis-[W(PMe$_2$Ph)$_4$(N$_2$)$_2$] (9.0 mg, 11 μmol, 1.0 eq.) and B(C$_6$F$_5$)$_3$ (5.8 mg, 11 μmol, 1.0 eq.) were dissolved in toluene-d_8. The resulting red/orange solution was sealed in a J-Young NMR tube and analysed by NMR spectroscopy at room temperature after 30 minutes and 2 hours of reaction. ^{31}P and ^{19}F NMR spectra of the crude reaction revealed a complex mixture of species, including B(C$_6$F$_5$)$_3$·P(Me$_2$Ph) adduct.[15]

2 NMR spectroscopic data

Figure S1. ^{1}H-NMR spectrum (400.0 MHz, C_6D_6, 298K) of compound 1_{Al}.

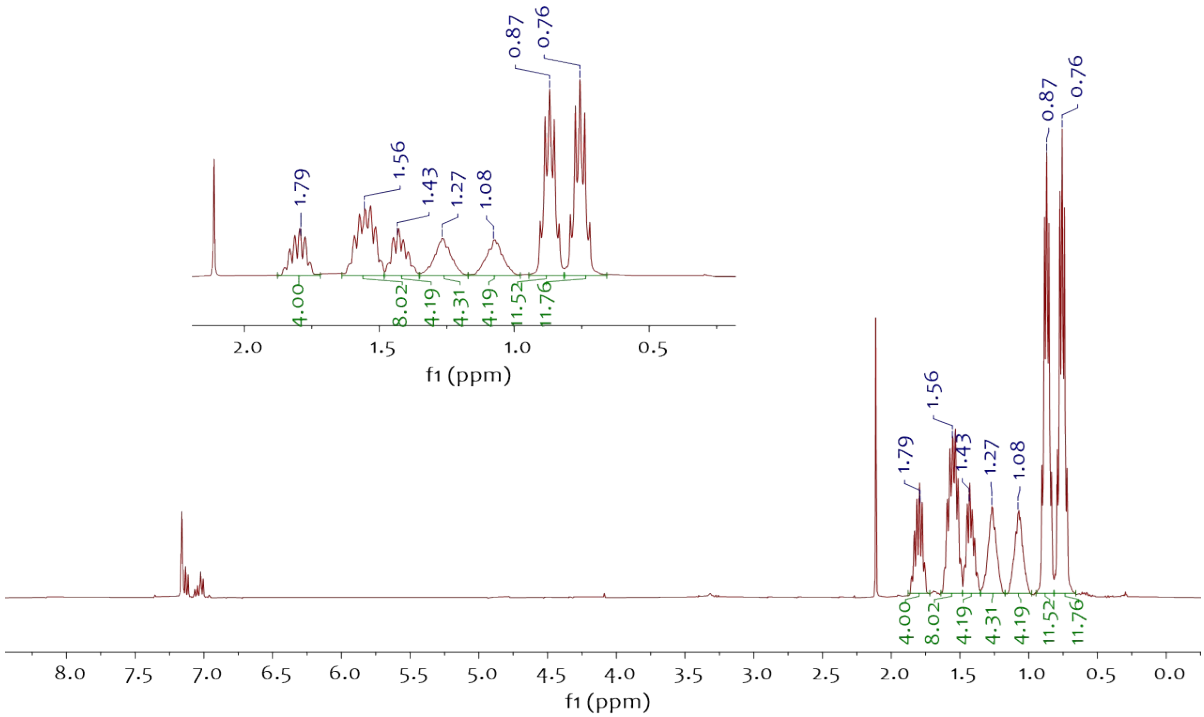

Figure S2. ^{1}H-NMR spectrum (400.0 MHz, C_6D_6, 298K) of another batch of compound 1_{Al} at a different concentration (note that ^{19}F-NMR and ^{31}P-NMR spectra of both batches are identical).

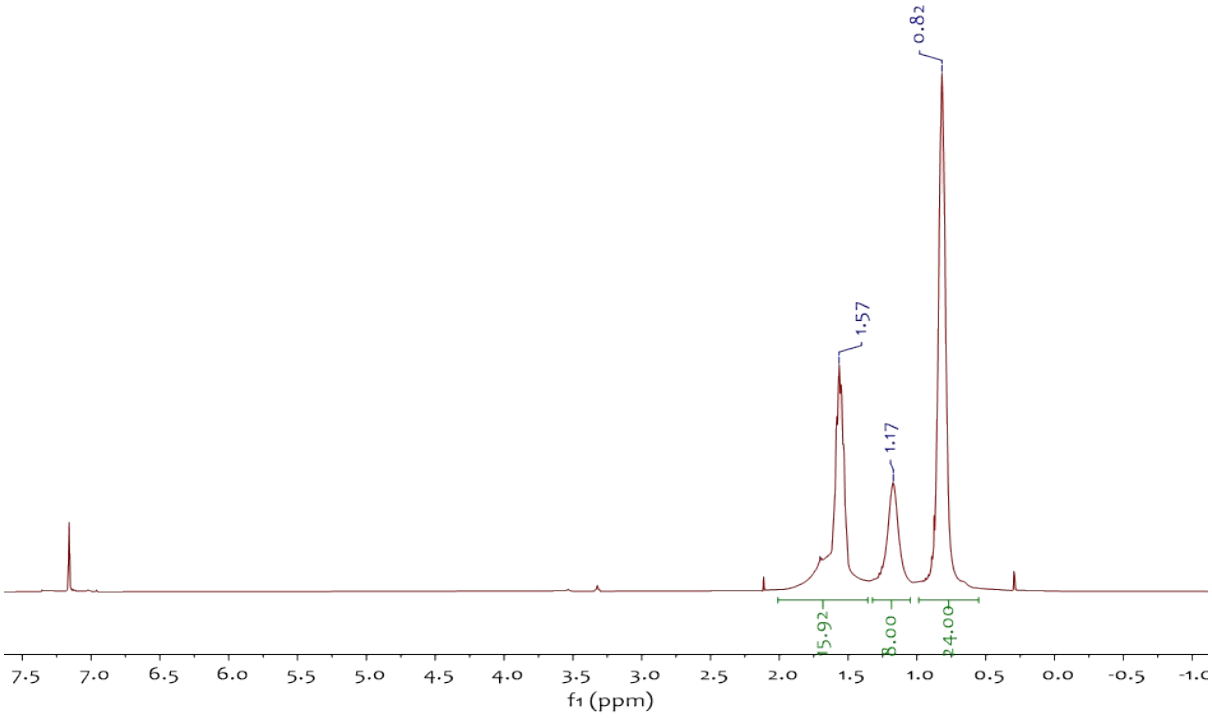

Figure S3. Stacking of Figure S1 and Figure S2 showing that the spectrum of batch 2 displays a coalescence phenomenon. The latter is assigned to the different concentrations between batch 1 and batch 2 (c.a. 14 mM *vs* 26 mM).

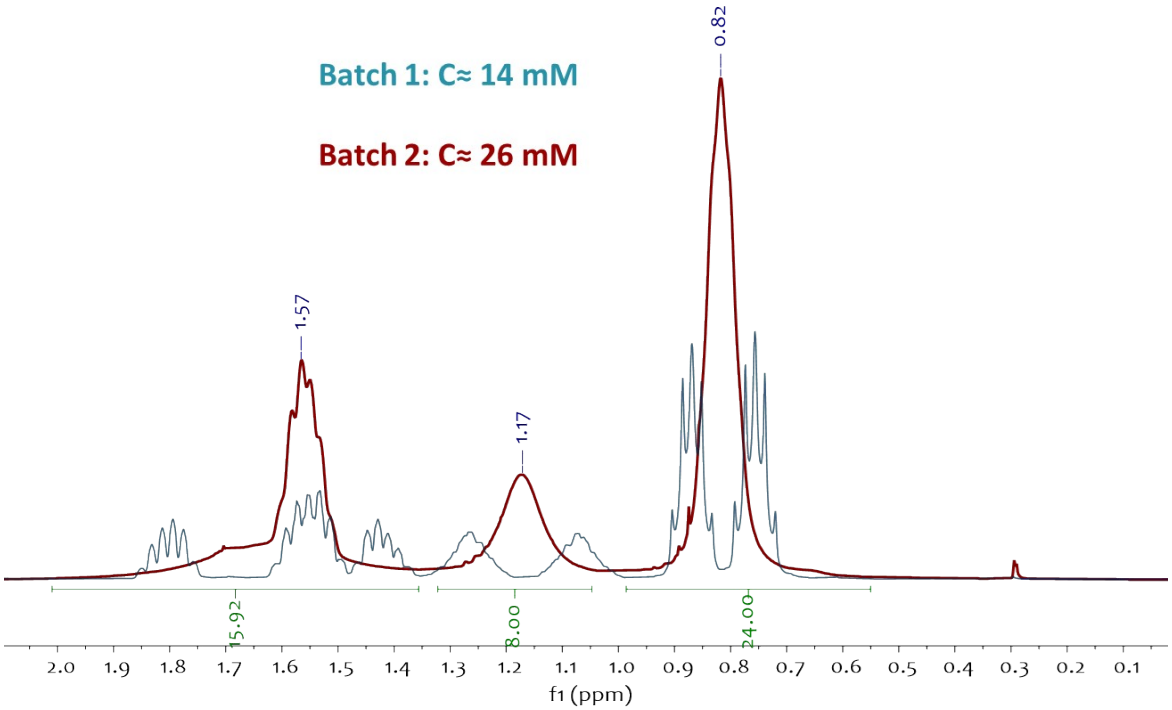

Figure S4. ^{19}F-NMR spectrum (376.2 MHz, C_6D_6, 298K) of compound $\mathbf{1}_{Al}$.

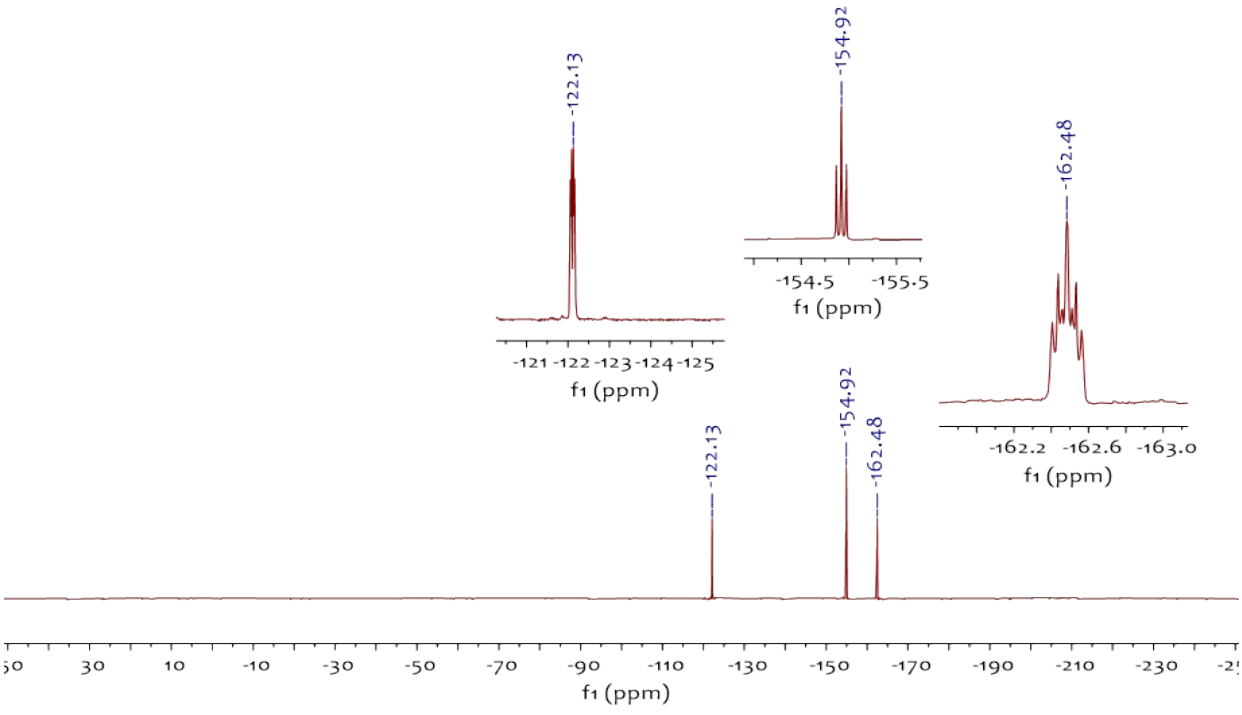

Figure S5. $^{13}C\{^{1}H\}$-NMR spectrum (100 MHz, C_6D_6, 298K) of compound 1_{Al}.

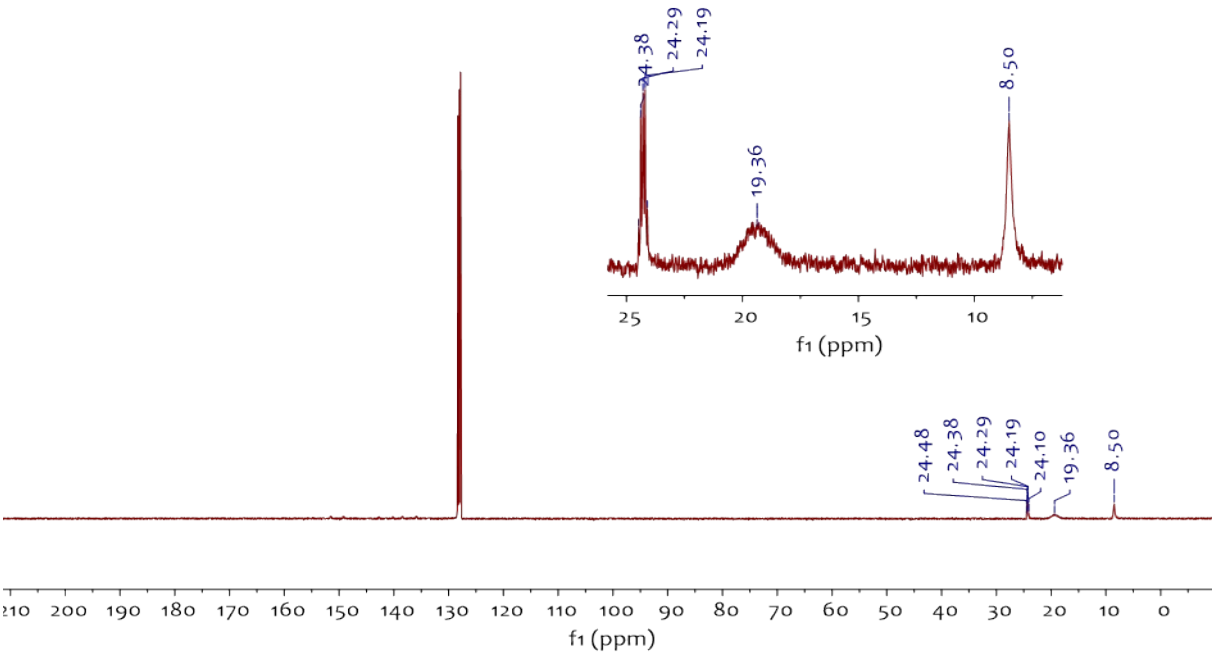

Figure S6. $^{31}P\{^{1}H\}$-NMR spectrum (163.2 MHz, C_6D_6, 298K) of compound 1_{Al}.

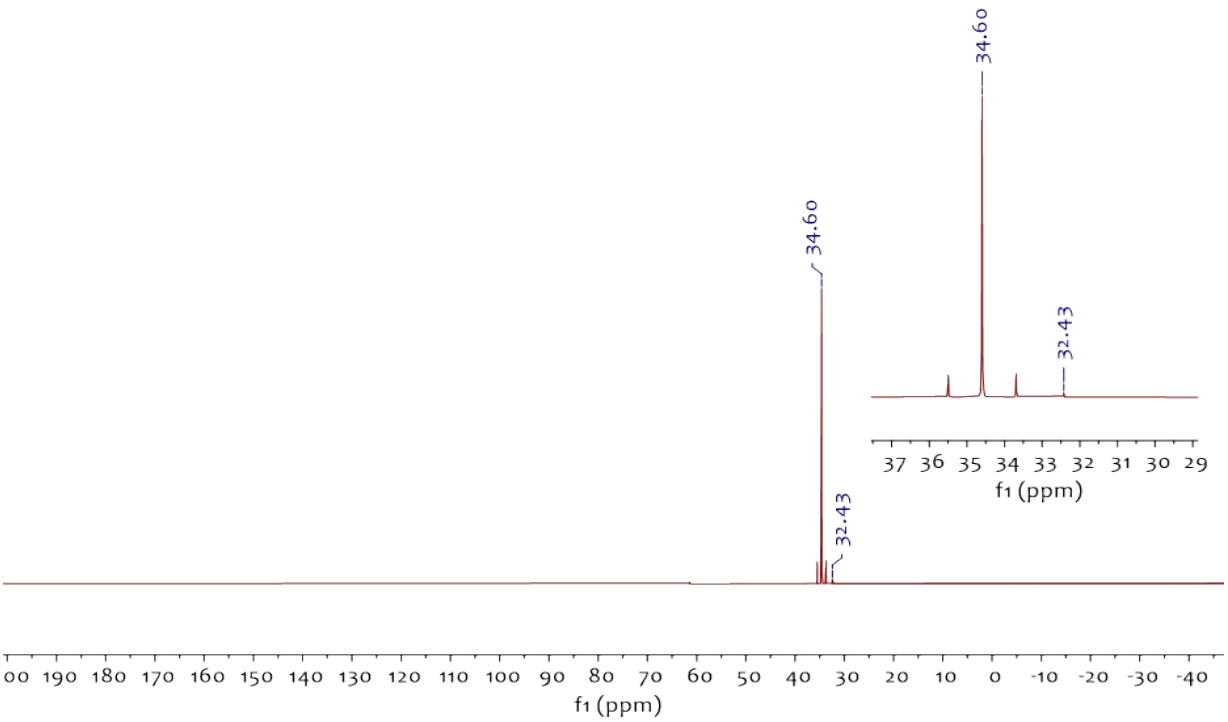

Figure S7. $^{15}N\{^{1}H\}$-INVGATED NMR spectrum (40.5 MHz, C_6D_6, 298K) of compound ^{15}N-1_{Al}.

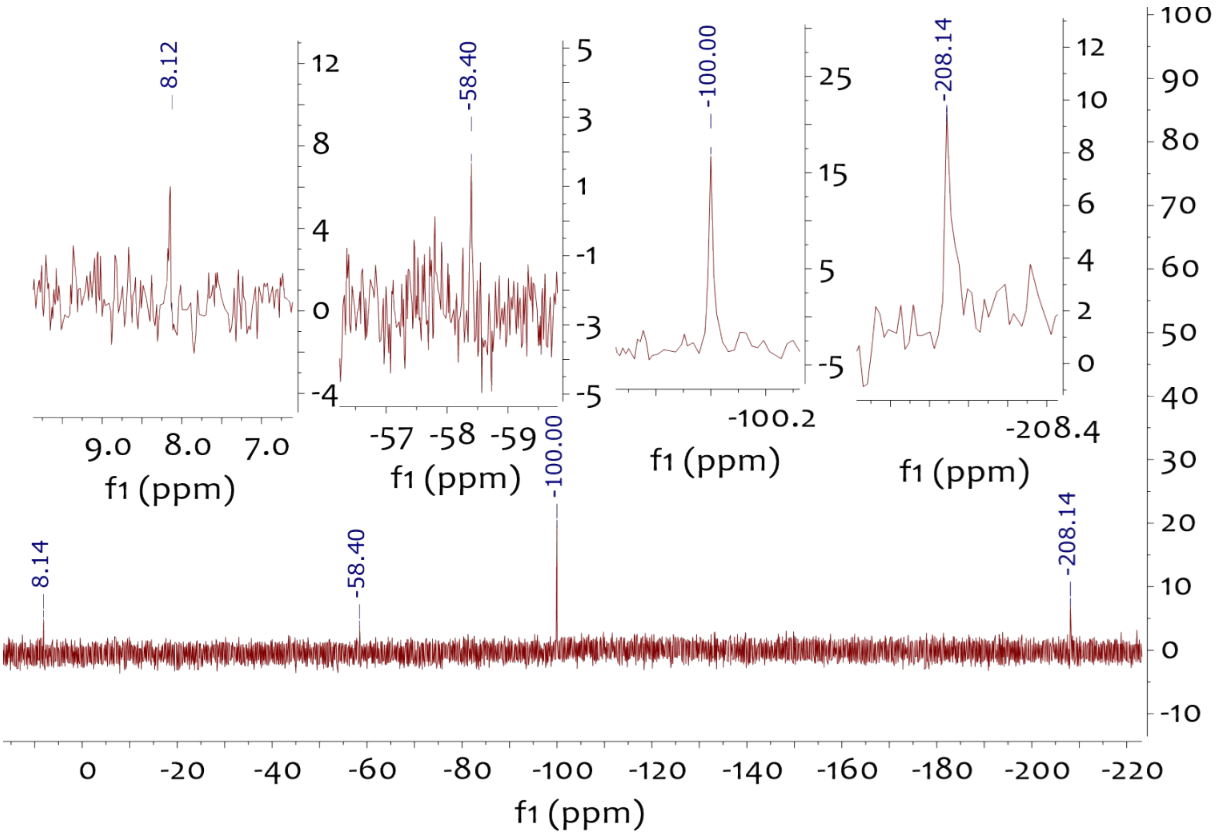

Figure S8. ^{19}F-NMR spectrum (376.2 MHz, C_6D_6, 298K) monitoring of the reaction of 1_B + AlCF leading to species 1_{Al} +BCF.

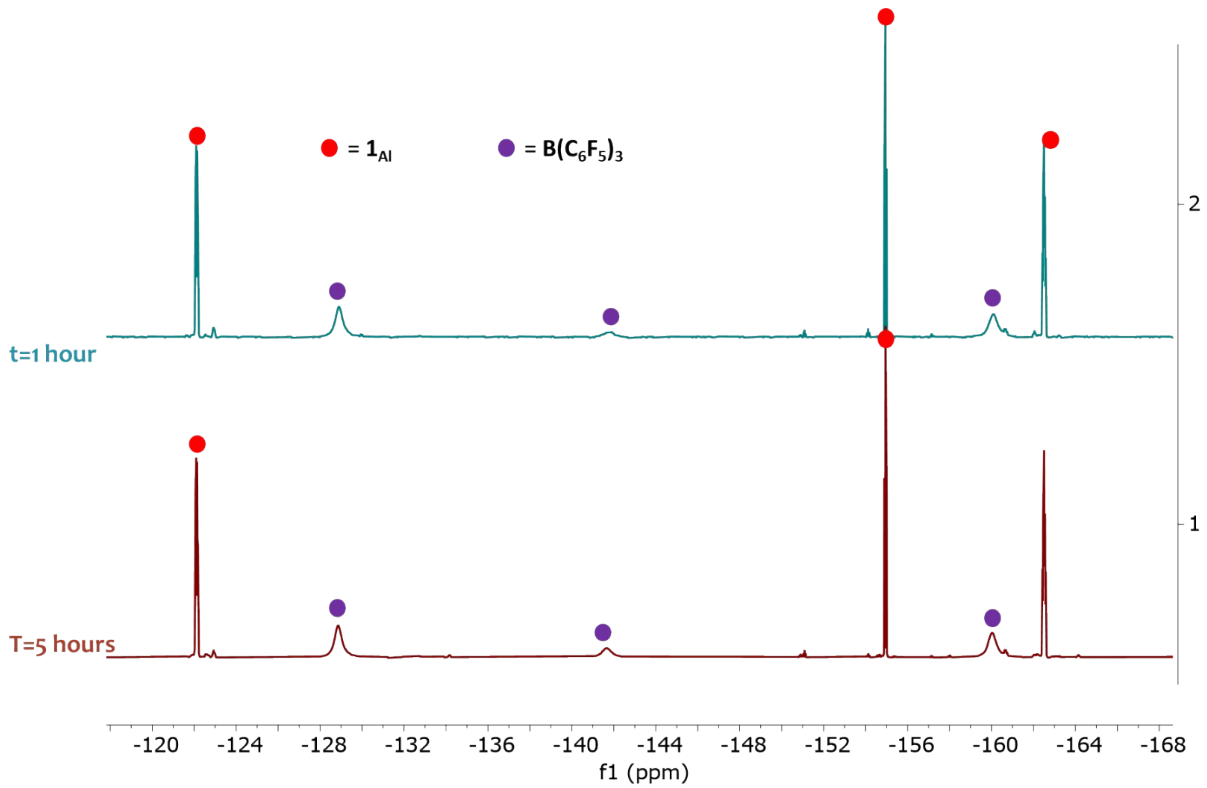

Figure S9. $^{31}P\{^{1}H\}$-NMR spectrum (163.2 MHz, C_6D_6, 298K) monitoring of the reaction of 1_B + AlCF leading to species 1_{Al} + BCF. The weak signals at 33.7 and 35.5 ppm correspond to the W satellites of 1_{Al} ($^{1}J_{W-P}$ = 146 Hz).

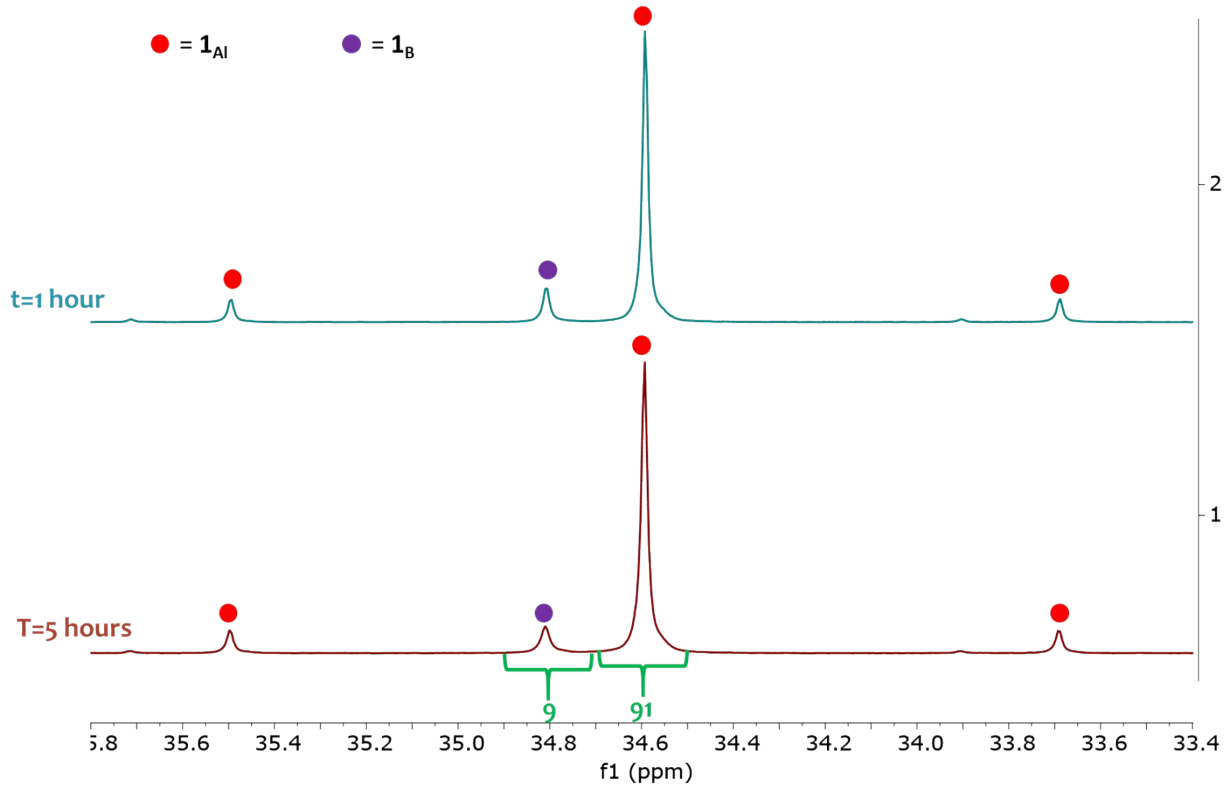

Figure S10. ^{1}H-NMR spectrum (400 MHz, C_6D_6, 298K) of compound 2_{Al}

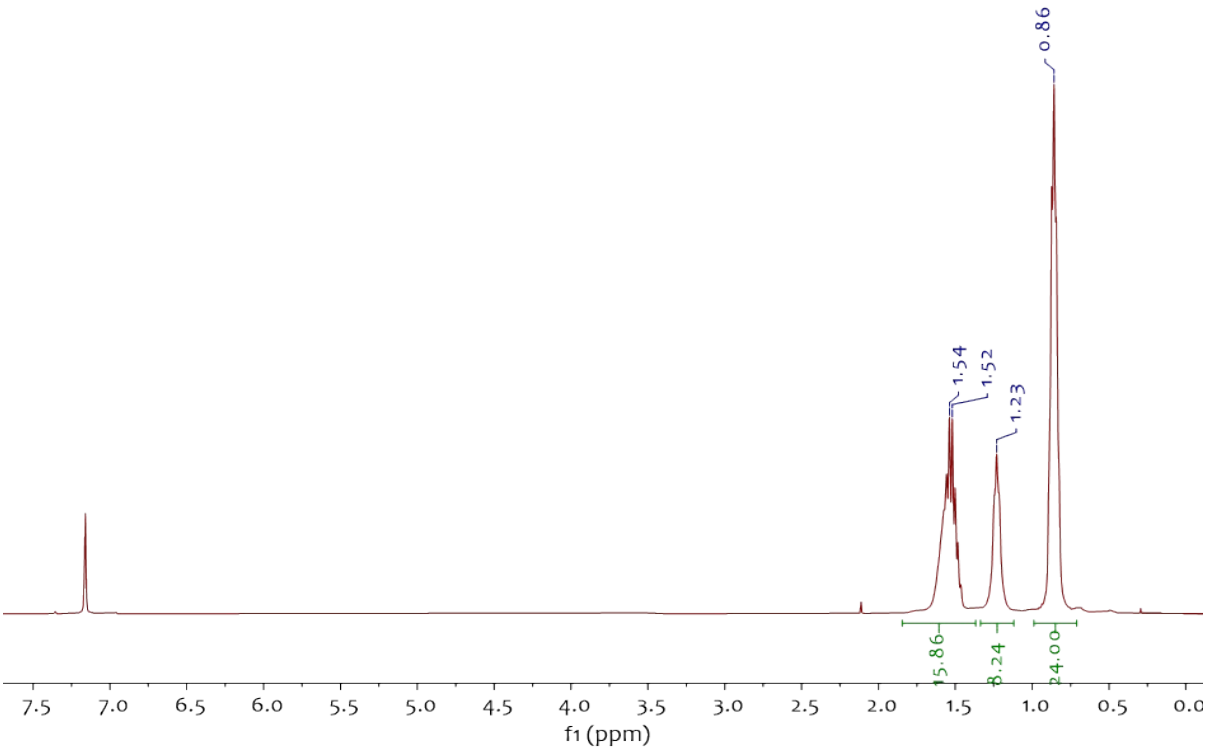

Figure S11. ^{19}F-NMR spectrum (376.2 MHz, C_6D_6, 298K) of compound 2_{Al}.

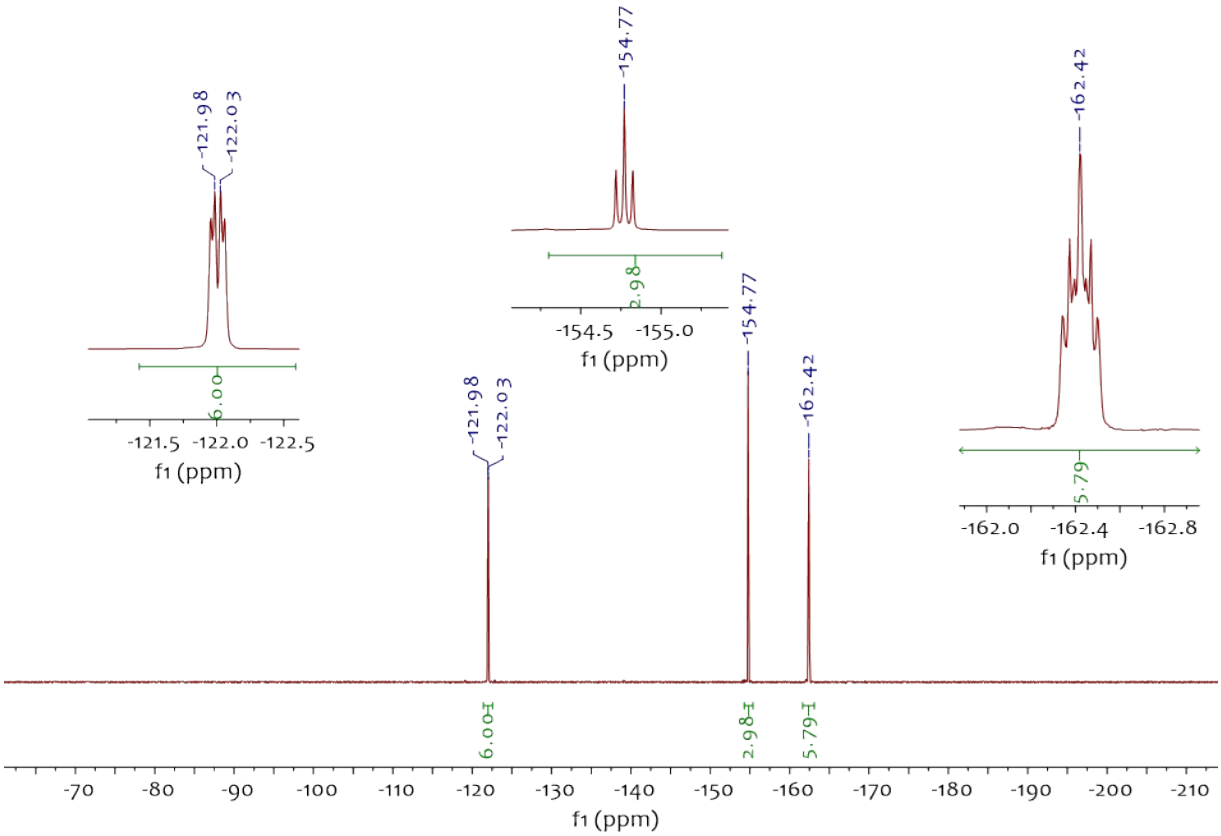

Figure S12. $^{13}C\{^1H\}$-NMR spectrum (100 MHz, C_6D_6, 298K) of compound 2_{Al}

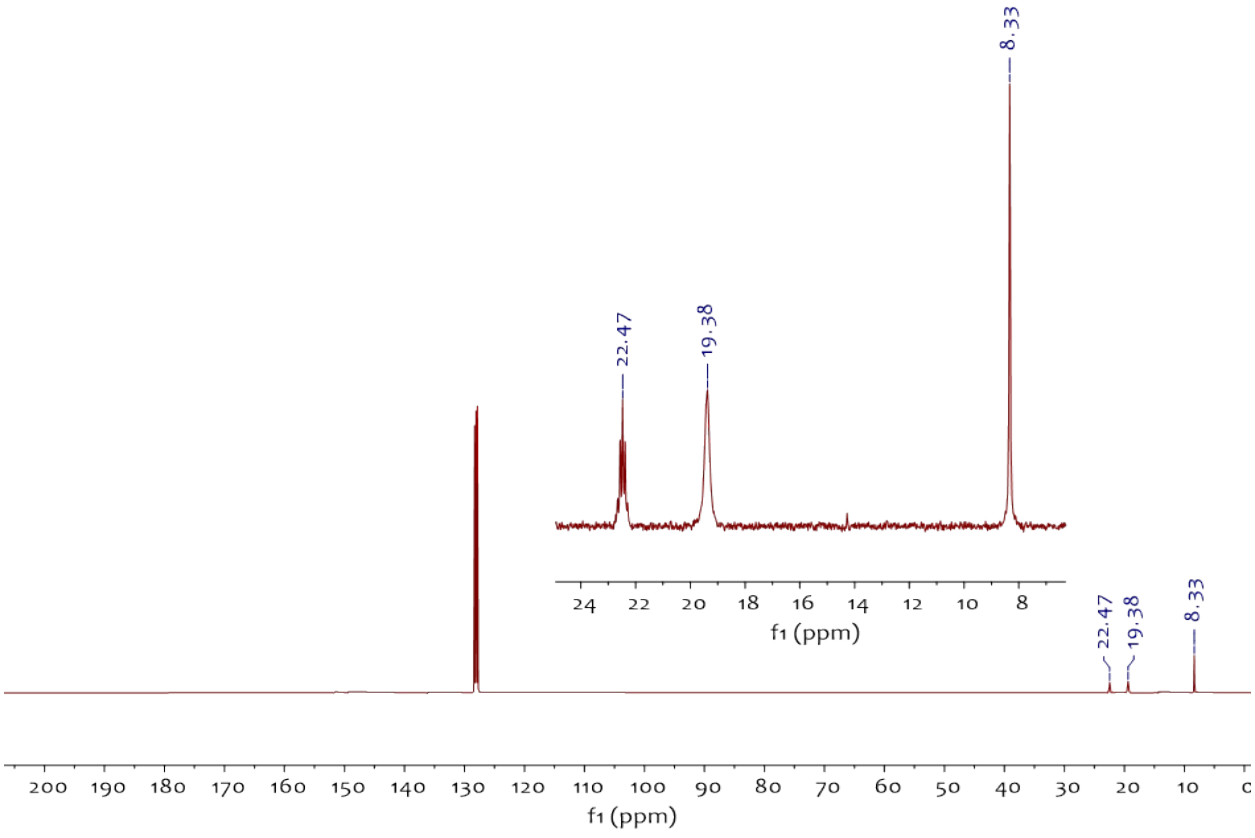

Figure S13. $^{31}P\{^{1}H\}$-NMR spectrum (163.2 MHz, C_6D_6, 298K) of compound 2_{Al}.

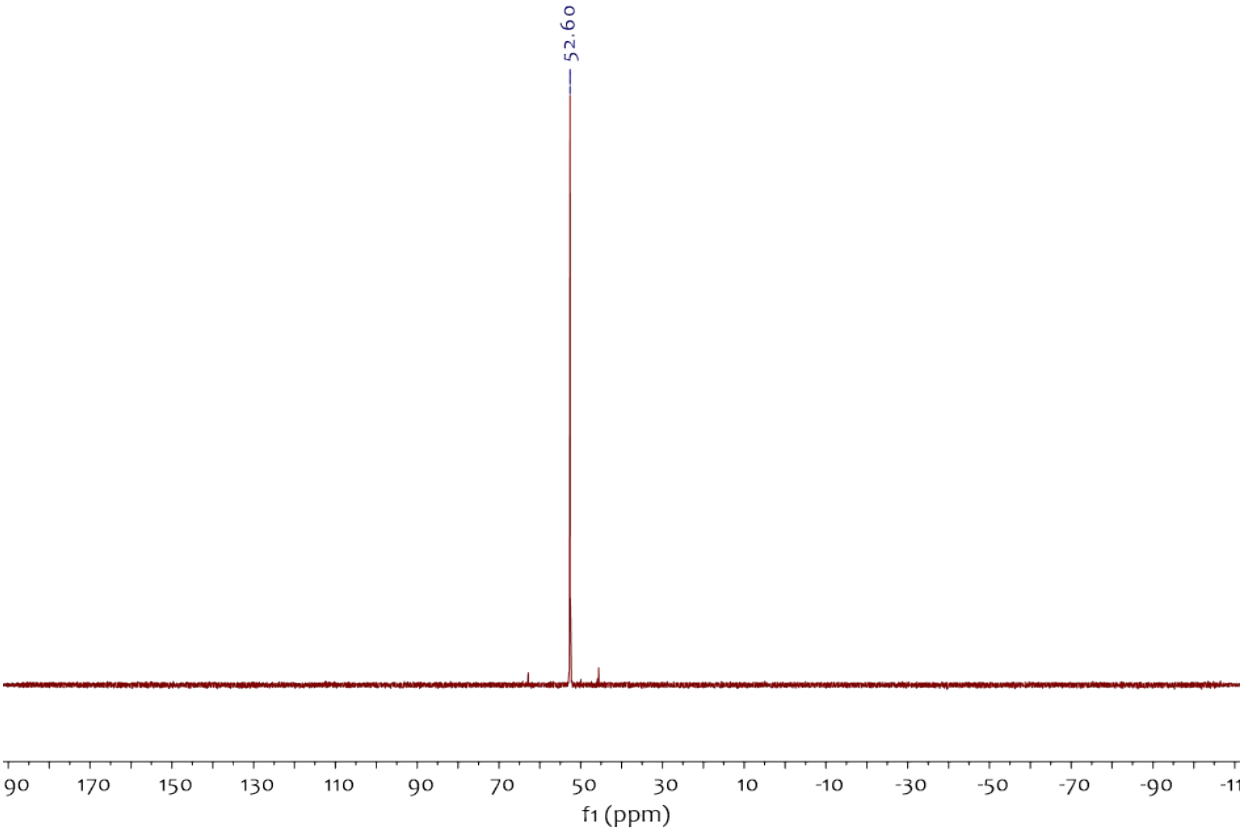

Figure S14. ^{1}H-NMR spectrum (400 MHz, C_6D_6, 298K) of compound 5_{Al}

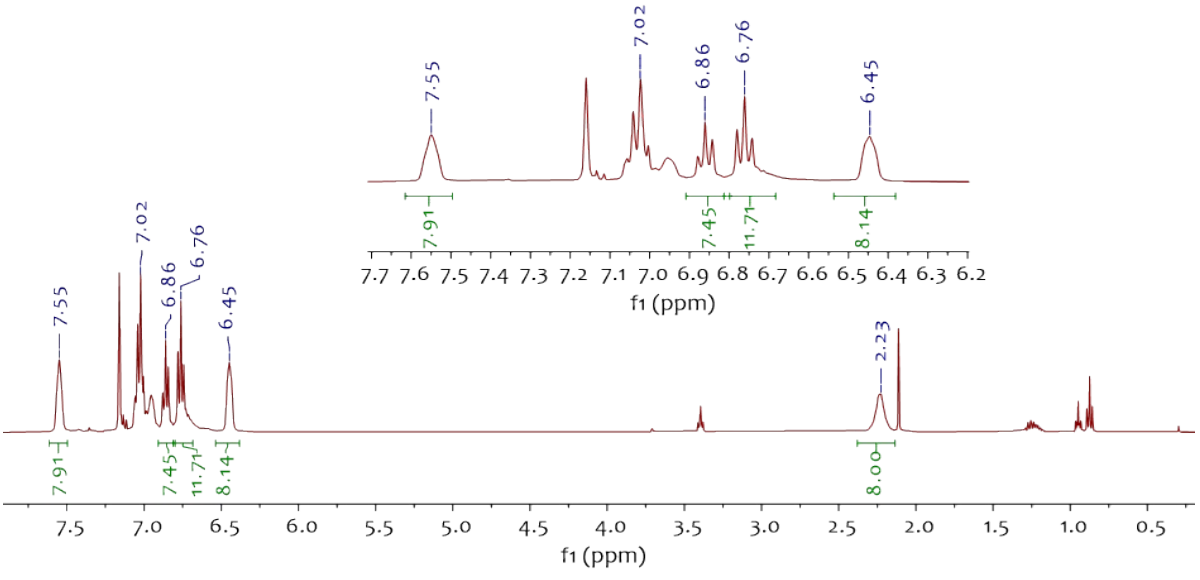

Figure S15. ^{19}F-NMR spectrum (376.2 MHz, C_6D_6, 298K) of compound 5_{Al}.

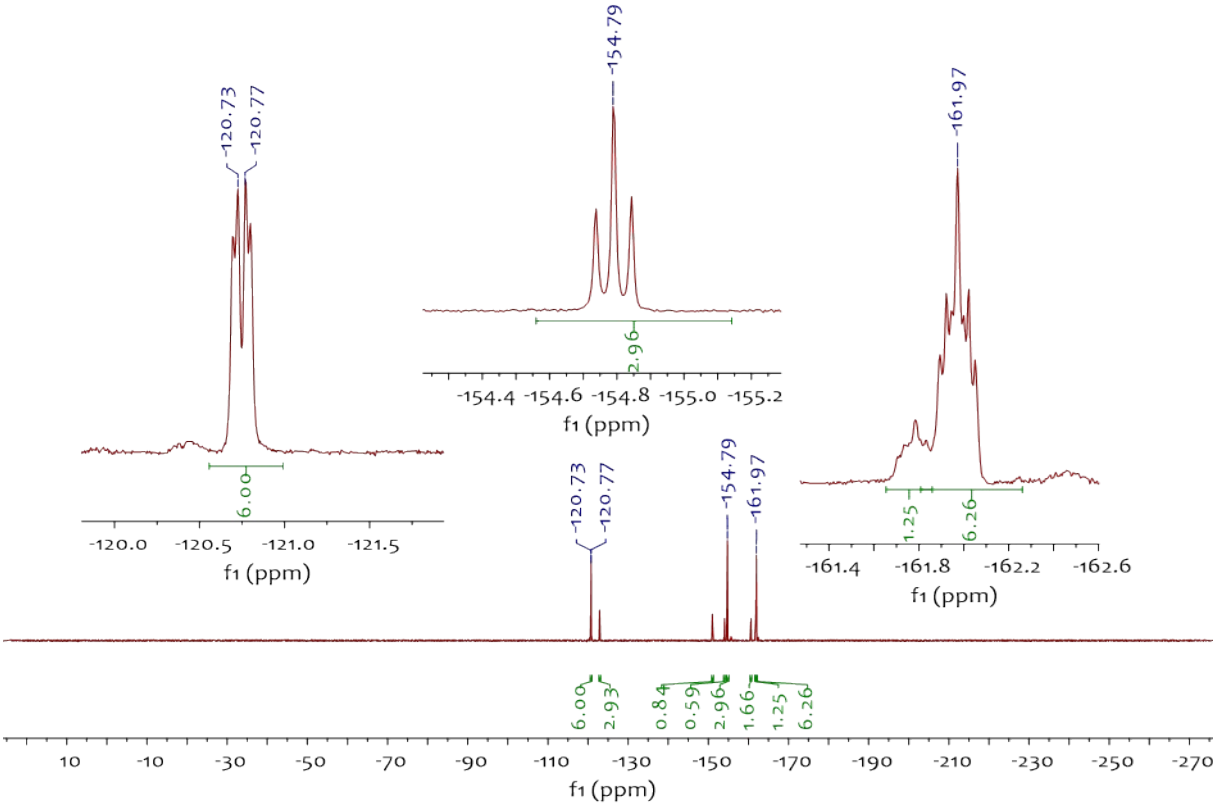

Figure S16. ^{13}C{^{1}H}-NMR spectrum (100 MHz, C_6D_6, 298K) of compound 5_{Al}.

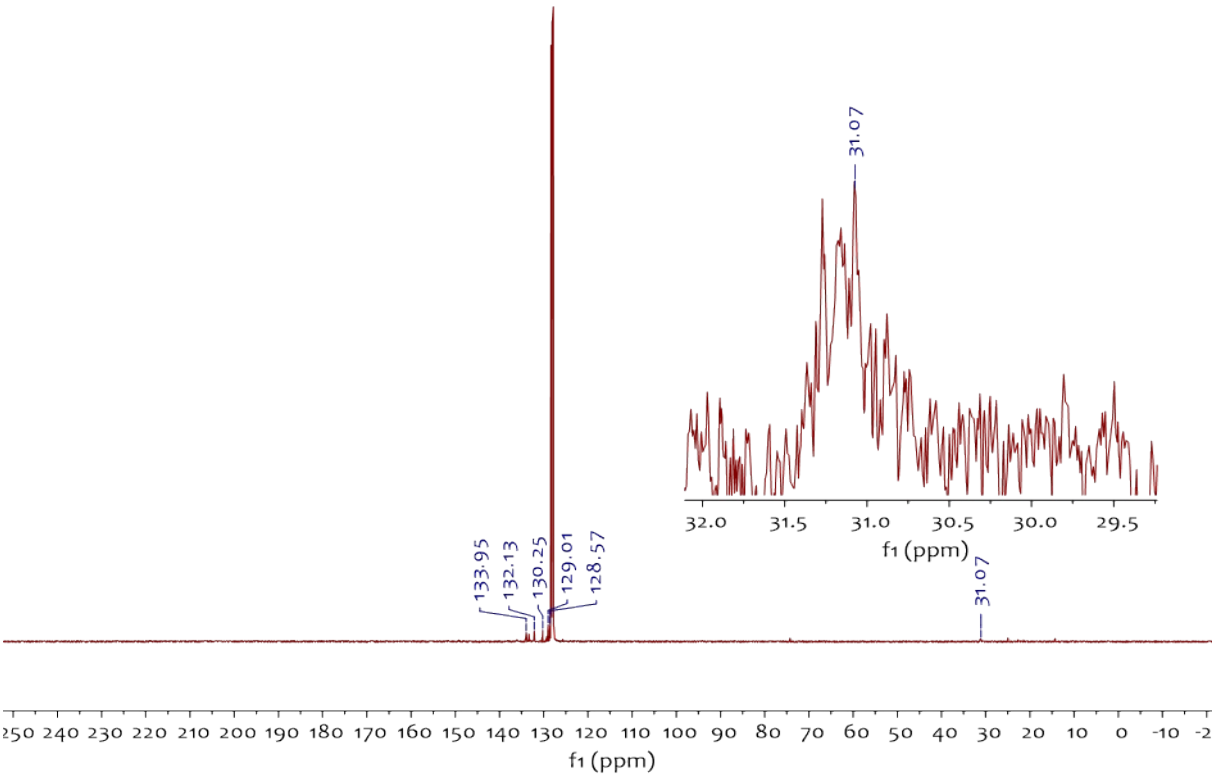

Figure S17. ^{1}H-^{13}C-HSQC NMR spectrum (400 MHz, C_6D_6, 298K) of compound 5_{Al}.

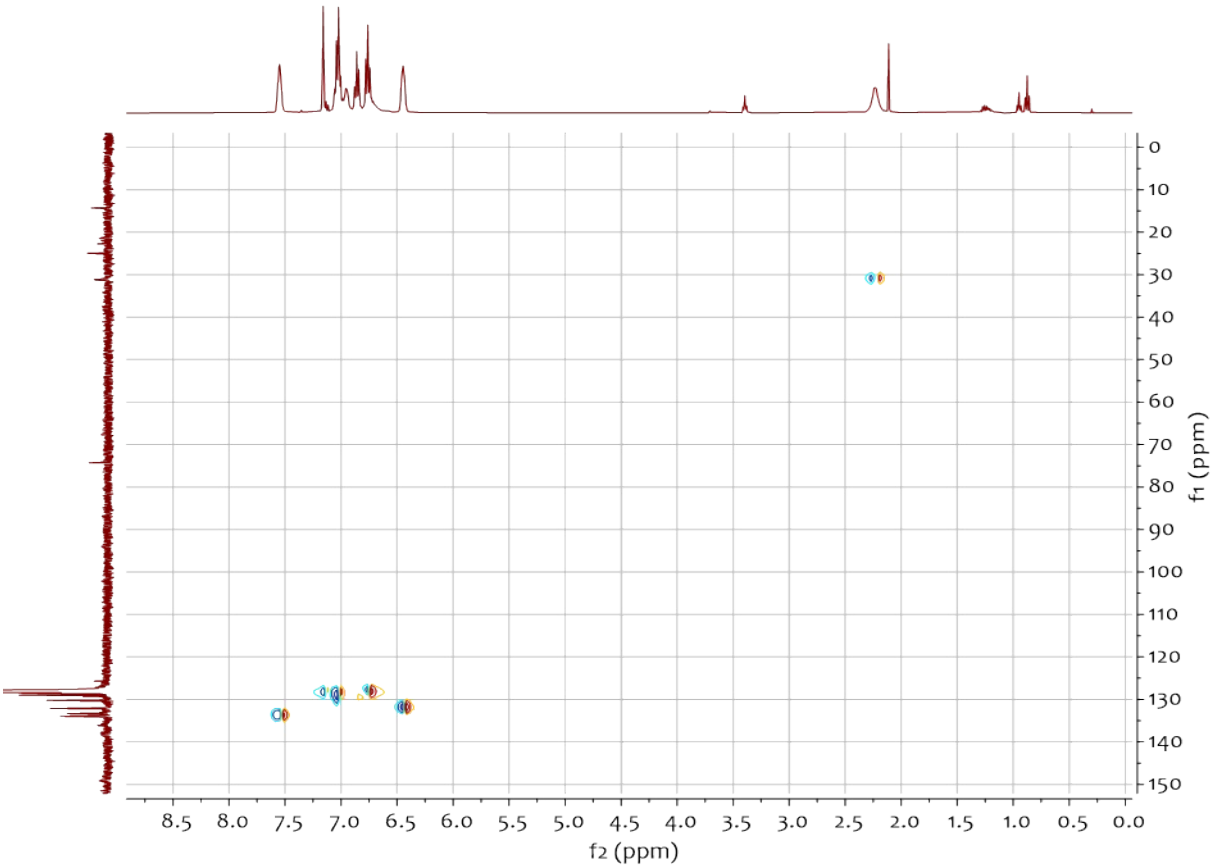

Figure S18. $^{31}P\{^{1}H\}$-NMR spectrum (163.2 MHz, C_6D_6, 298K) of compound 5_{Al}.

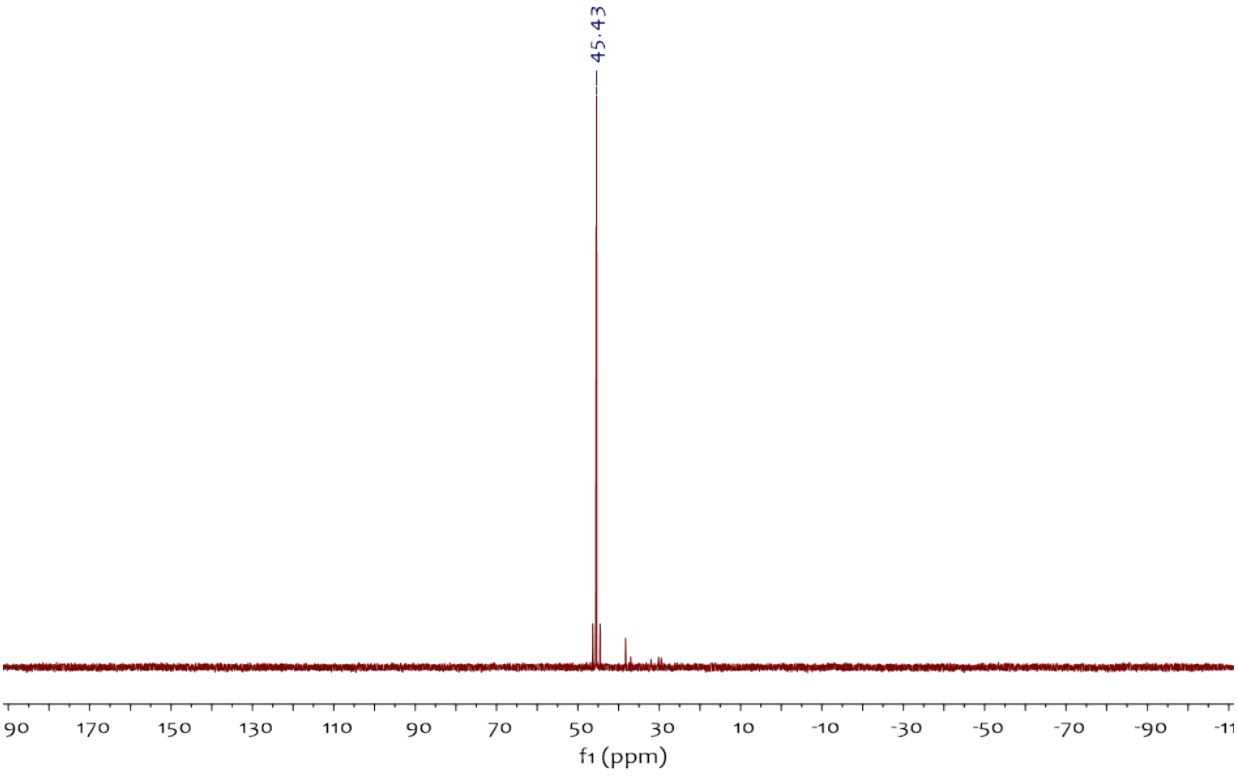

Figure S19. ^{1}H-NMR spectra (400.0 MHz, C_6D_6, 298K) relating to the reaction of $[W(dppe)_2(N_2)_2]$ + $Al(C_6F_5)_3(tol)$ under an atmosphere of nitrogen (turquoise line) or argon (red line). This experiment shows two identical spectra where the compound 5_{Al} is predominant.

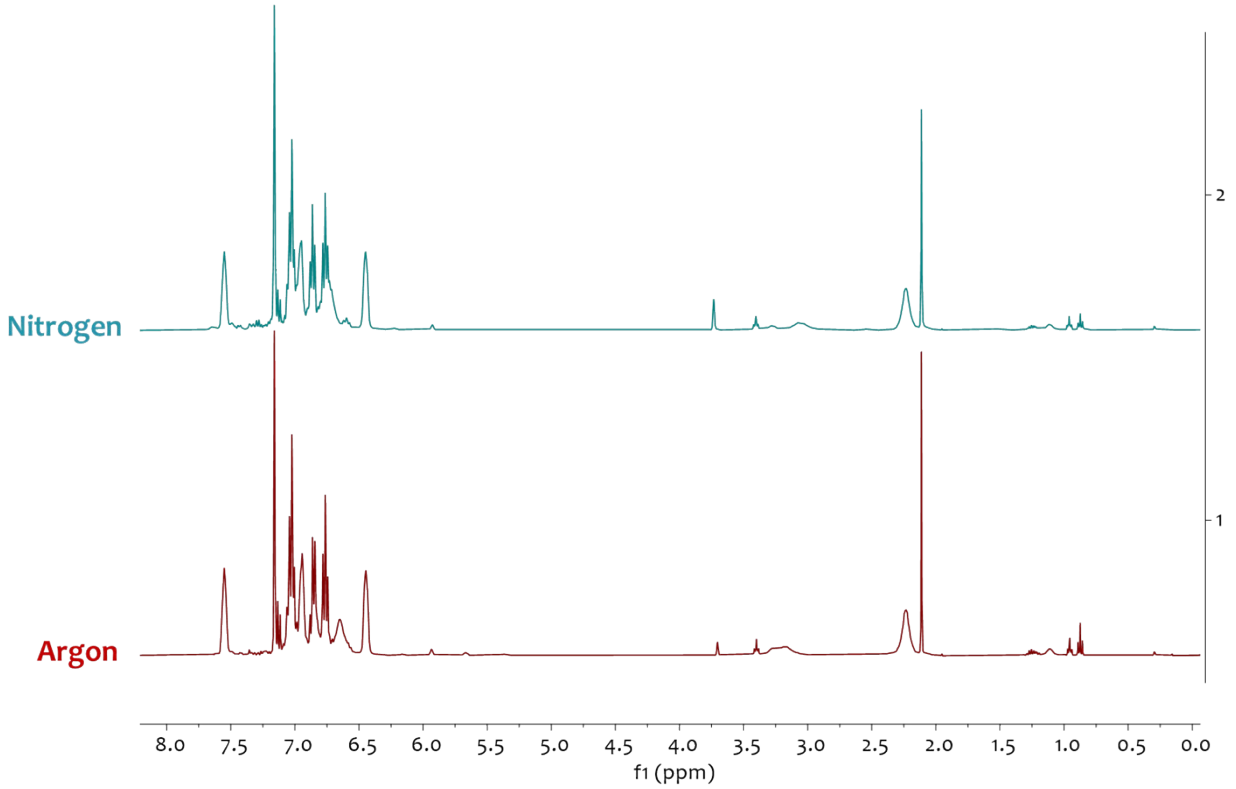

Figure S20. ^{1}H-NMR spectrum (400 MHz, C_6D_6, 298K) of compound 6_{Al}.

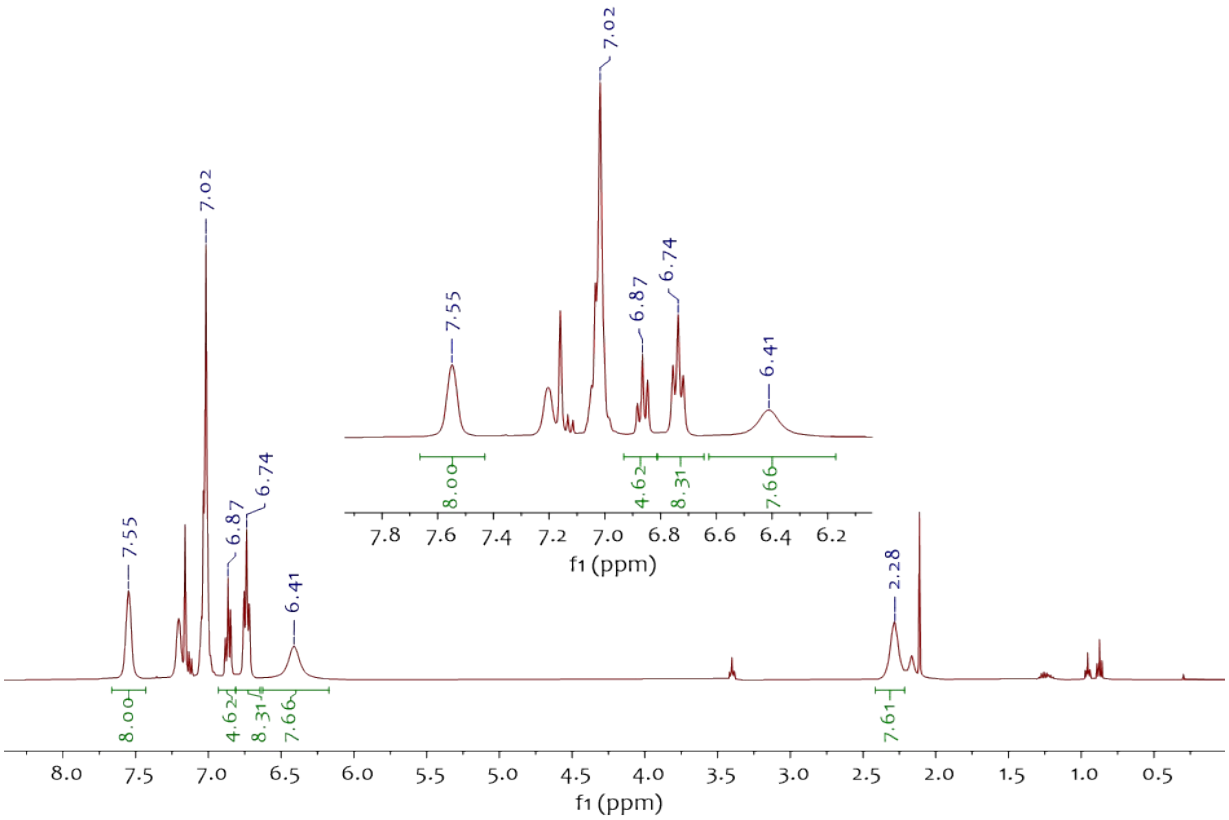

Figure S21. ^{19}F-NMR spectrum (376.2 MHz, C_6D_6, 298K) of compound 6_{Al}.

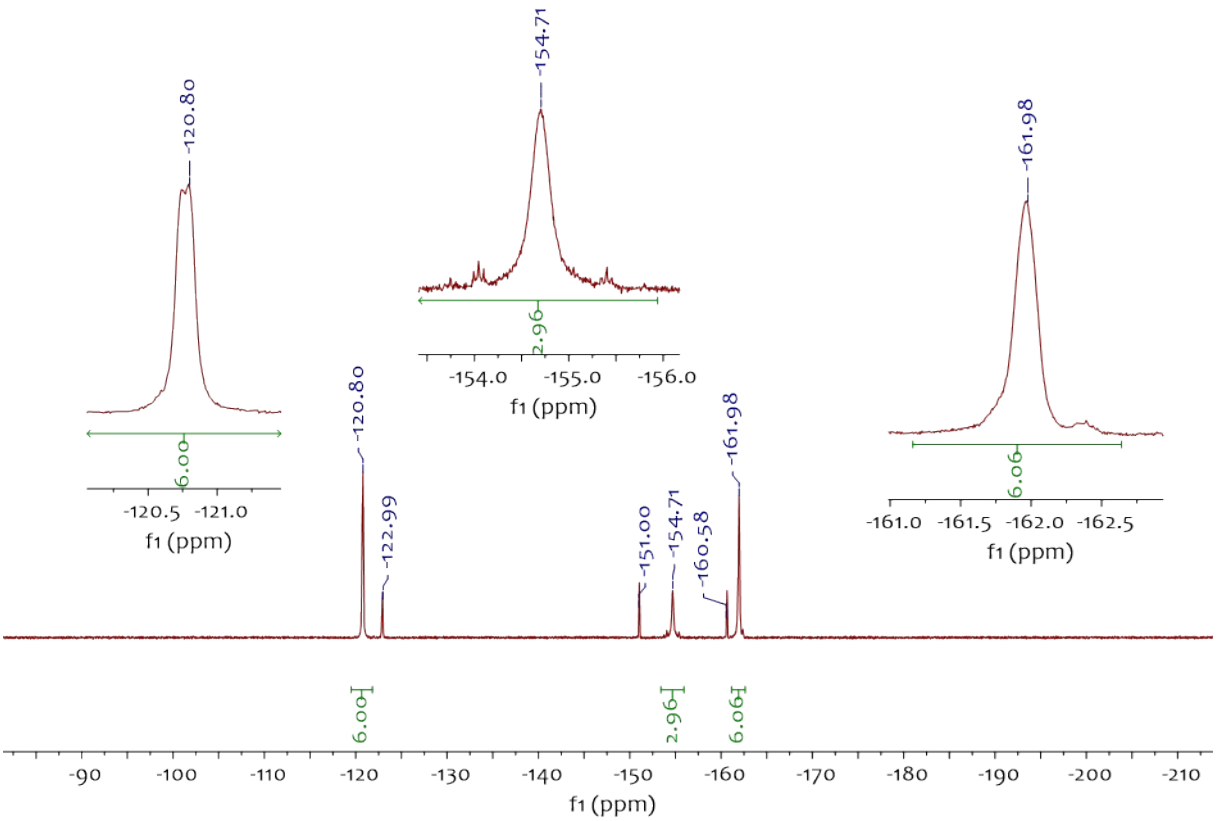

Figure S22. ^{13}C{^{1}H}-NMR spectrum (100 MHz, C_6D_6, 298K) of compound 6_{Al}.

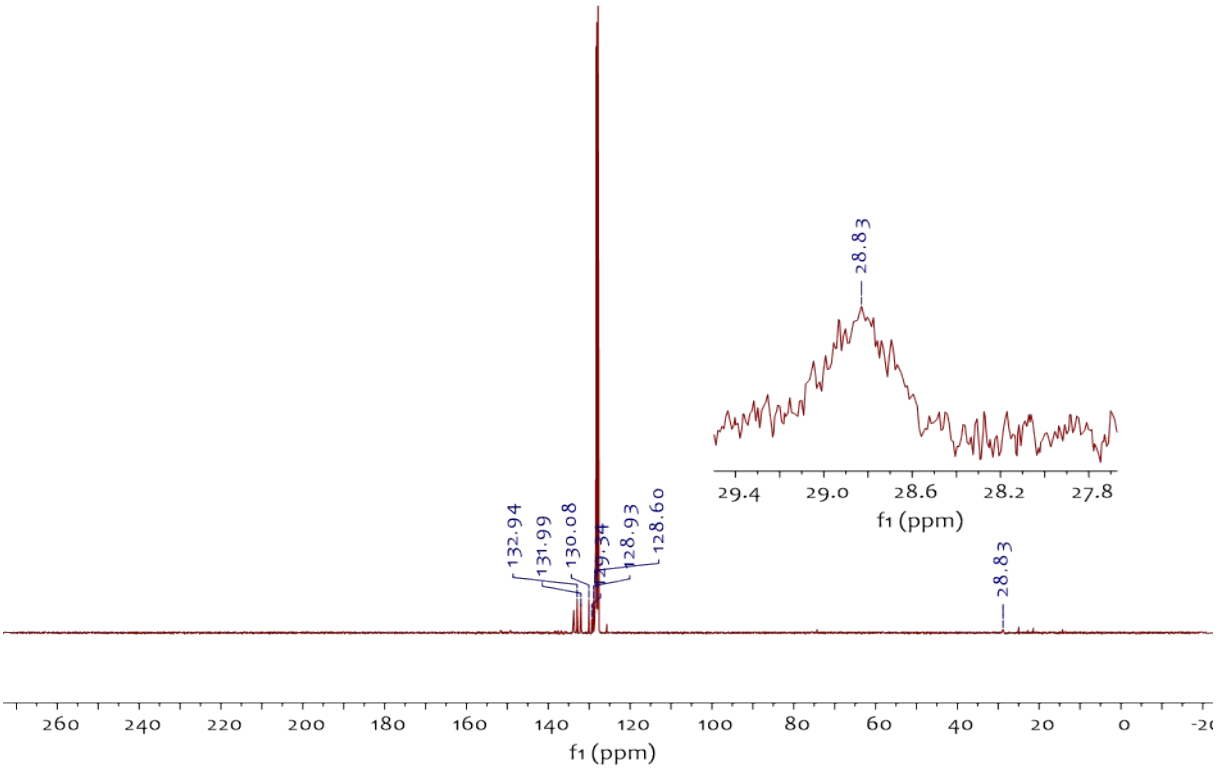

Figure S23. ^{1}H-^{13}C-HSQC NMR spectrum (400 MHz, C_6D_6, 298K) of compound 6_{Al}.

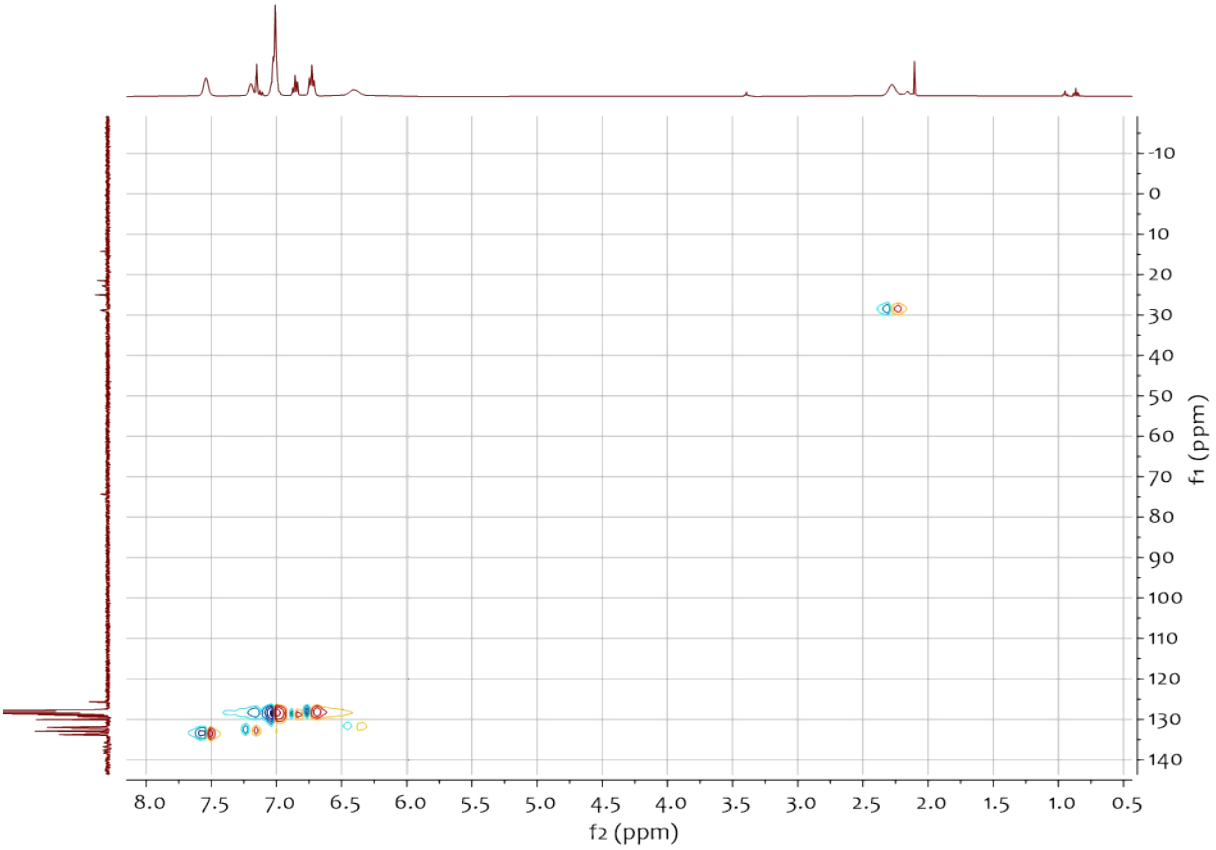

Figure S24. $^{31}P\{^{1}H\}$-NMR spectrum (163.2 MHz, C_6D_6, 298K) of compound 6_{Al}.

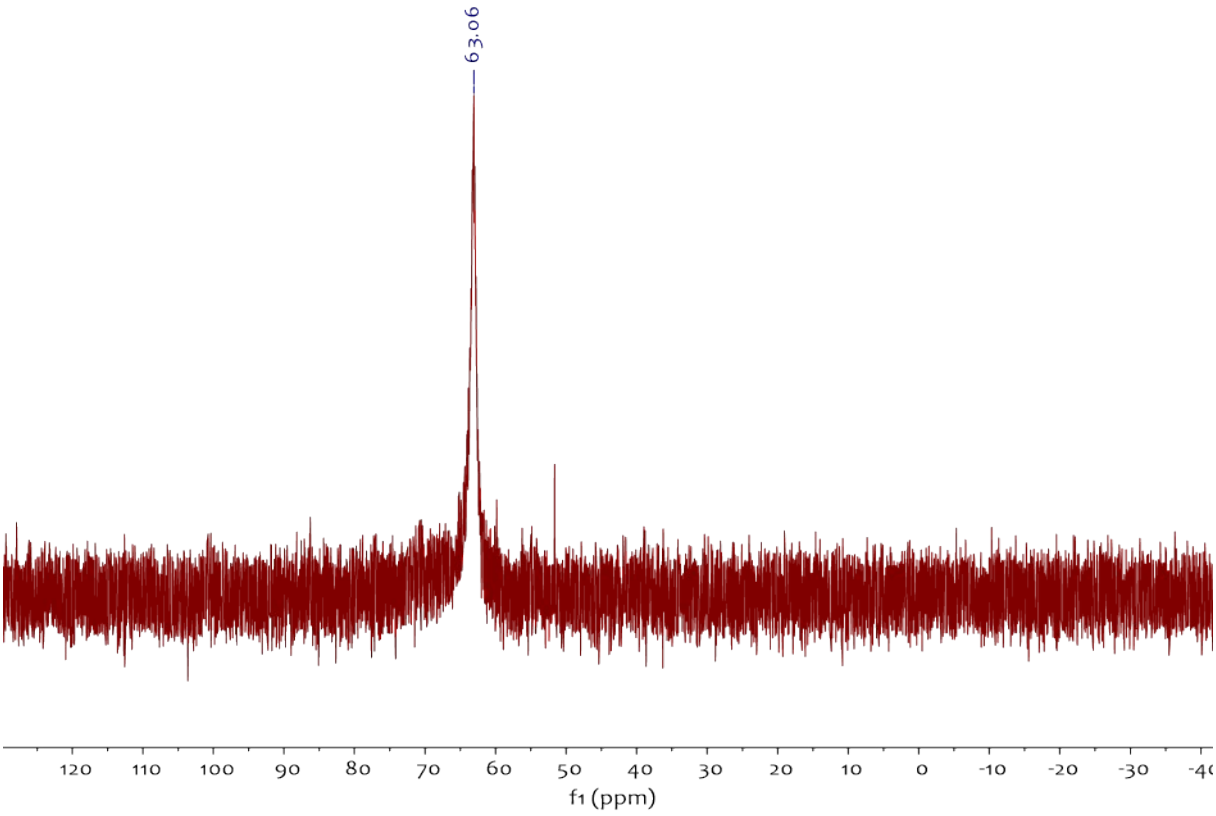

Figure S25. ^{1}H-NMR spectrum (400.0 MHz, C_6D_6, 298K) of the crude reaction of $[Mo(dppe)_2(N_2)_2]$+$Al(C_6F_5)_3$(tol) in an argon glovebox showing the predominant formation of product 4_{Al} along with minor amounts of product 6_{Al}.

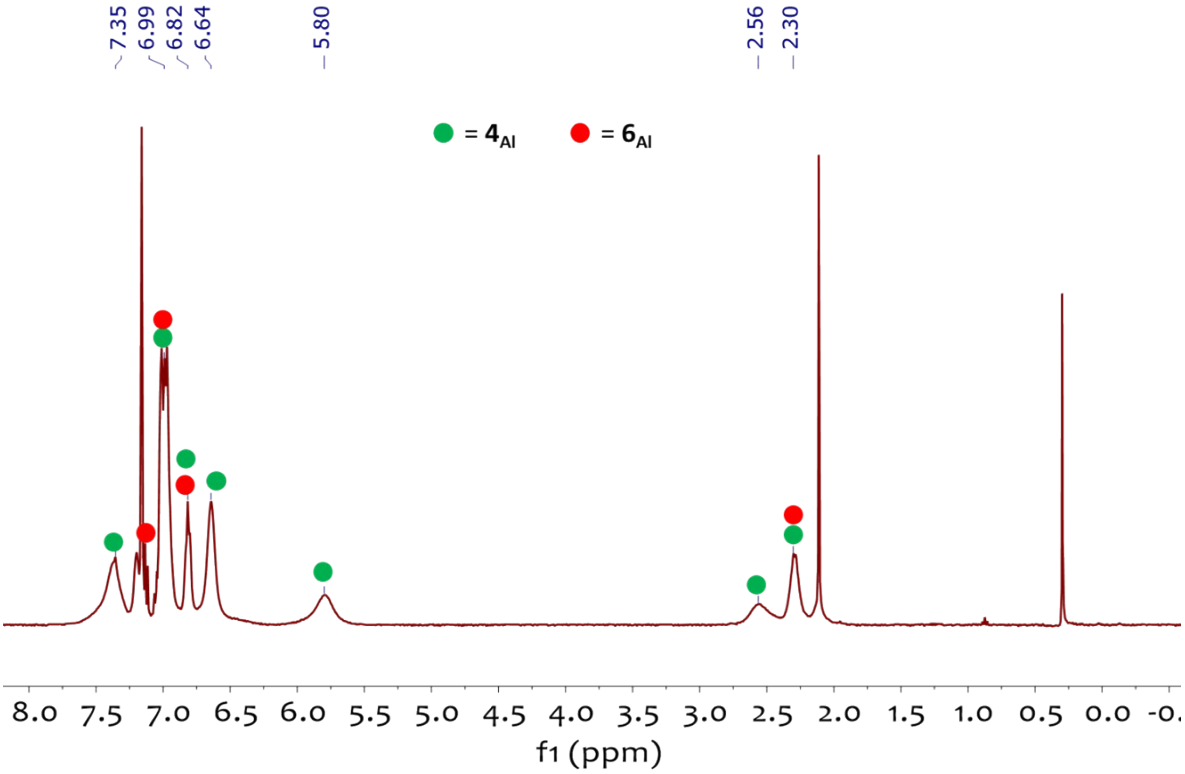

Figure S26. ^{19}F-NMR spectrum (376.2 MHz, C_6D_6, 298K) of the crude reaction of $[Mo(dppe)_2(N_2)_2]$+$Al(C_6F_5)_3$(tol) in an argon glovebox showing the predominant formation of product 4_{Al} along with minor amounts of product 6_{Al} and free AlCF.

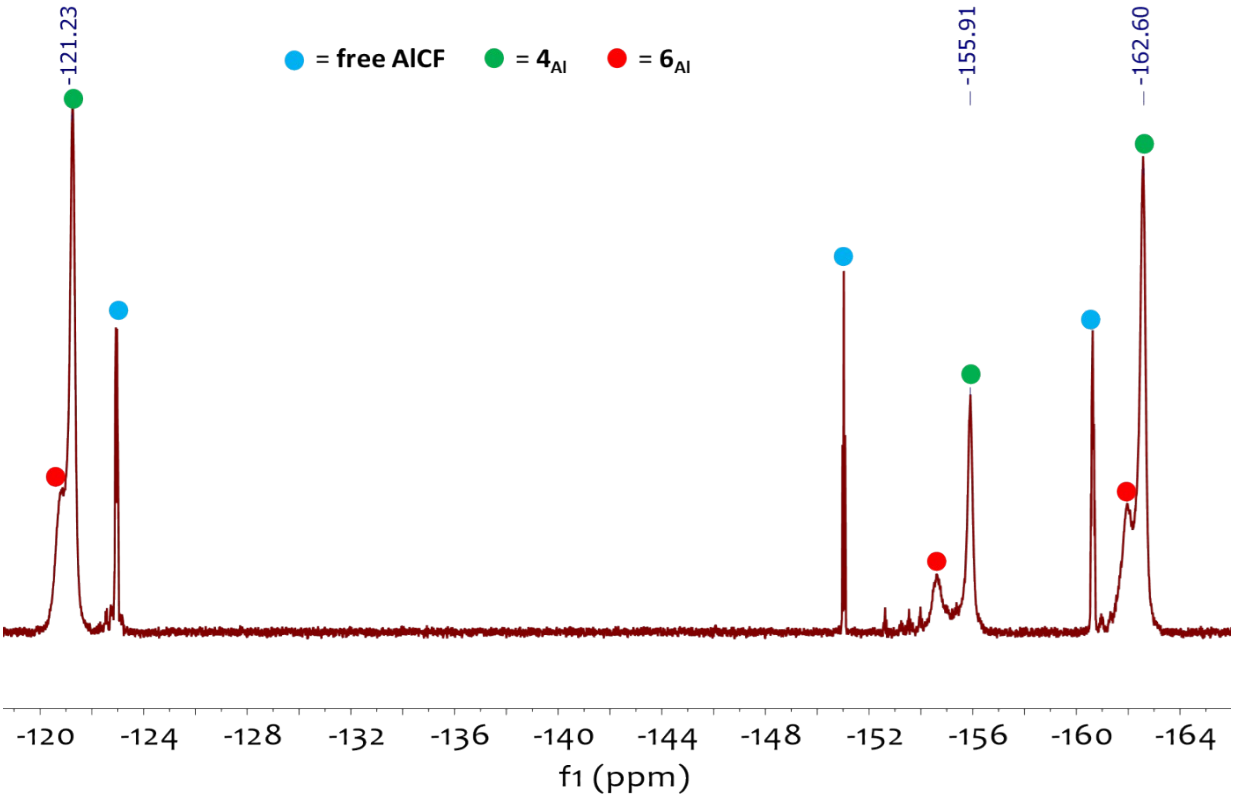

Figure S27. $^{31}P\{^{1}H\}$-NMR spectrum (163.2 MHz, C_6D_6, 298K) of the crude reaction of $[Mo(dppe)_2(N_2)_2]$+$Al(C_6F_5)_3$(tol) in an argon glovebox showing the predominant formation of product 4_{Al} (73%, δ=70.9 ppm) along with minor amounts of product 6_{Al} (27%, δ=63.0 ppm).

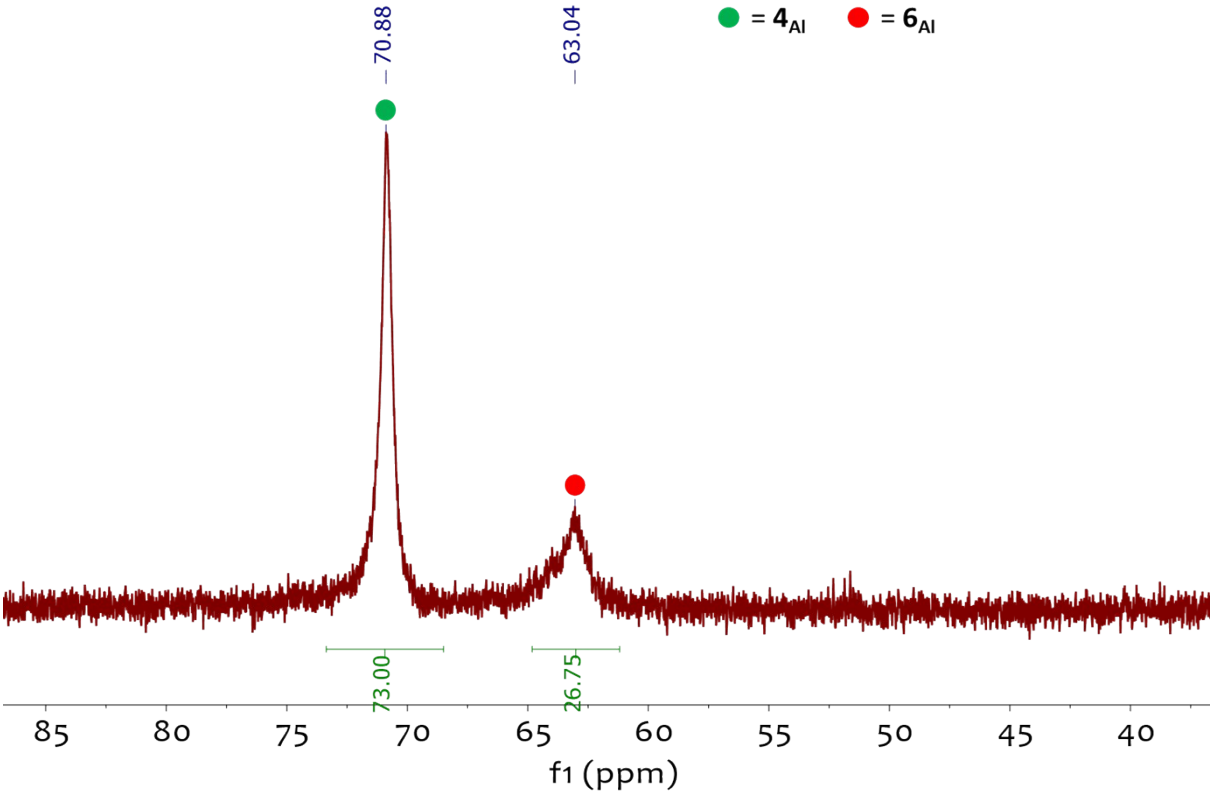

Figure S28. ^{19}F-NMR spectrum (376.2 MHz, C_6D_6, 298K) relating to the reaction of trans-$[W(dppe)_2(\mu\text{-}N_2)BCF]$ (3_B) + $Al(C_6F_5)_3$(tol) (argon glovebox) showing the predominant formation of 5_{Al} - trans-$[W(dppe)_2(N_2)(\mu\text{-}N_2)AlCF]$ - and free BCF.

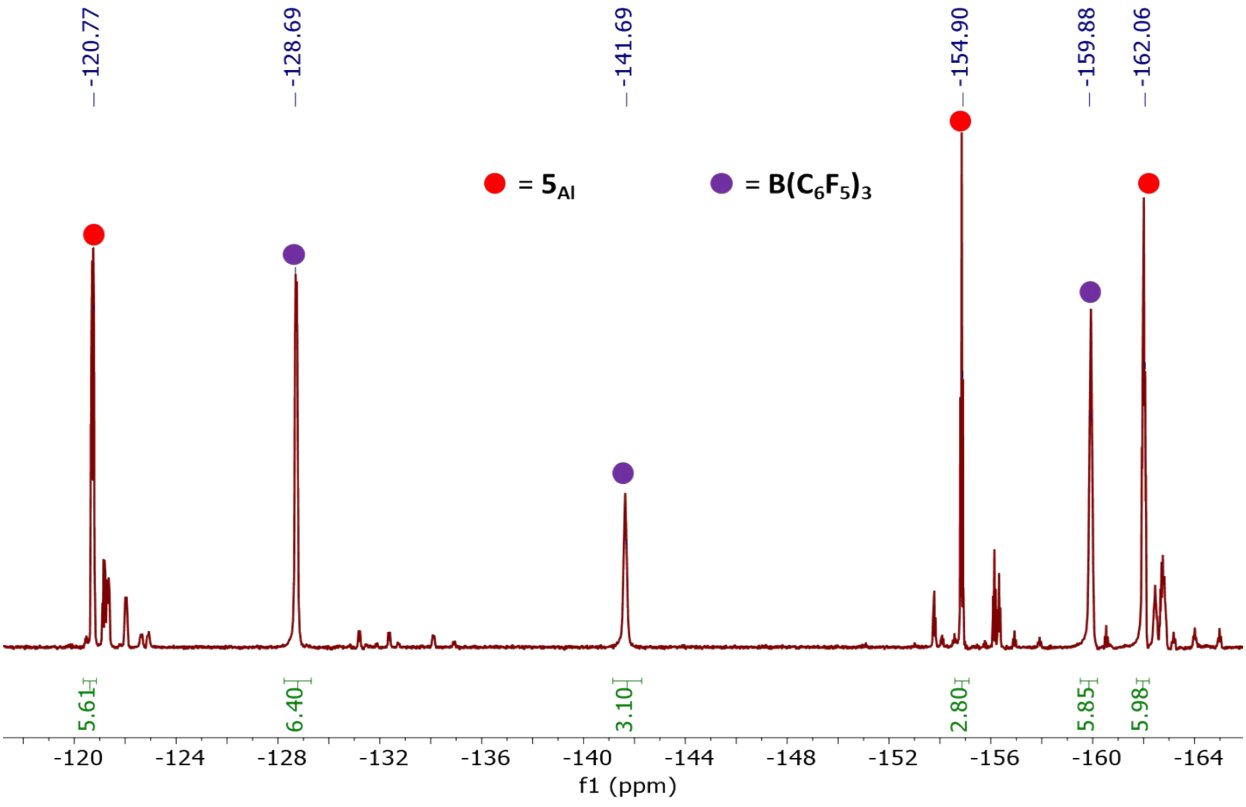

Figure S29. ^{19}F-NMR spectrum (376.2 MHz, C_6D_6, 298K) relating to the reaction of *trans*-[Mo(dppe)$_2$(μ-N$_2$)BCF] (4_B) + Al(C_6F_5)$_3$(tol) under dinitrogen atmosphere showing the predominant formation of 6_{Al} - *trans*-[Mo(dppe)$_2$(N$_2$)(μ-N$_2$)AlCF] - and free BCF.

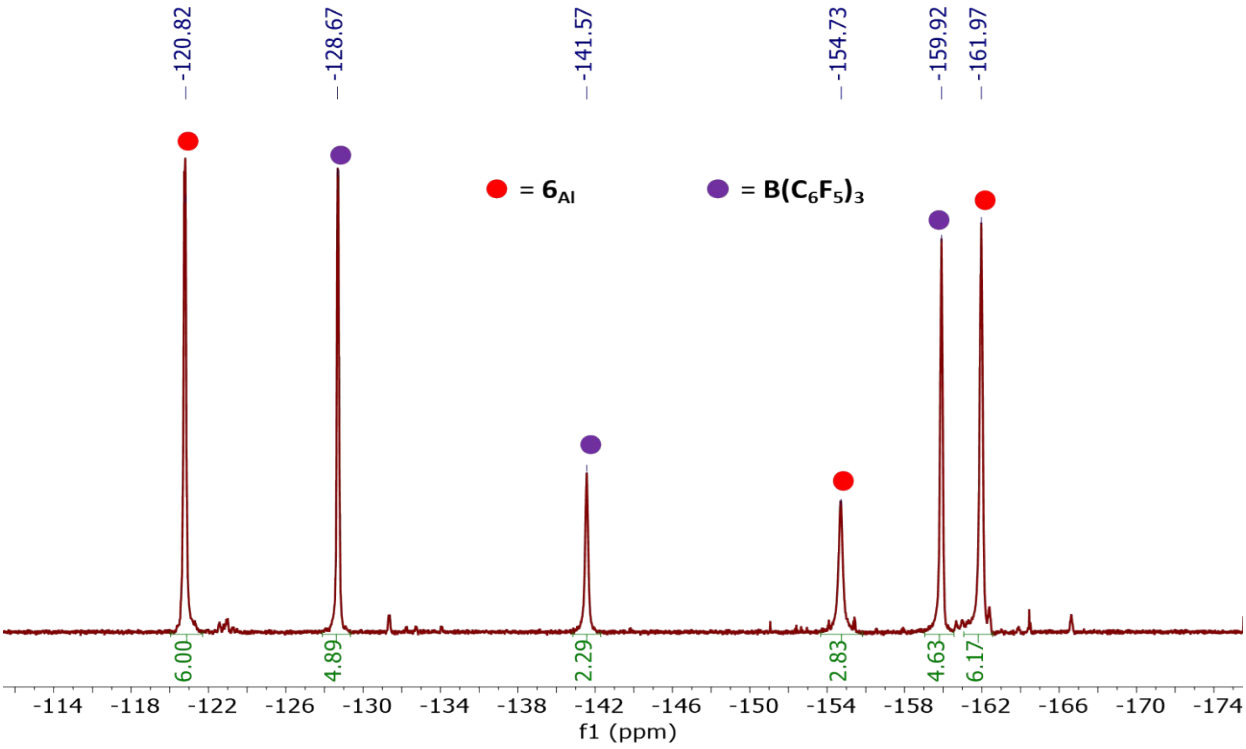

Figure S30. ^{19}F-NMR spectrum (376.2 MHz, C_6D_6, 298K) relating to the reaction of *trans*-[Mo(dppe)$_2$(μ-N$_2$)BCF] (4_B) + Al(C_6F_5)$_3$(tol) under argon atmosphere showing the predominant formation of 4_{Al} - *trans*-[Mo(dppe)$_2$(μ-N$_2$)AlCF] – along with free BCF and minor amounts of 6_{Al}.

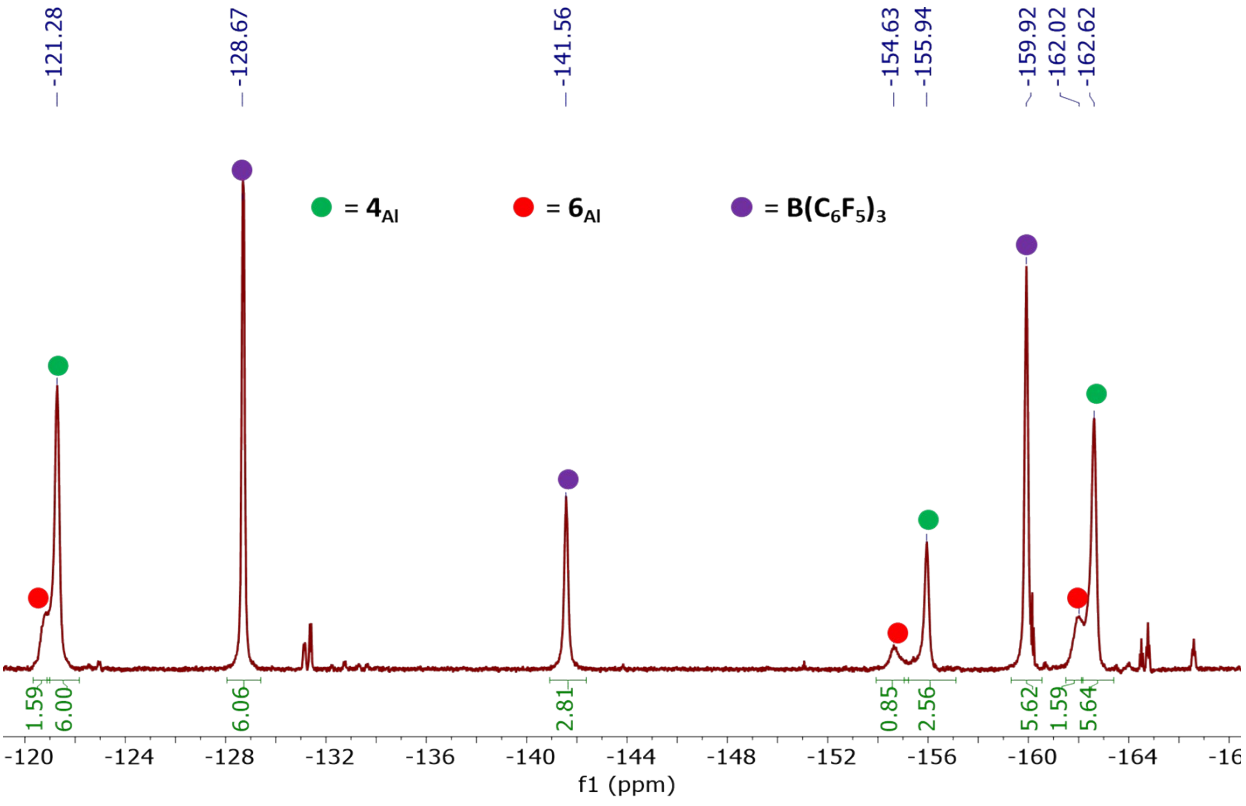

Figure S31. $^{31}P\{^{1}H\}$-NMR spectrum (163.2 MHz, C_6D_6, 298K) relating to the reaction of *trans*-[Mo(dppe)$_2$(μ-N$_2$)BCF] (4_B) + Al(C_6F_5)$_3$(tol) under argon atmosphere showing the predominant formation of 4_{Al} - *trans*-[Mo(dppe)$_2$(μ-N$_2$)AlCF] – along with minor amounts of 6_{Al} and 4_B.

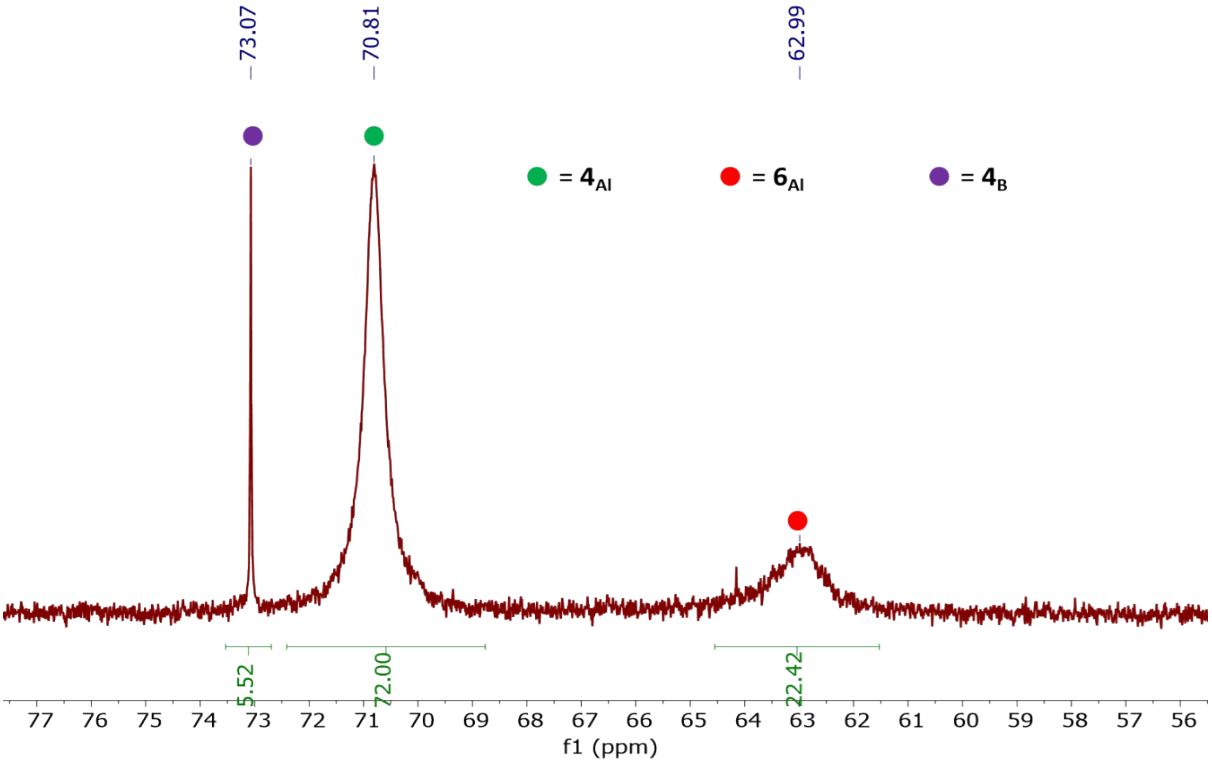

Figure S32. $^{31}P\{^{1}H\}$-NMR spectra (163.2 MHz, C_6D_6, 298K) relating to the monitoring of the reaction of *trans*-[W(dppe)$_2$(N$_2$)$_2$] + B(C_6F_5)$_3$ under dinitrogen atmosphere producing products 5_B/3_B = 69/31 after one night.

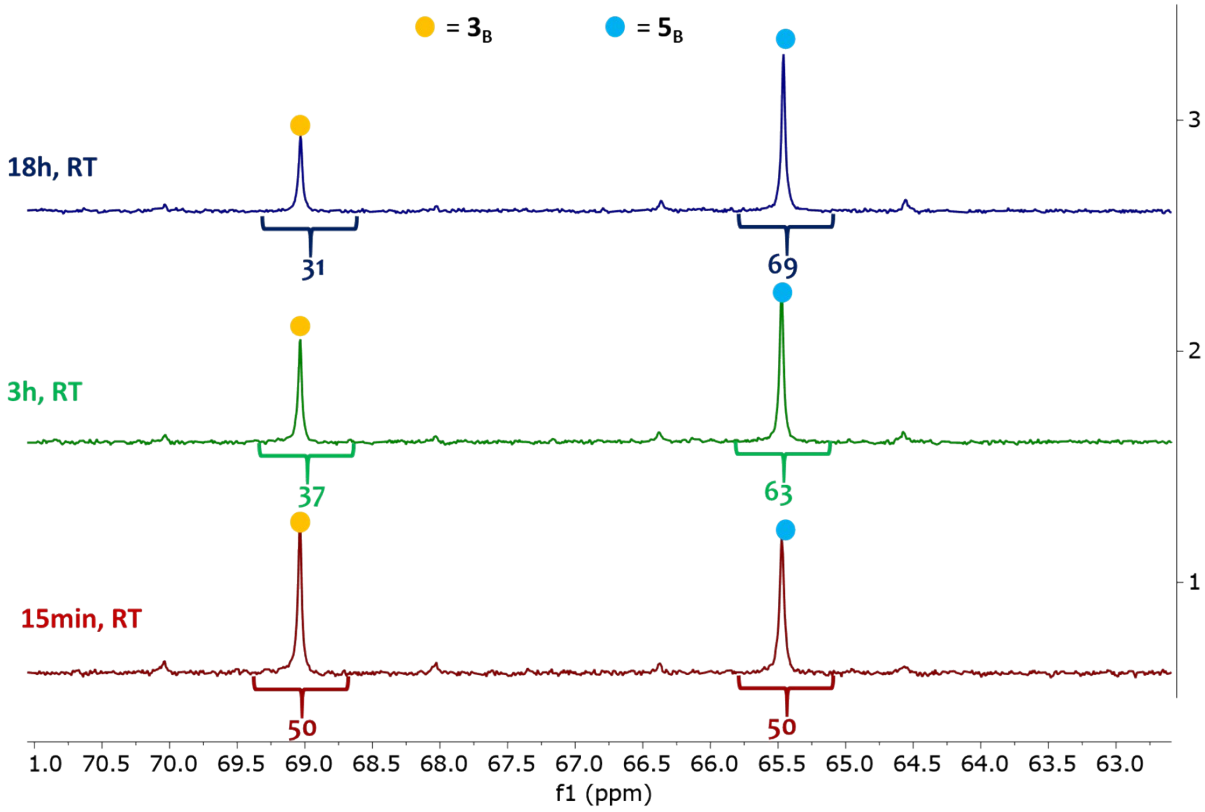

Figure S33. ^{1}H-NMR spectrum (400 MHz, C_6D_6, 298K) of compound 7_{Al}

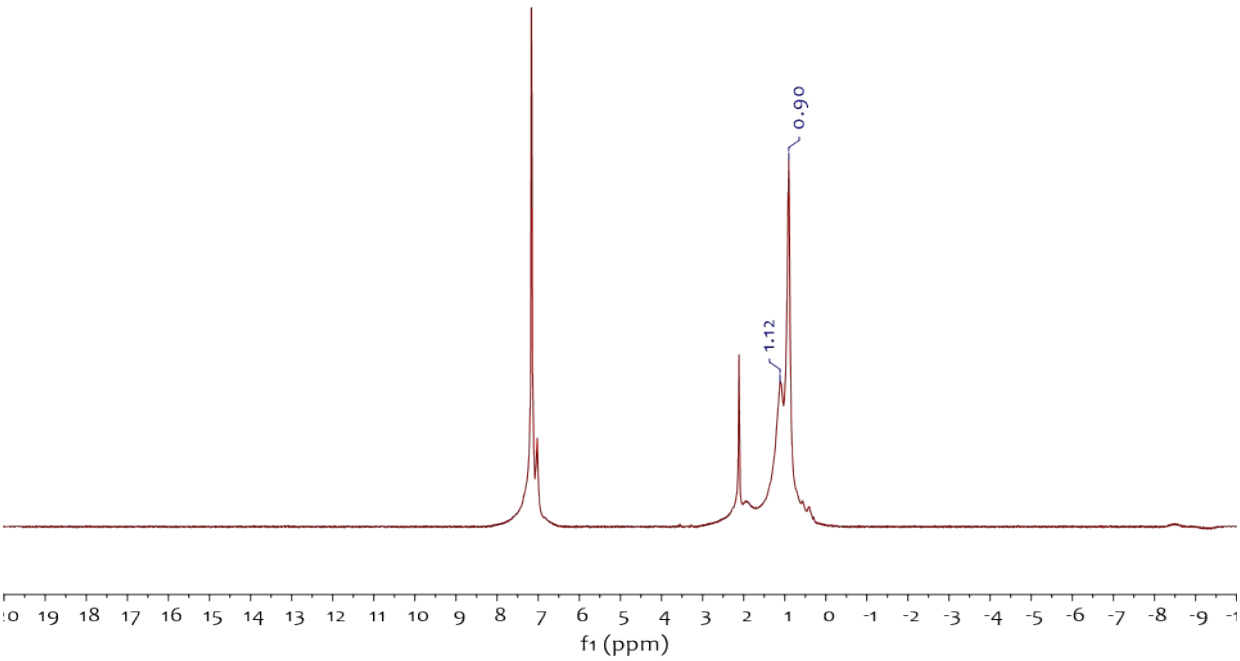

Figure S34. ^{19}F-NMR spectrum (376.2 MHz, C_6D_6, 298K) of compound 7_{Al}.

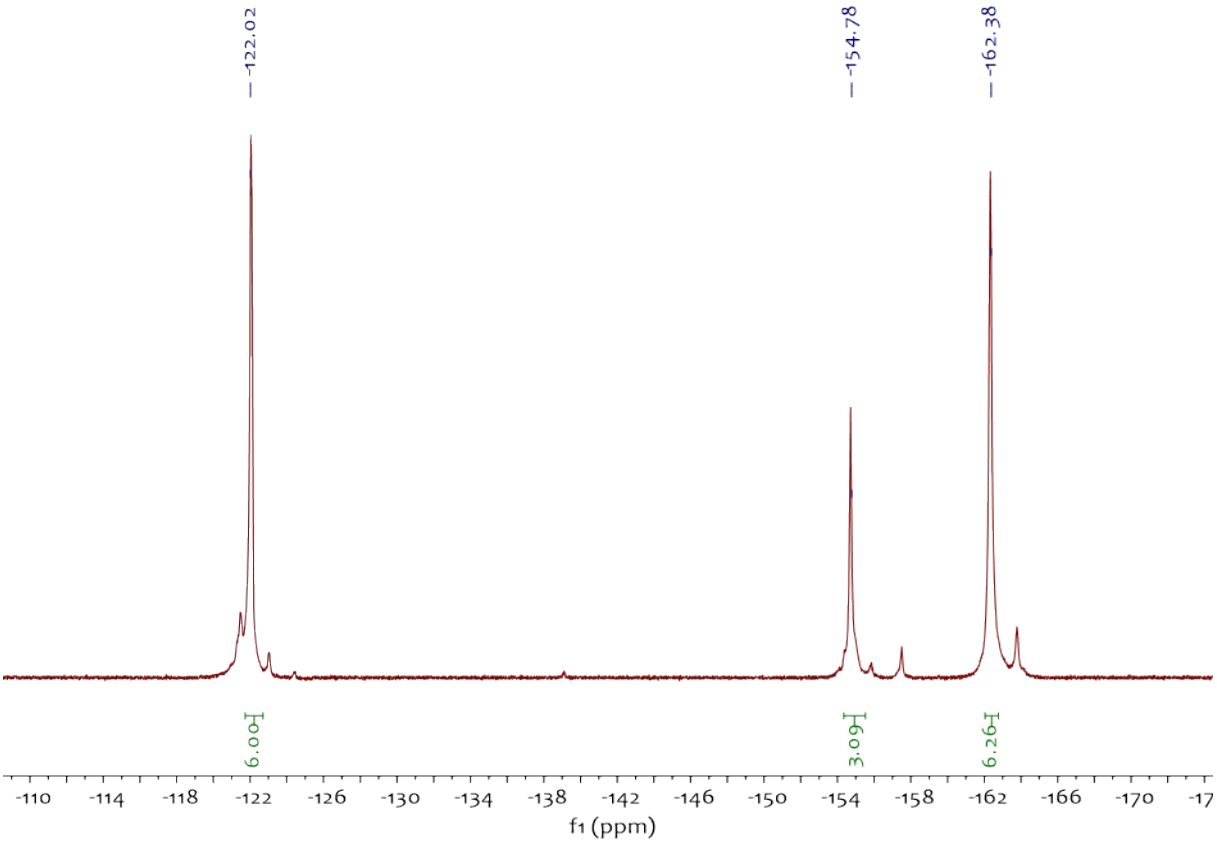

Figure S35. $^{31}P\{^{1}H\}$-NMR spectrum (163.2 MHz, C_6D_6, 298K) of compound 7_{Al}.

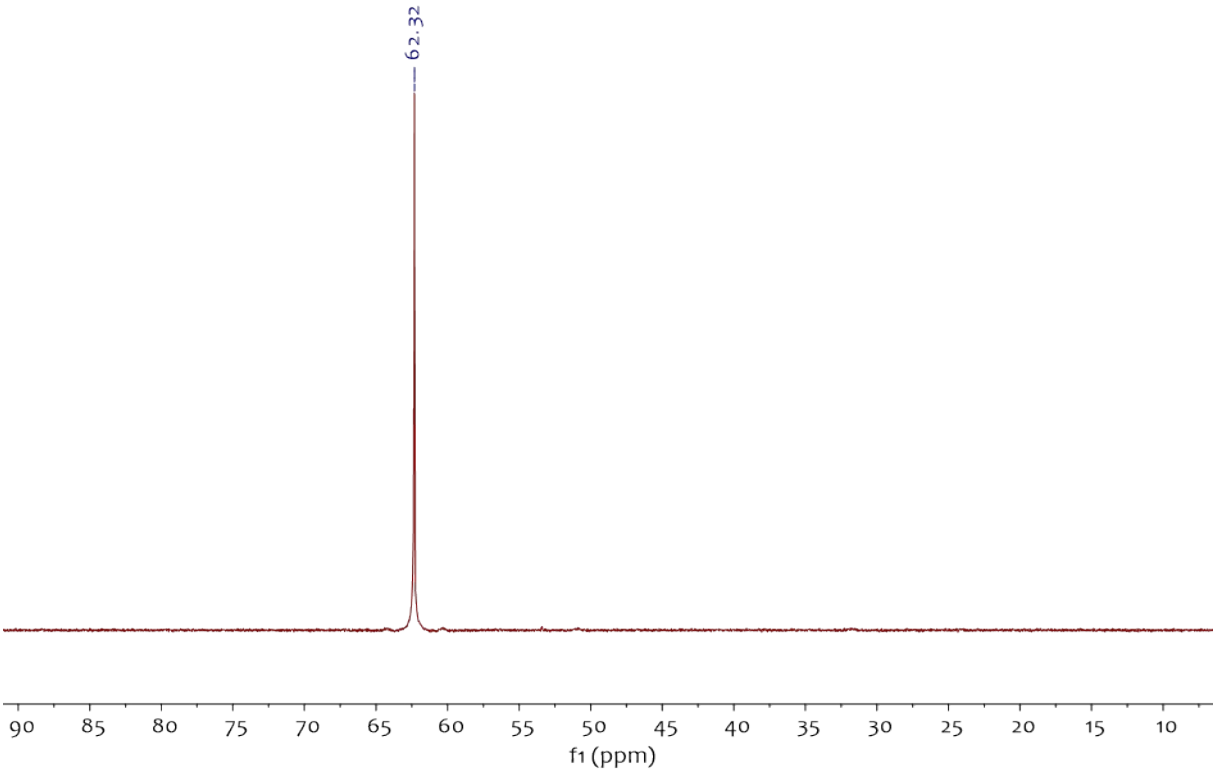

Figure S36. ^{1}H-NMR spectrum (400 MHz, C_6D_6, 298K) of the reaction of $B(C_6F_5)_3$ (1 eq.) + *trans*-$[Cr(dmpe)_2(N_2)_2]$.

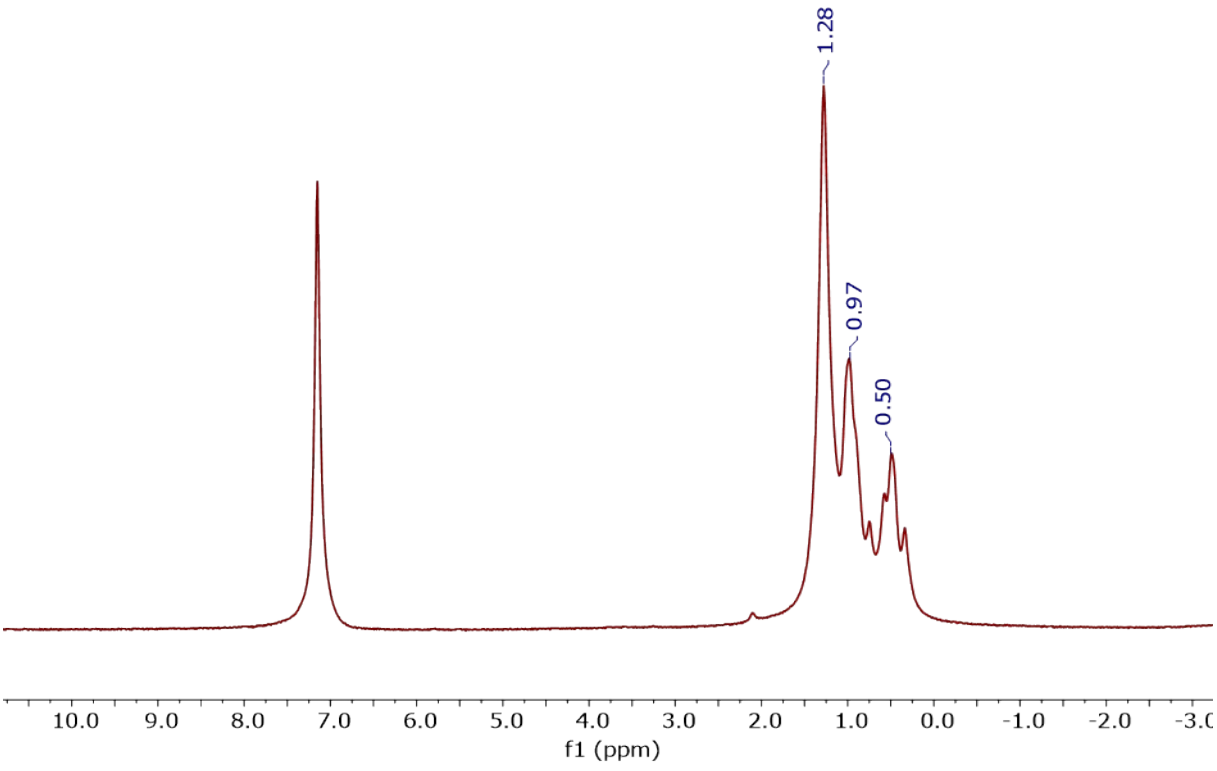

Figure S37. ^{19}F-NMR spectrum (376.2 MHz, C_6D_6, 298K) of the reaction of $B(C_6F_5)_3$ (1 eq.) + *trans*-$[Cr(dmpe)_2(N_2)_2]$.

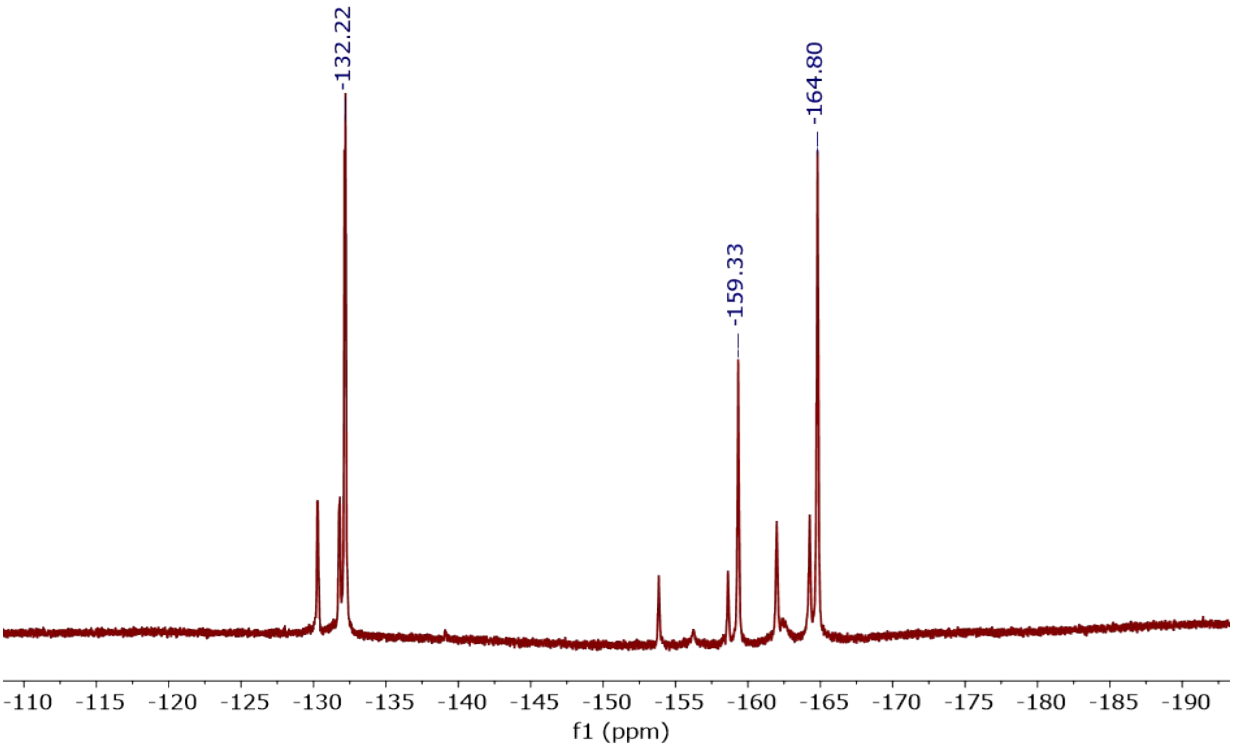

Figure S38. $^{31}P\{^1H\}$-NMR spectrum (163.2 MHz, C_6D_6, 298K) of the reaction of $B(C_6F_5)_3$ (1 eq.) + *trans*-$[Cr(dmpe)_2(N_2)_2]$.

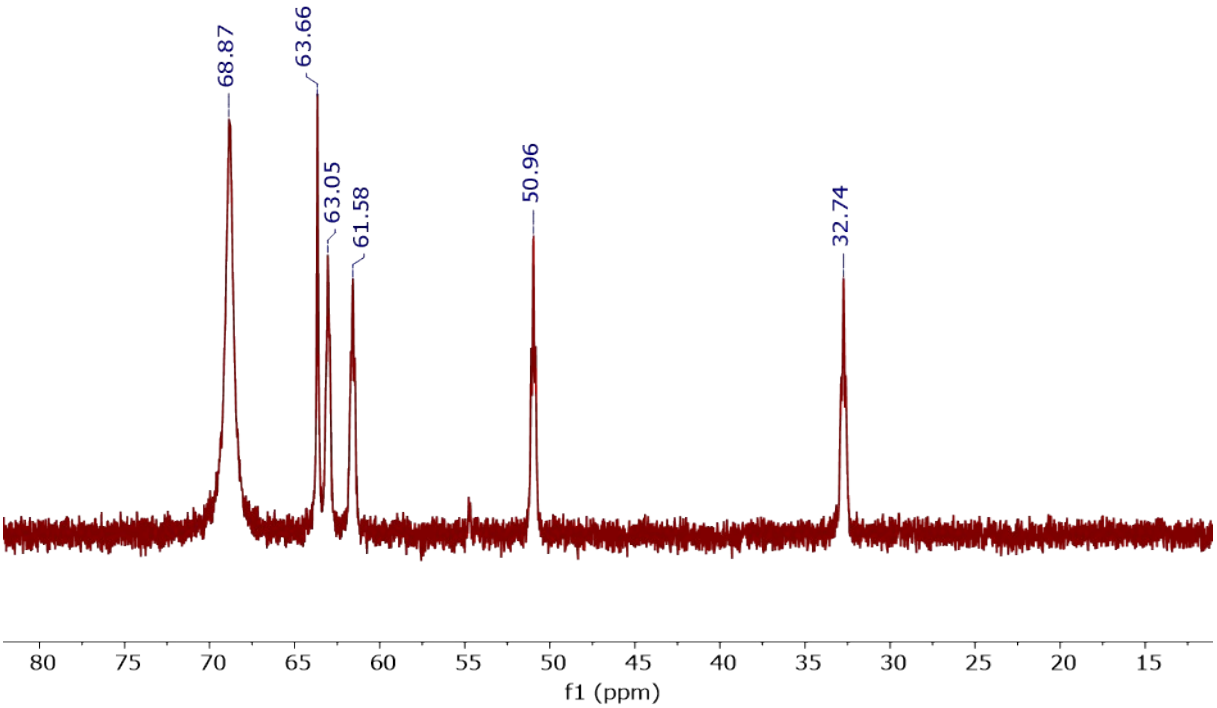

Figure S39. ^{11}B-NMR spectrum (128.3 MHz, C_6D_6, 298K) of the reaction of $B(C_6F_5)_3$ (1 eq.) + *trans*-$[Cr(dmpe)_2(N_2)_2]$.

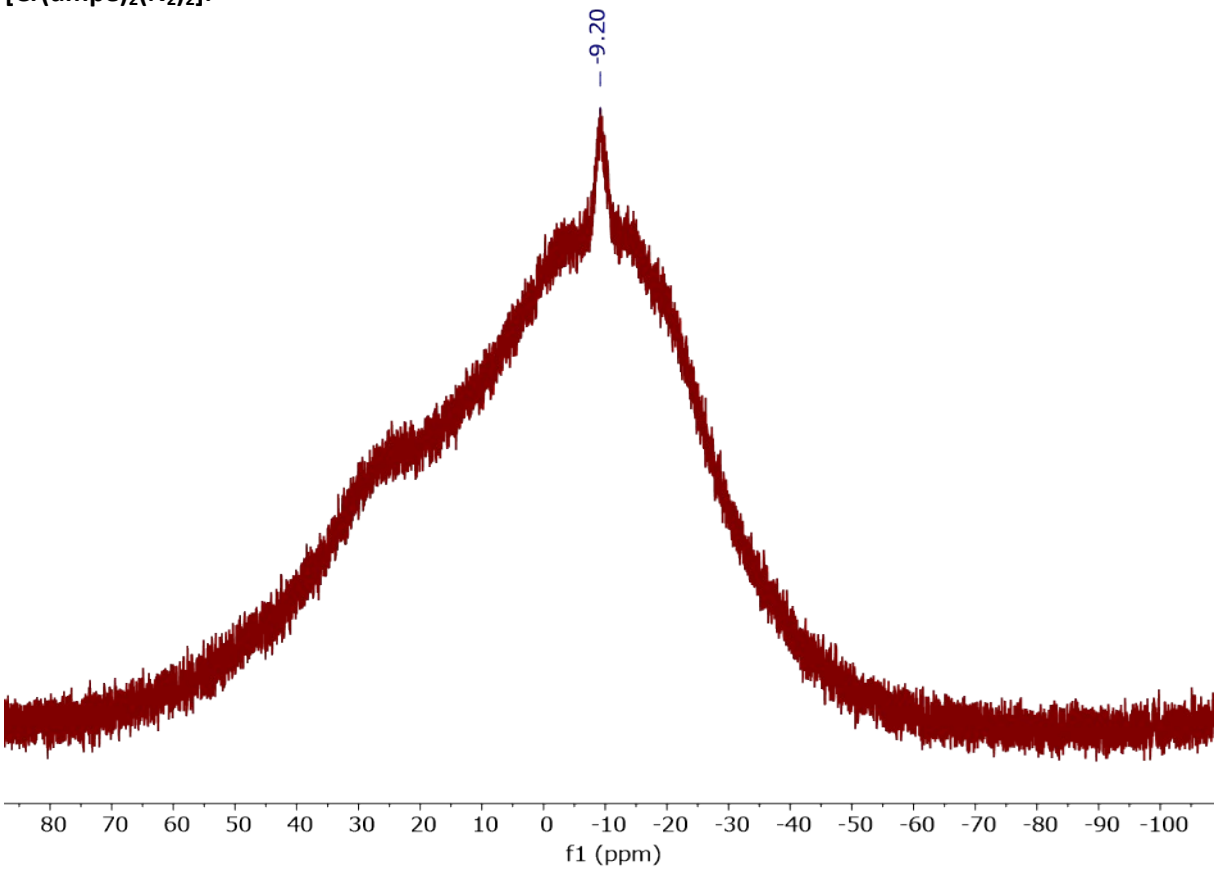

Figure S40. a) ^{1}H-NMR spectra in toluene-d_8 (400 MHz). b) ^{19}F-NMR spectra in toluene-d_8 (377 MHz). c) Zoom of ^{19}F NMR spectrum at -60 °C in toluene-d_8. d) ^{31}P{^{1}H}-NMR spectrum (163.2 MHz, toluene-d_8, 298K). Captions are the followings: Green colour=adduct 1_B - [W(depe)$_2$(N$_2$)(μ-N$_2$){B(C$_6$F$_5$)$_3$}]. Purple colour= Reaction of [W(N$_2$)$_2$(depe)$_2$] with 2 equivalents of B(C$_6$F$_5$)$_3$ at 298K, we assigned the three ^{1}H-NMR depe signals to i) either the formation of a putative double adduct or ii) to the coalescence of the six resonances of adduct 1_B due to a concentration effect (phenomenon also observed for adduct 1_{Al}, see spectra page 11). Turquoise colour= Reaction of [W(N$_2$)$_2$(depe)$_2$] with 2 equivalents of B(C$_6$F$_5$)$_3$ at -60°C. This set of experiments shows the concomitant formation of free BCF with adduct 1_B in equilibrium with a putative double adduct.

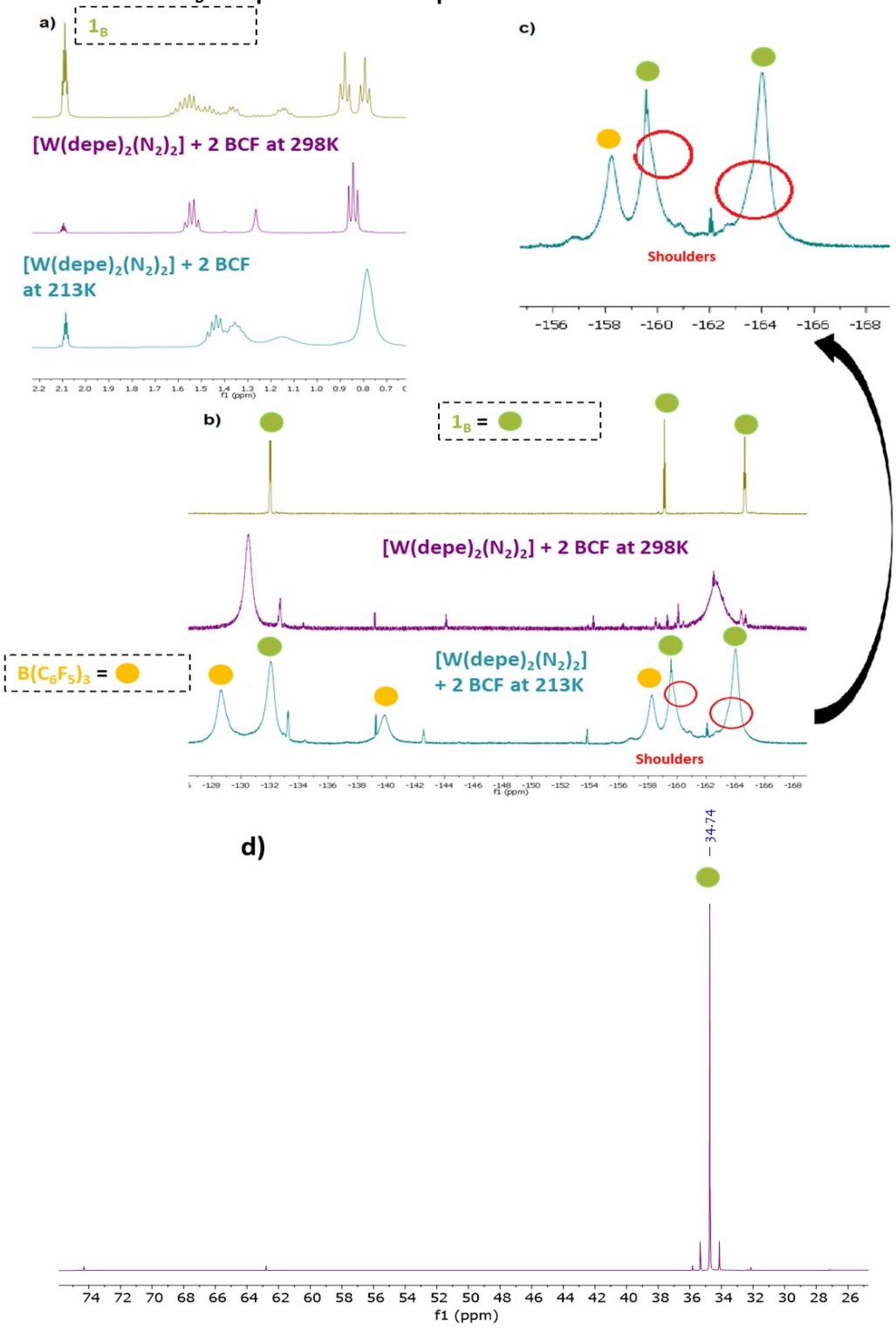

Figure S41. ^{1}H-NMR spectrum (400 MHz, C_6D_6, 298K) of compound 8_{Al} (coming from reaction monitoring between $[W(depe)_2(N_2)_2]$ + 2 eq. of $Al(C_6F_5)_3(tol)$ after 1 hour).

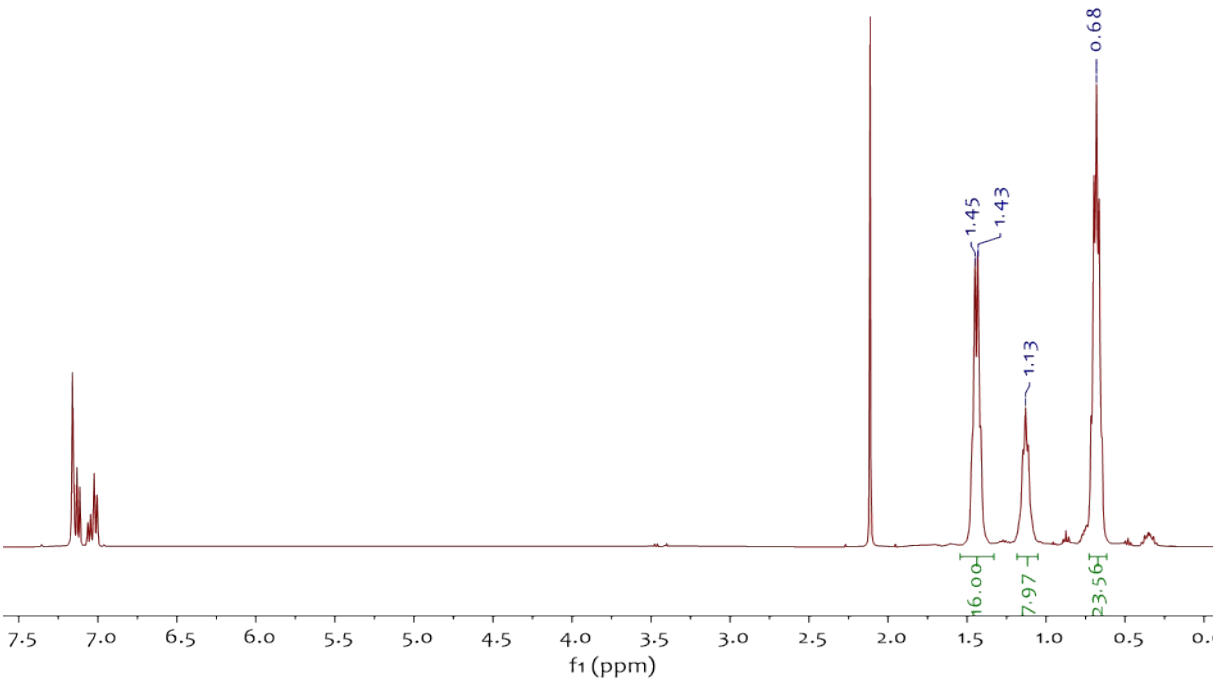

Figure S42. ^{19}F-NMR spectrum (376.2 MHz, C_6D_6, 298K) of compound 8_{Al} (coming from reaction monitoring between $[W(depe)_2(N_2)_2]$ + 2 eq. of $Al(C_6F_5)_3(tol)$ after 1 hour).

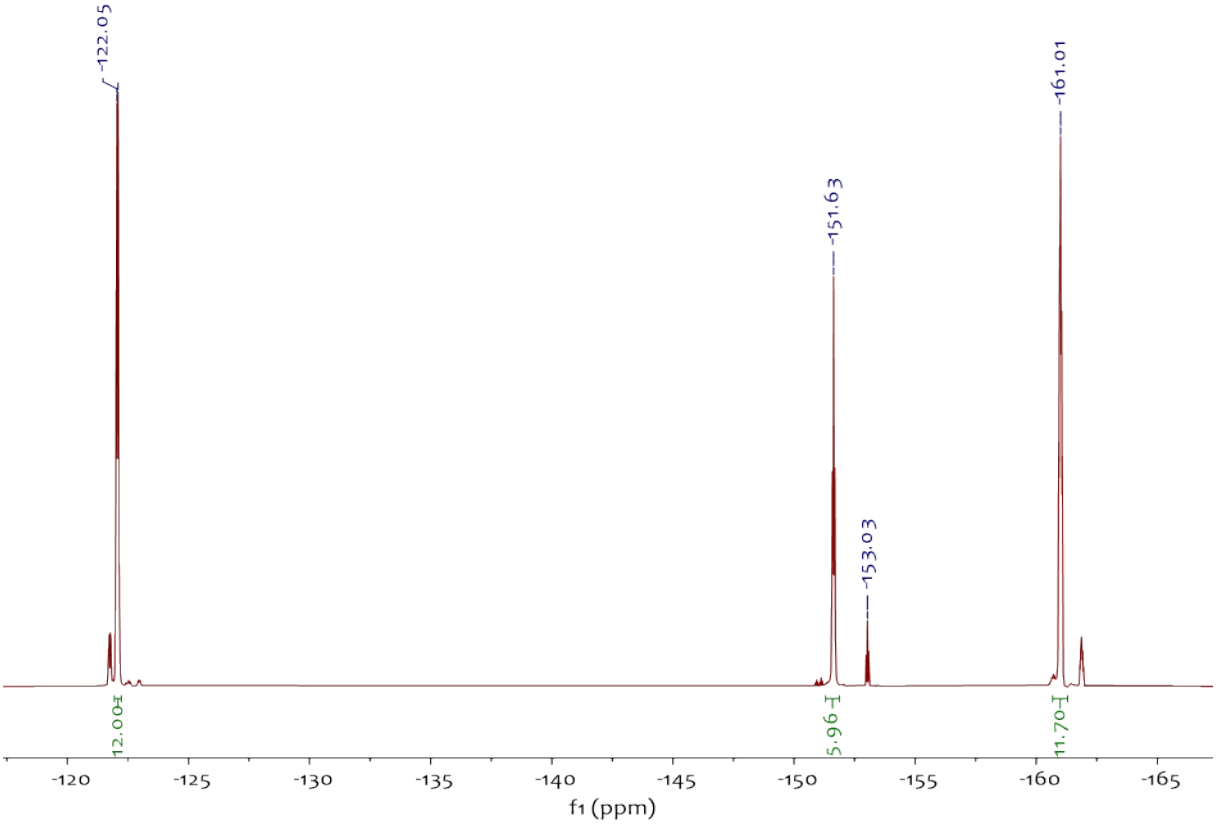

Figure S43. $^{31}P\{^{1}H\}$-NMR spectrum (163.2 MHz, C_6D_6, 298K) of compound 8_{Al} (coming from reaction monitoring between $[W(depe)_2(N_2)_2]$ + 2 eq. of $Al(C_6F_5)_3(tol)$ after 1 hour)

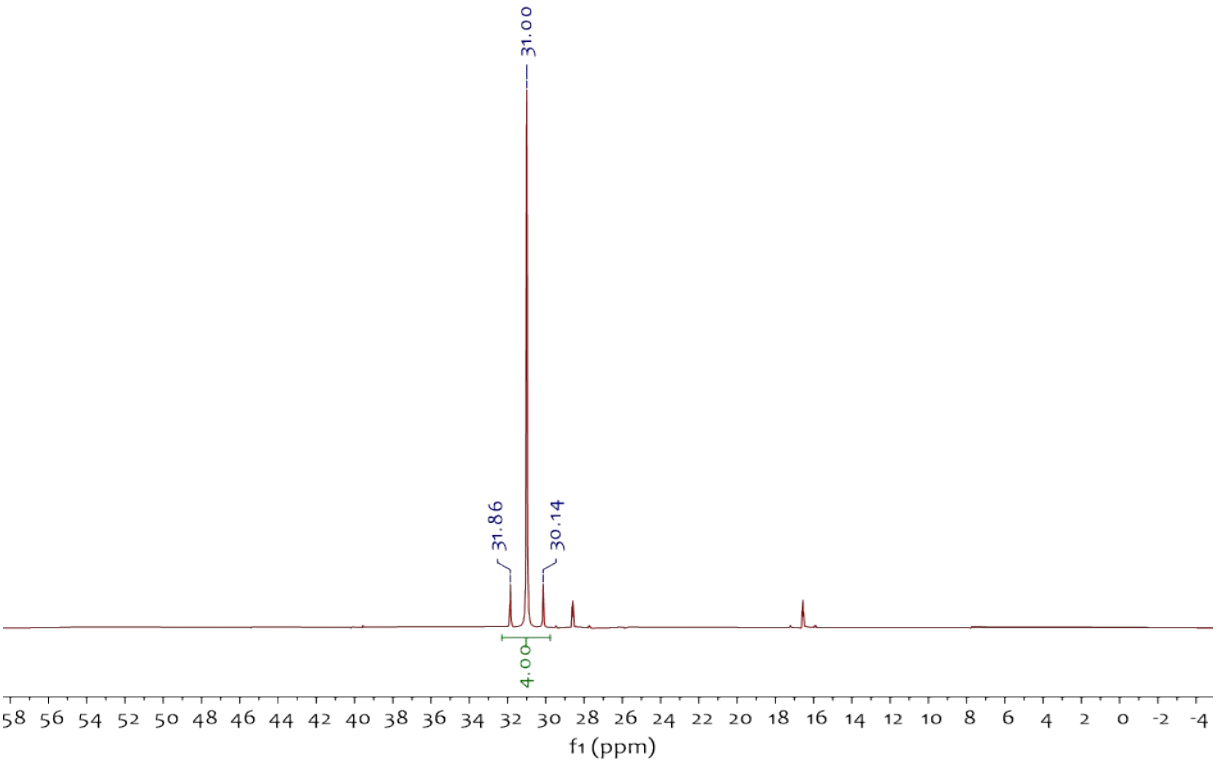

Figure S44. ^{1}H-NMR spectrum (400 MHz, C_6D_6, 298K) of compound 11_{Al} (coming from reaction monitoring between $[W(depe)_2(N_2)_2]$ + 2 eq. of $Al(C_6F_5)_3(tol)$ after 24 hours). Note that most of 11_{Al} came out of the C_6D_6 solution as brown crystalline materials (explaining then its low concentration in solution).

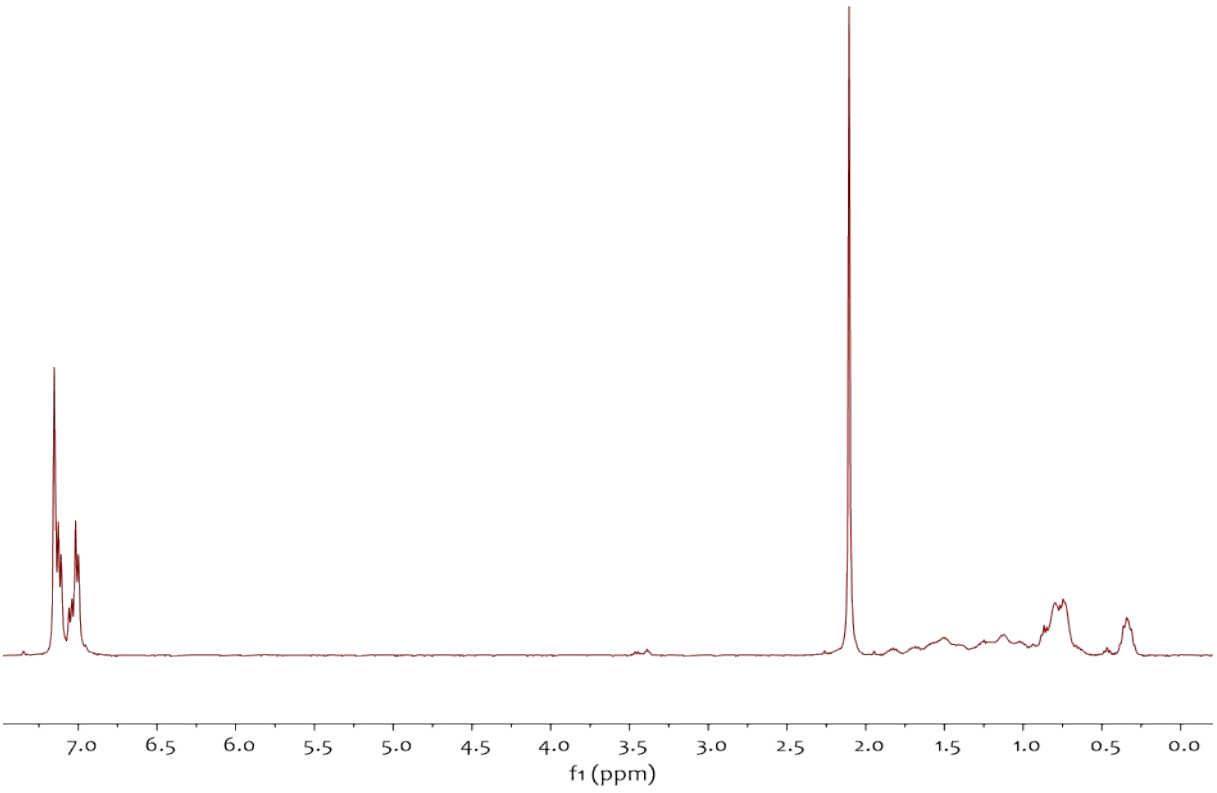

Figure S45. ^{19}F-NMR spectrum (376.2 MHz, C_6D_6, 298K) of compound 11_{Al} (coming from reaction monitoring between $[W(depe)_2(N_2)_2]$ + 2 eq. of $Al(C_6F_5)_3$(tol) after 24 hours). Note that most of 11_{Al} came out of the C_6D_6 solution as brown crystalline materials (explaining then its low concentration in solution).

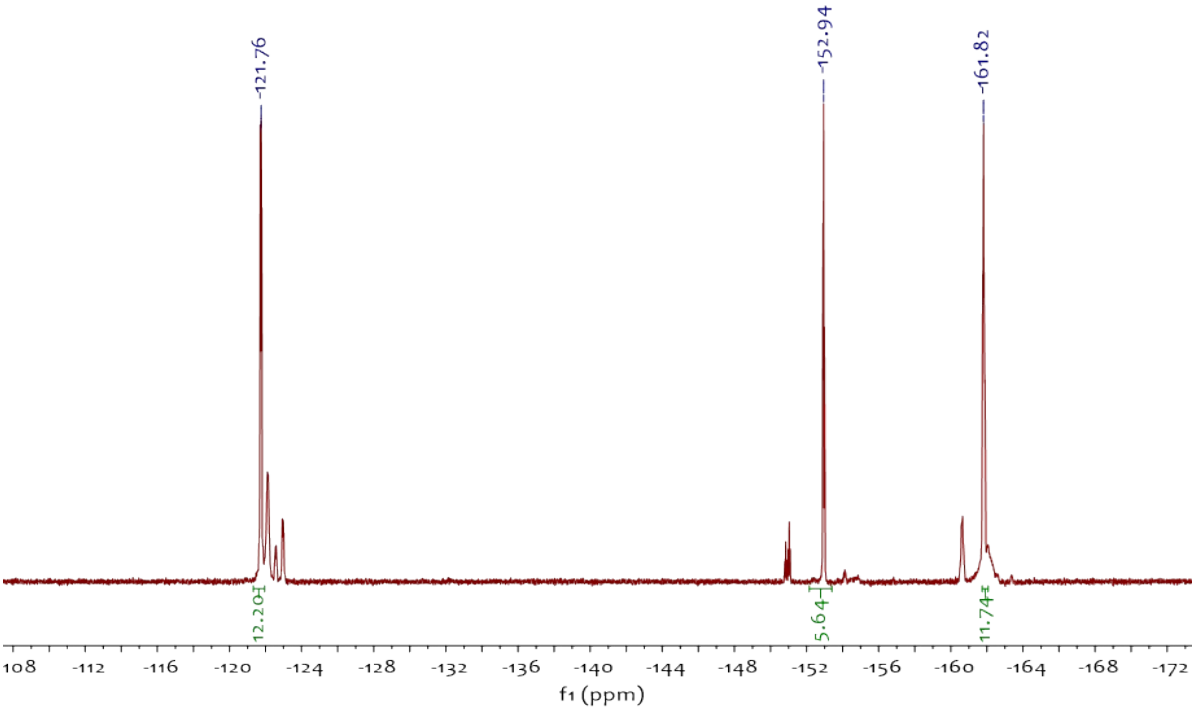

Figure S46. $^{31}P\{^1H\}$-NMR spectrum (163.2 MHz, C_6D_6, 298K) of compound 11_{Al} (coming from reaction monitoring between $[W(depe)_2(N_2)_2]$ + 2 eq. of $Al(C_6F_5)_3$(tol) after 24 hours). Note that most of 11_{Al} came out of the C_6D_6 solution as brown crystalline materials (explaining then its low concentration in solution).

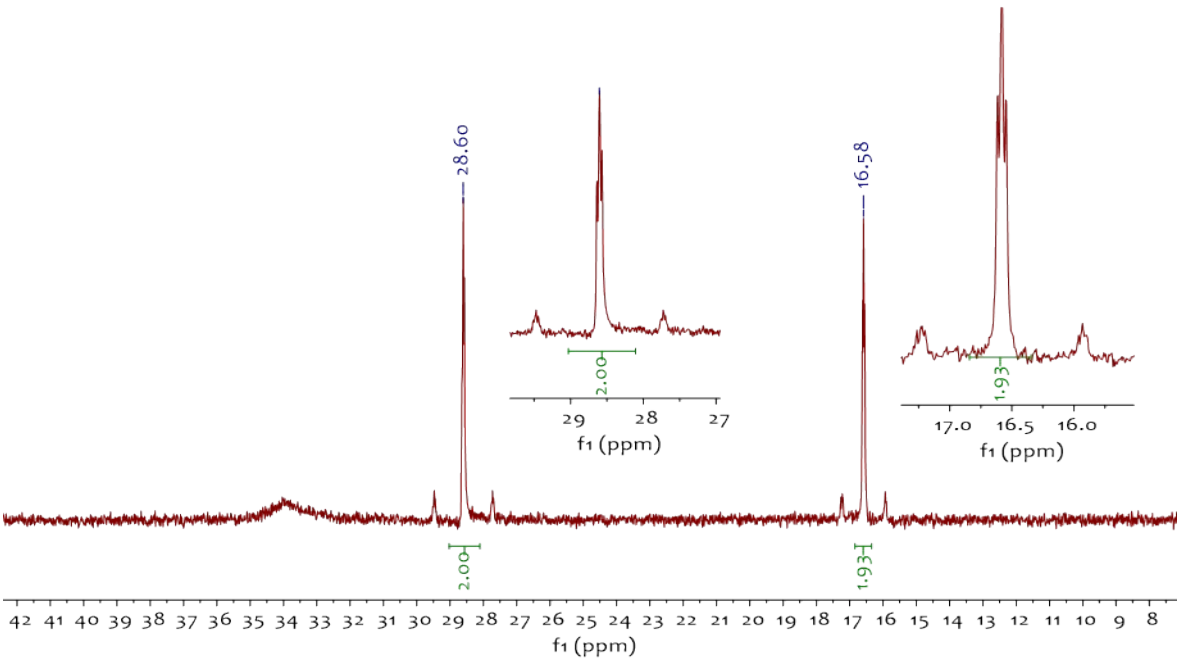

Figure S47. ^{1}H-NMR (400 MHz, C_6D_6, 298K) monitoring of the reaction between $[W(depe)_2(N_2)_2]$ + 2 eq. of $Al(C_6F_5)_3(tol)$. Note that most of 11_{Al} came out of the C_6D_6 solution as brown crystalline materials from a time of 6 hours.

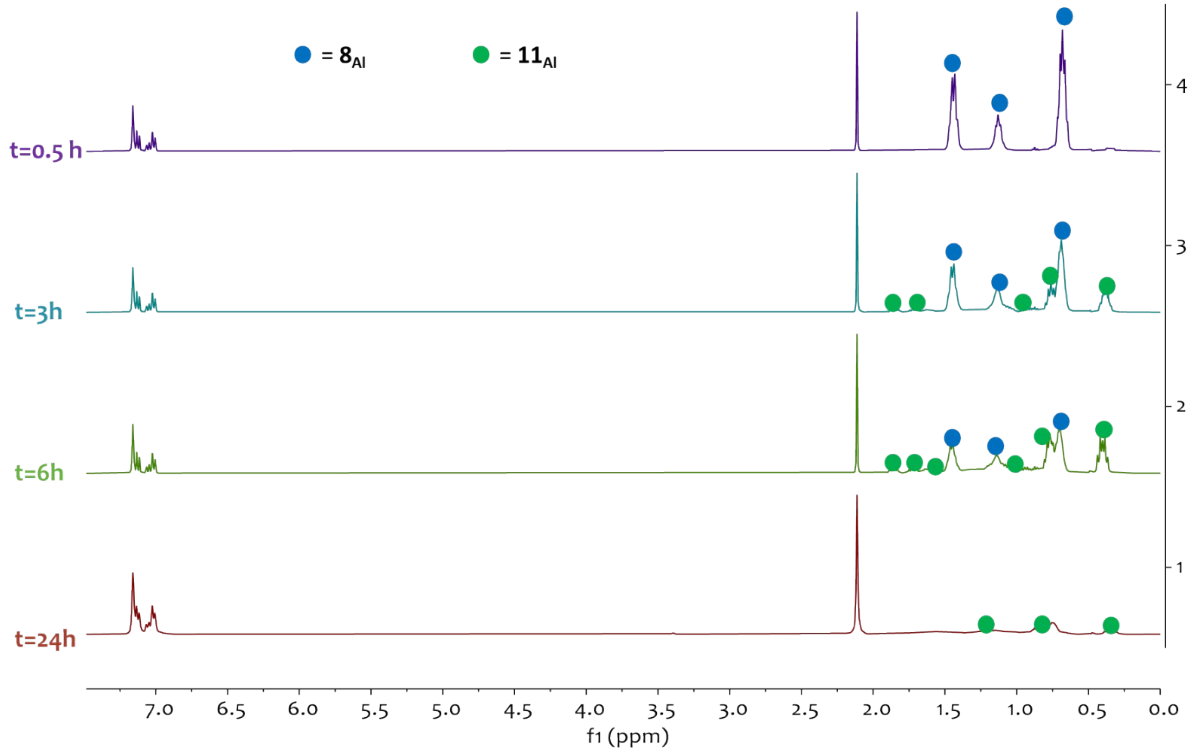

Figure S48. ^{19}F-NMR spectrum (376.2 MHz, C_6D_6, 298K) monitoring of the reaction between $[W(depe)_2(N_2)_2]$ + 2 eq. of $Al(C_6F_5)_3(tol)$. Note that most of 11_{Al} came out of the C_6D_6 solution as brown crystalline materials from a time of 6 hours.

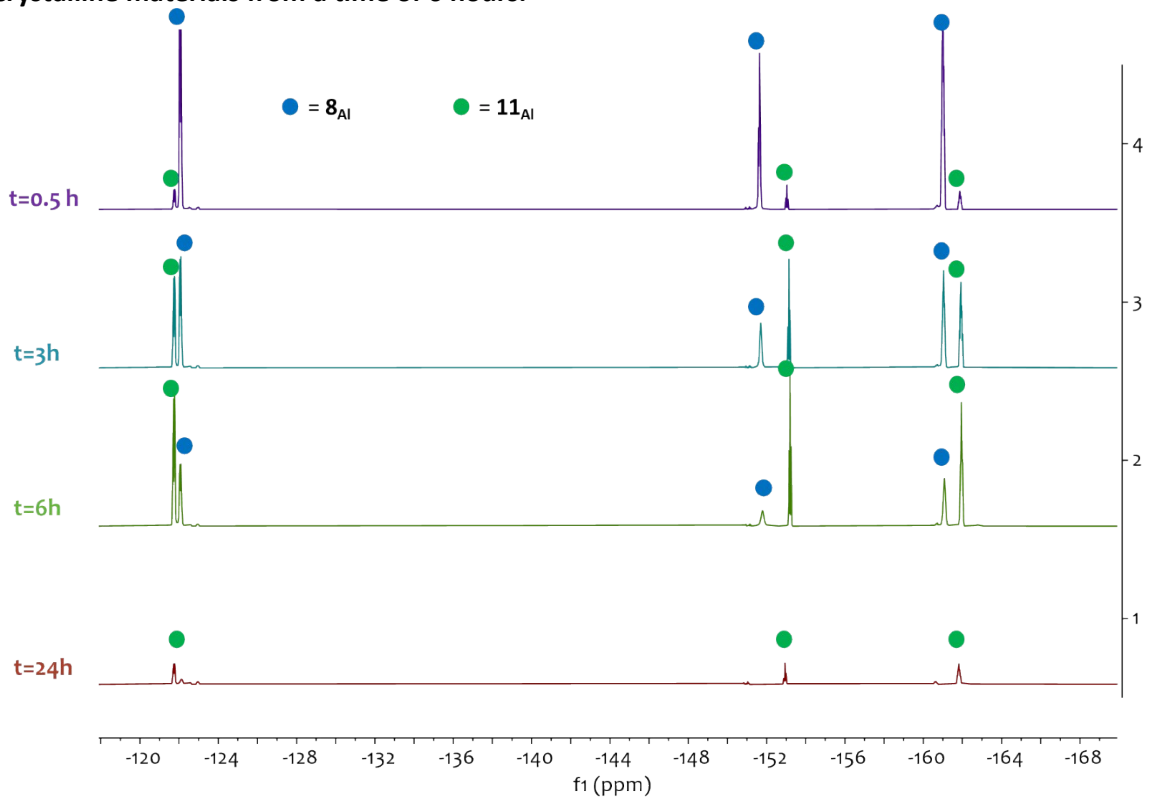

Figure S49. $^{31}P\{^{1}H\}$-NMR spectrum (163.2 MHz, C_6D_6, 298K) monitoring of the reaction between $[W(depe)_2(N_2)_2]$ + 2 eq. of $Al(C_6F_5)_3(tol)$. Note that most of 11_{Al} came out of the C_6D_6 solution as brown crystalline materials from a time of 6 hours.

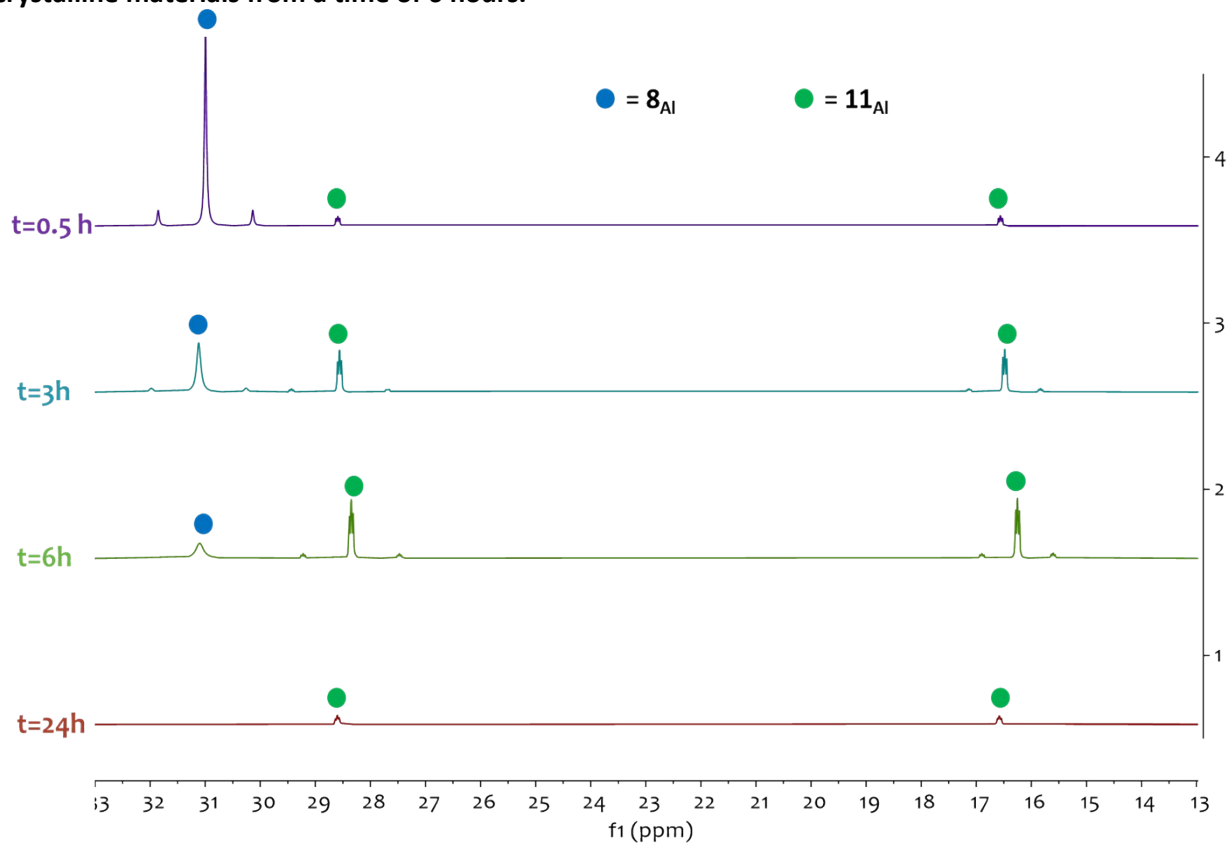

Figure S50. $^{15}N\{^{1}H\}$-INVGATED NMR (40.5 MHz, C_6D_6, 298K) spectrum of ^{15}N-11_{Al}.

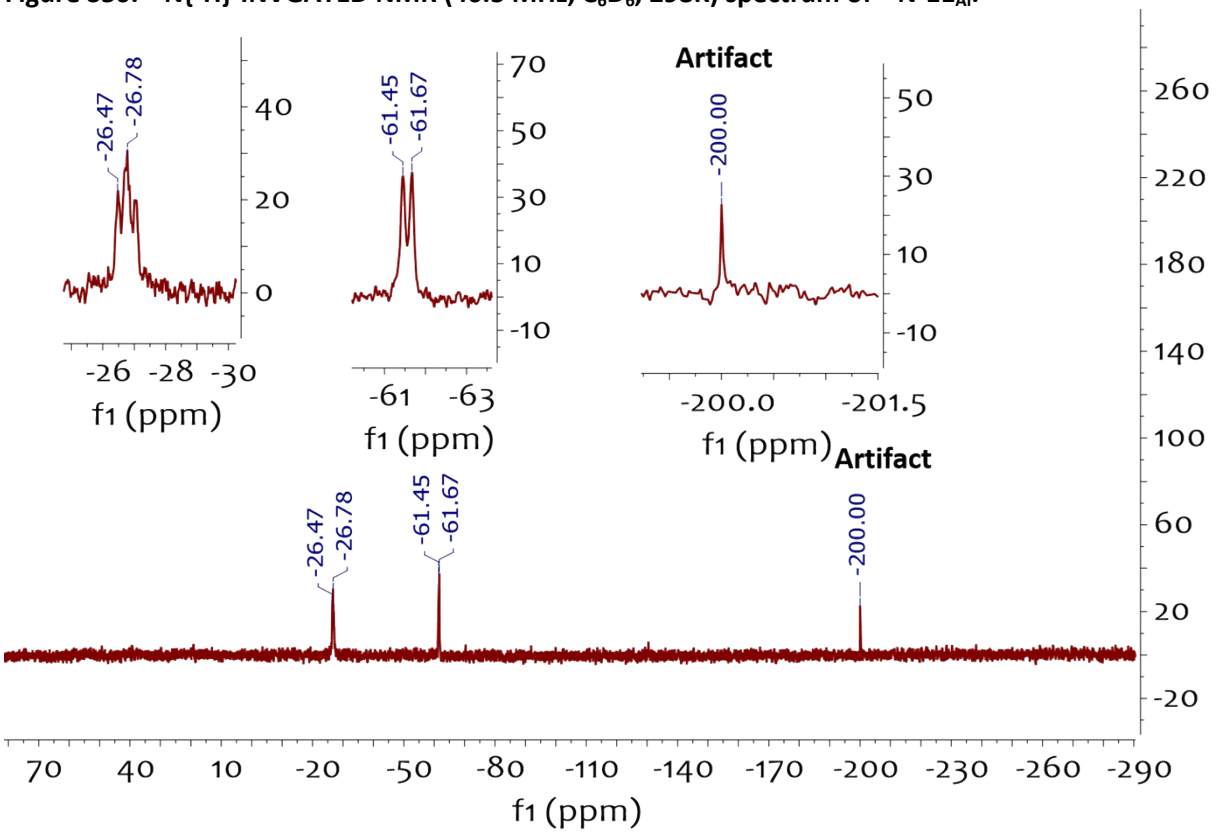

Figure S51. ^{1}H-NMR (400 MHz, tol-d_8, 298K) monitoring of the reaction between [Mo(depe)$_2$(N$_2$)$_2$] + 2 eq. of Al(C$_6$F$_5$)$_3$(tol).

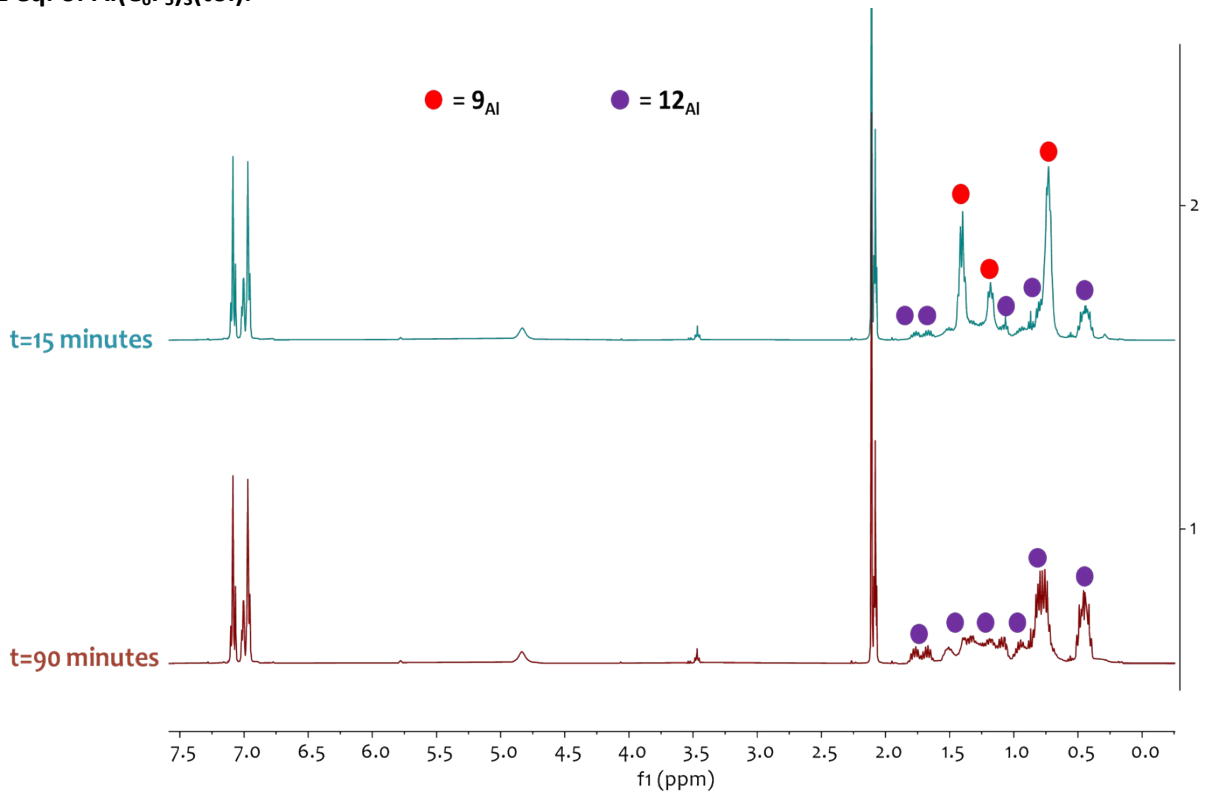

Figure S52. ^{19}F-NMR spectrum (376.2 MHz, tol-d_8, 298K) monitoring of the reaction between [Mo(depe)$_2$(N$_2$)$_2$] + 2 eq. of Al(C$_6$F$_5$)$_3$(tol).

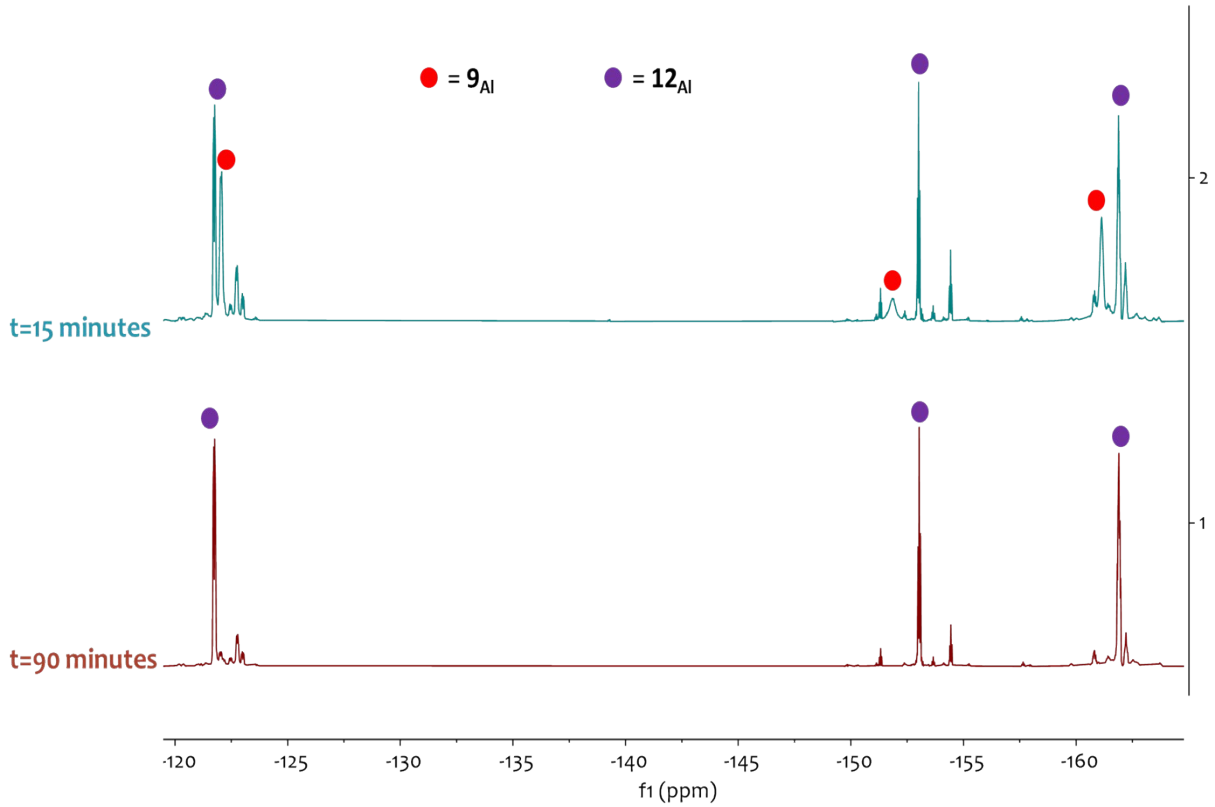

Figure S53. ^{31}P{^{1}H}-NMR spectrum (163.2 MHz, tol-d_8, 298K) monitoring of the reaction between [Mo(depe)$_2$(N$_2$)$_2$] + 2 eq. of Al(C$_6$F$_5$)$_3$(tol).

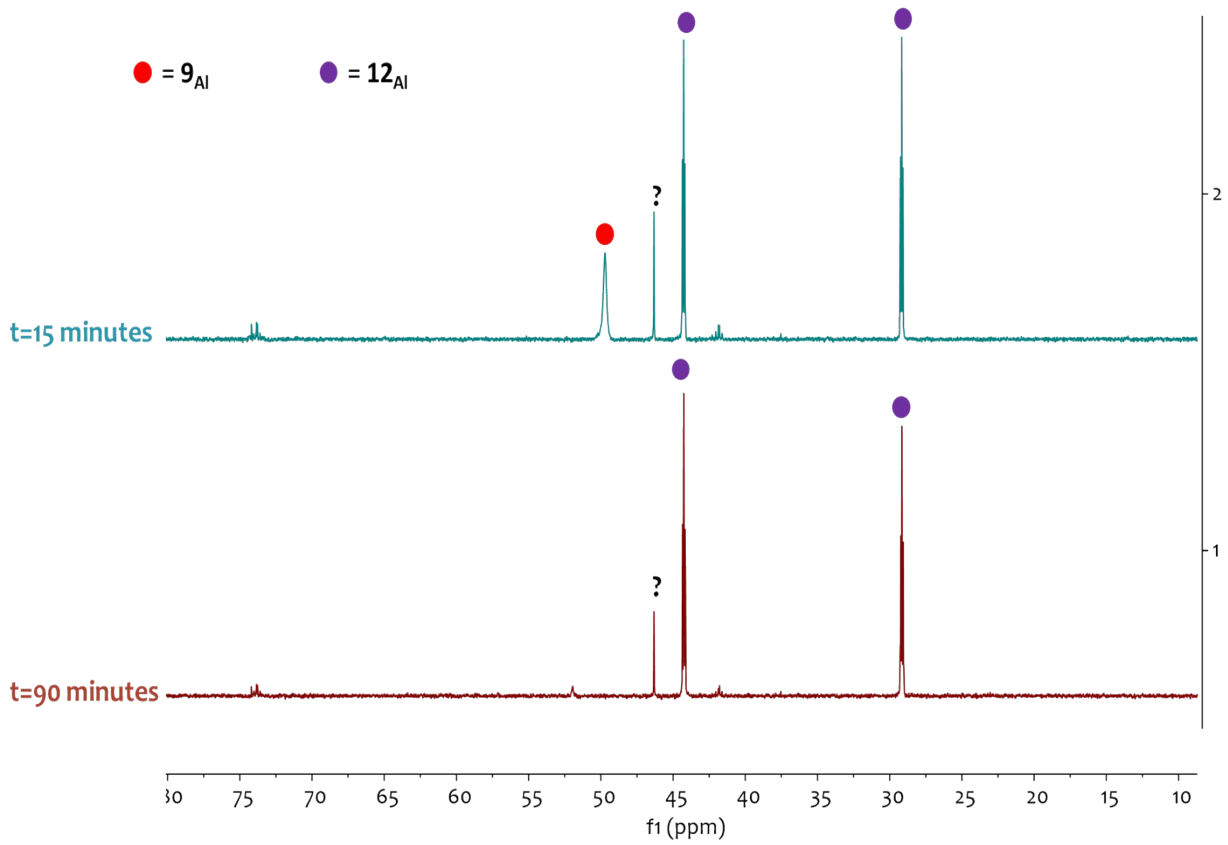

Figure S54. ^{1}H-NMR spectrum (400 MHz, C_6D_6, 298K) of compound 12_{Al}

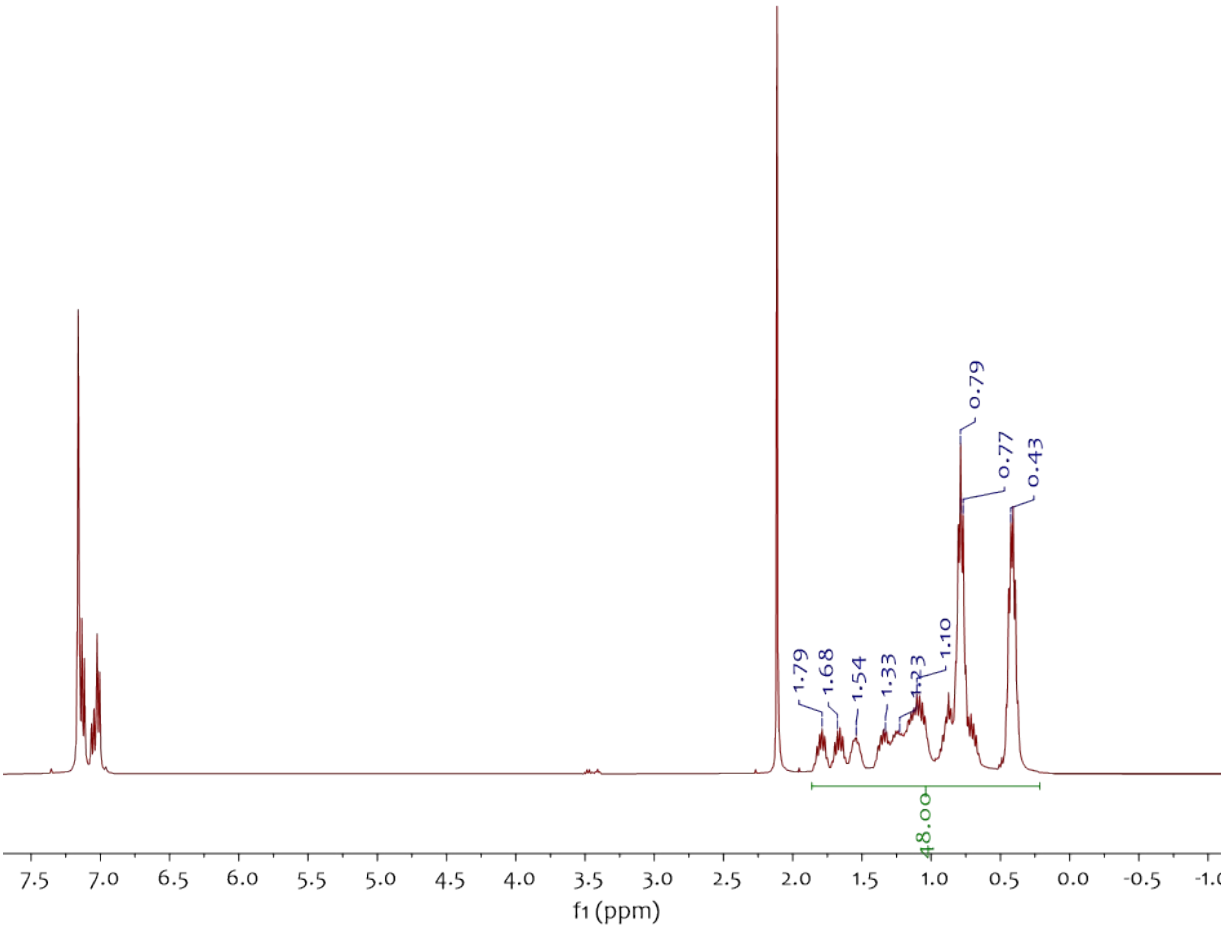

Figure S55. ^{19}F-NMR spectrum (376.2 MHz, C_6D_6, 298K) of compound 12_{Al}.

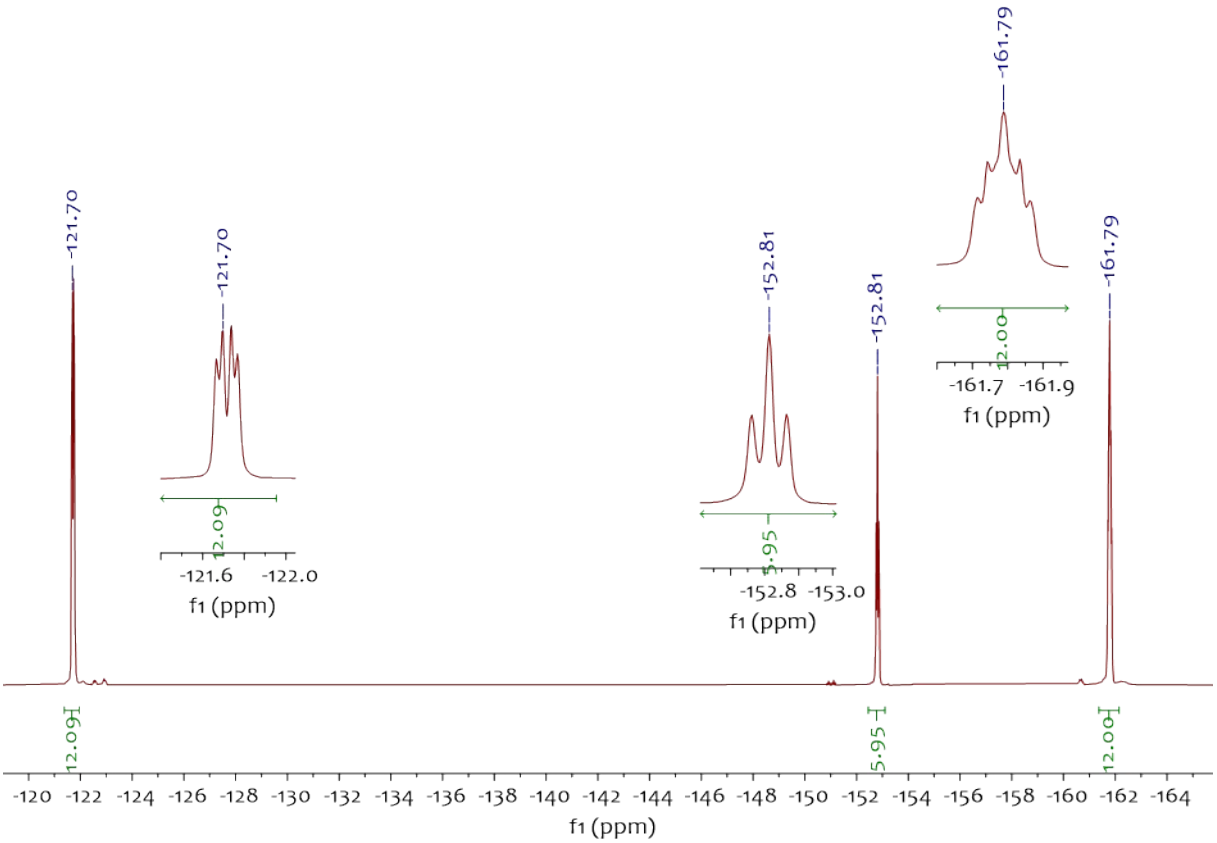

Figure S56. ^{31}P{^{1}H}-NMR spectrum (163.2 MHz, C_6D_6, 298K) of compound 12_{Al}.

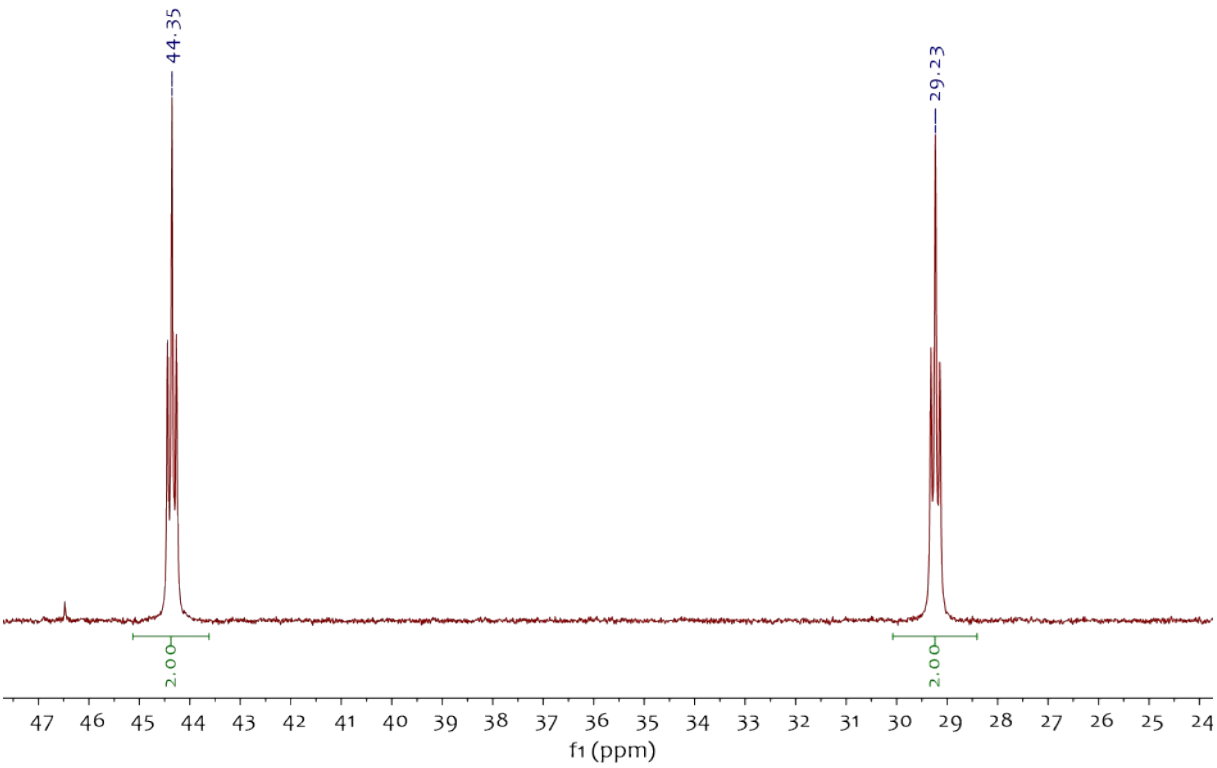

Figure S57. ^{1}H-NMR spectrum (400 MHz, C_6D_6, 298K) of compound 15_{Al}

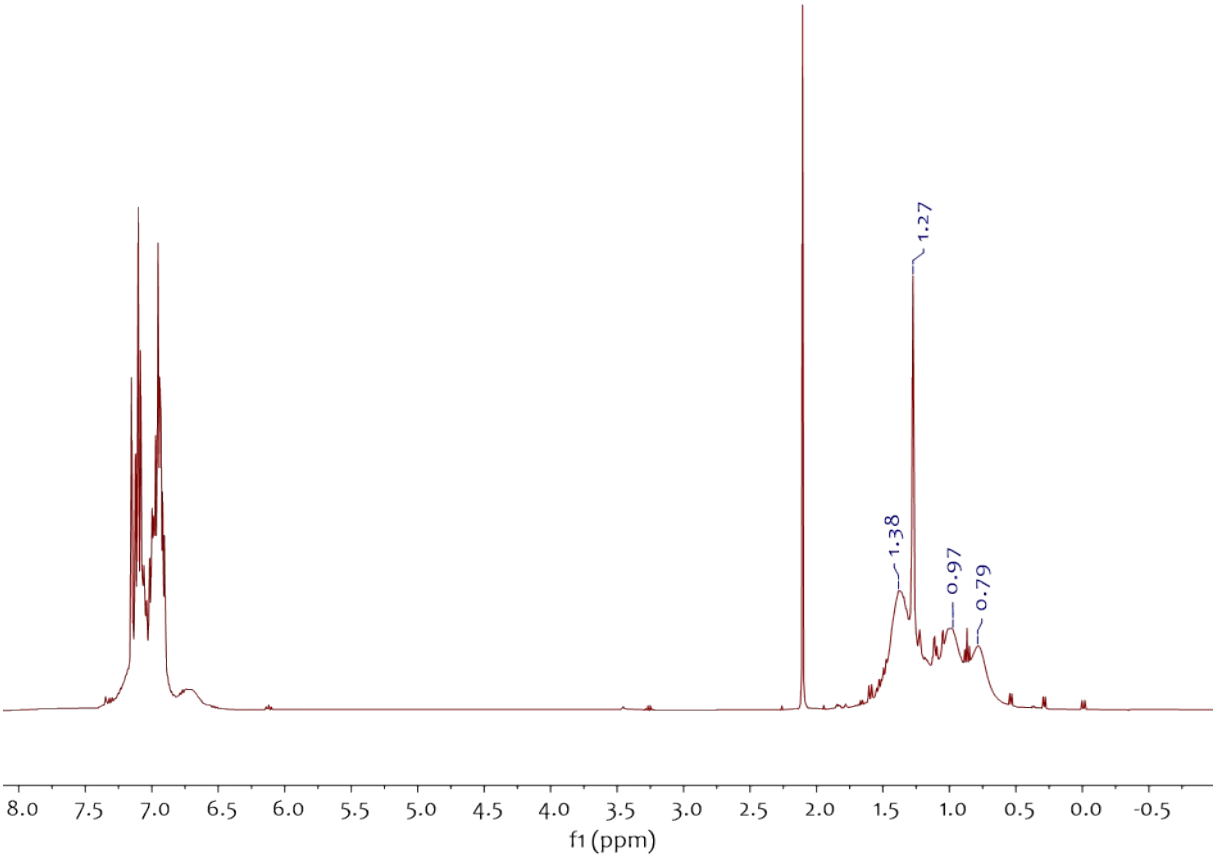

Figure S58. ^{19}F-NMR spectrum (376.2 MHz, C_6D_6, 298K) of compound 15_{Al}

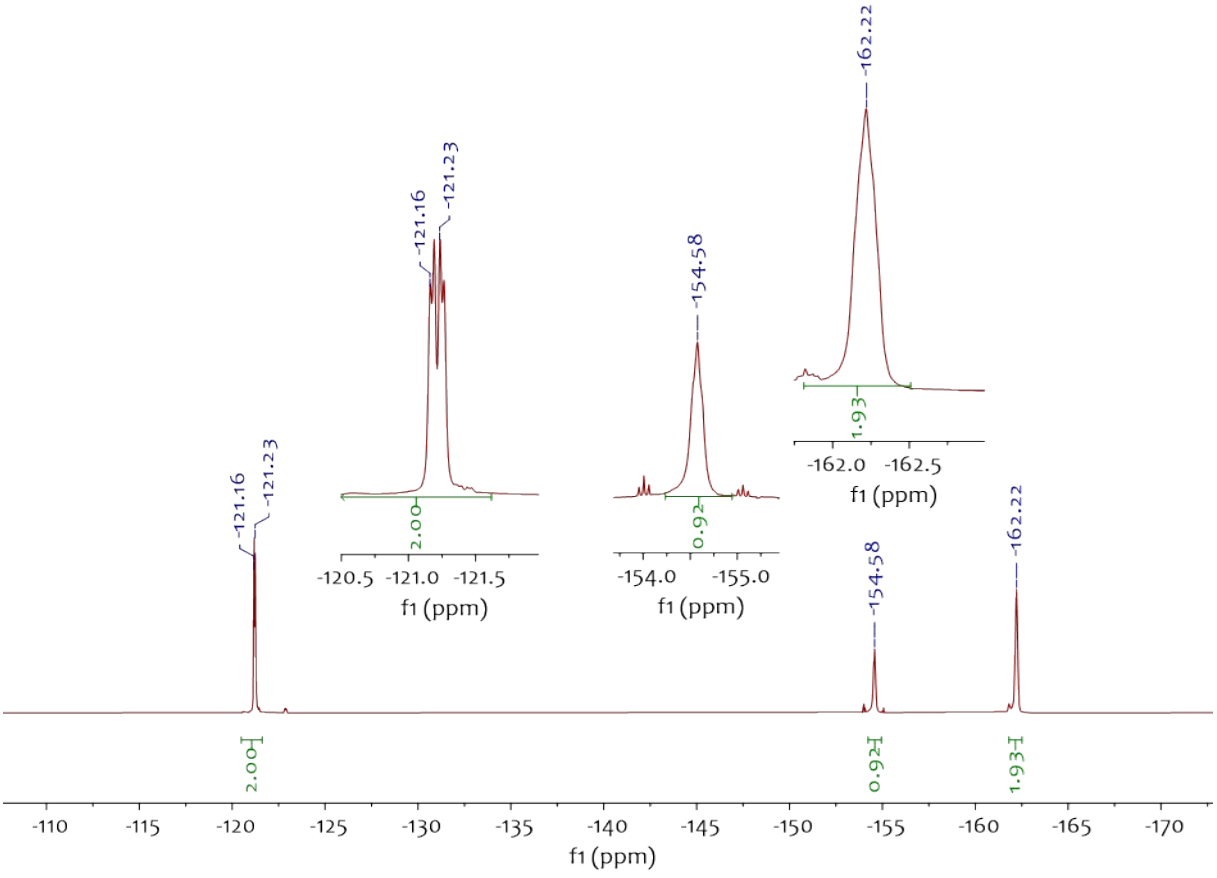

Figure S59. $^{31}P\{^{1}H\}$-NMR spectrum (163.2 MHz, C_6D_6, 298K) of compound 15_{Al}

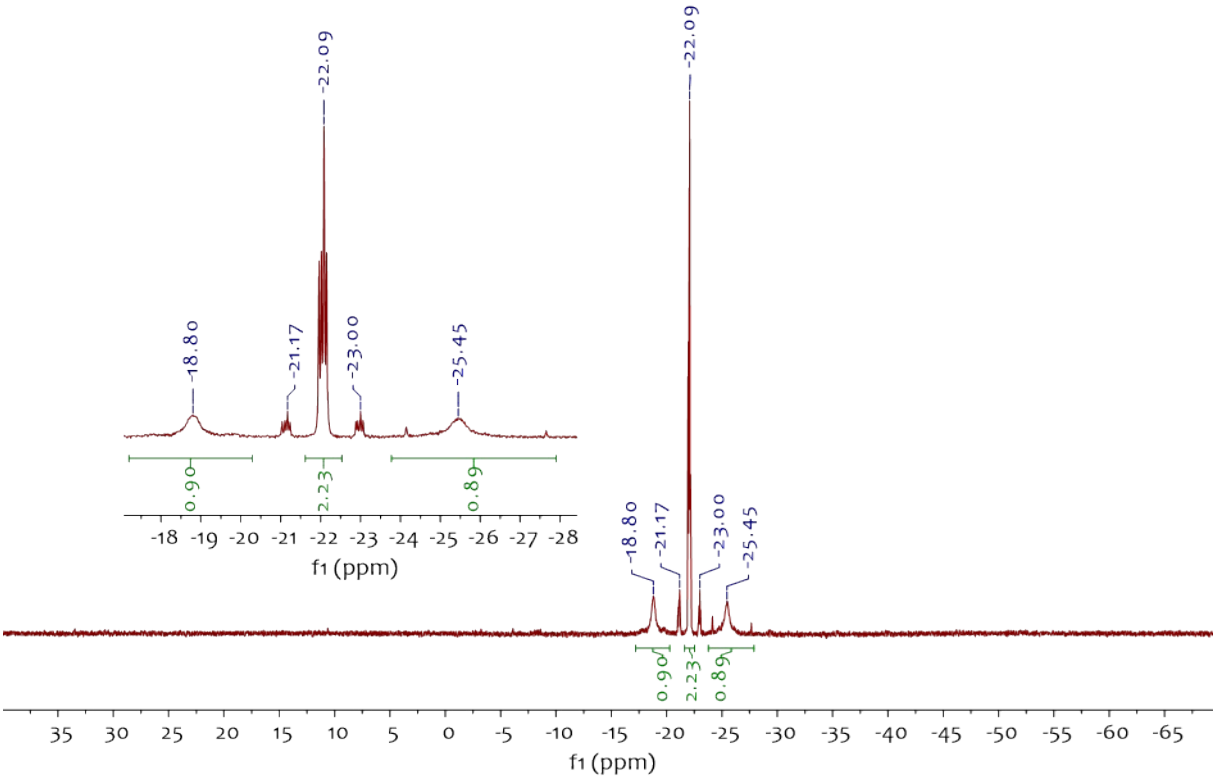

Figure S60. ^{1}H-NMR spectrum (400 MHz, C_6D_6, 298K) of compound 16_{Al}

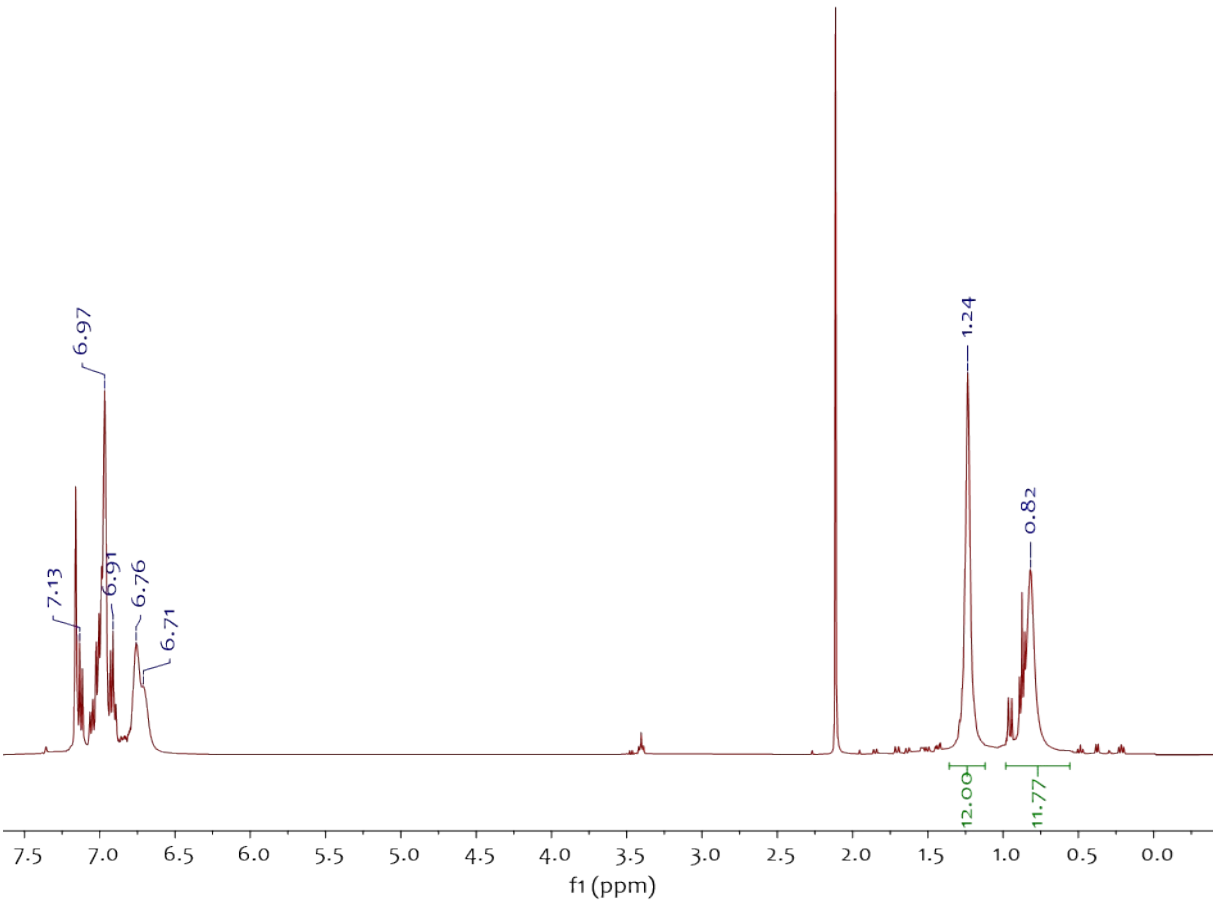

Figure S61. ^{19}F-NMR spectrum (376.2 MHz, C_6D_6, 298K) of compound 16_{Al}

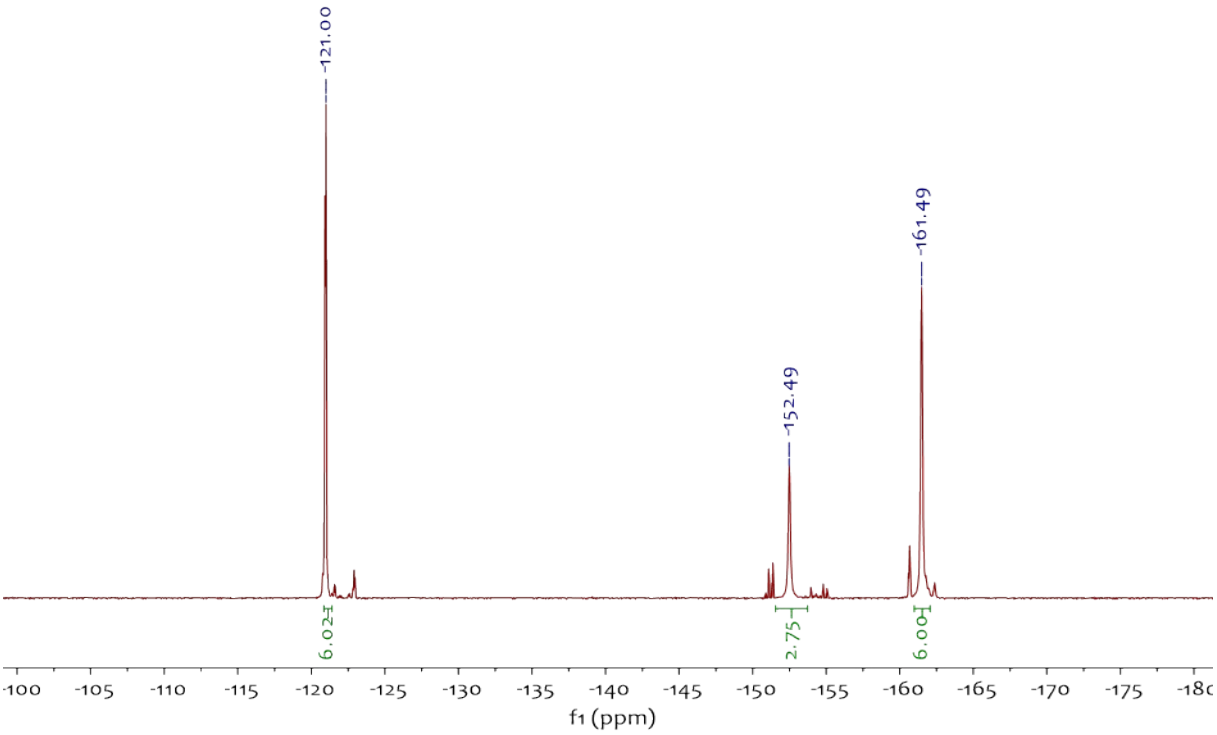

Figure S62. ^{31}P{^{1}H}-NMR spectrum (163.2 MHz, C_6D_6, 298K) of compound 16_{Al}

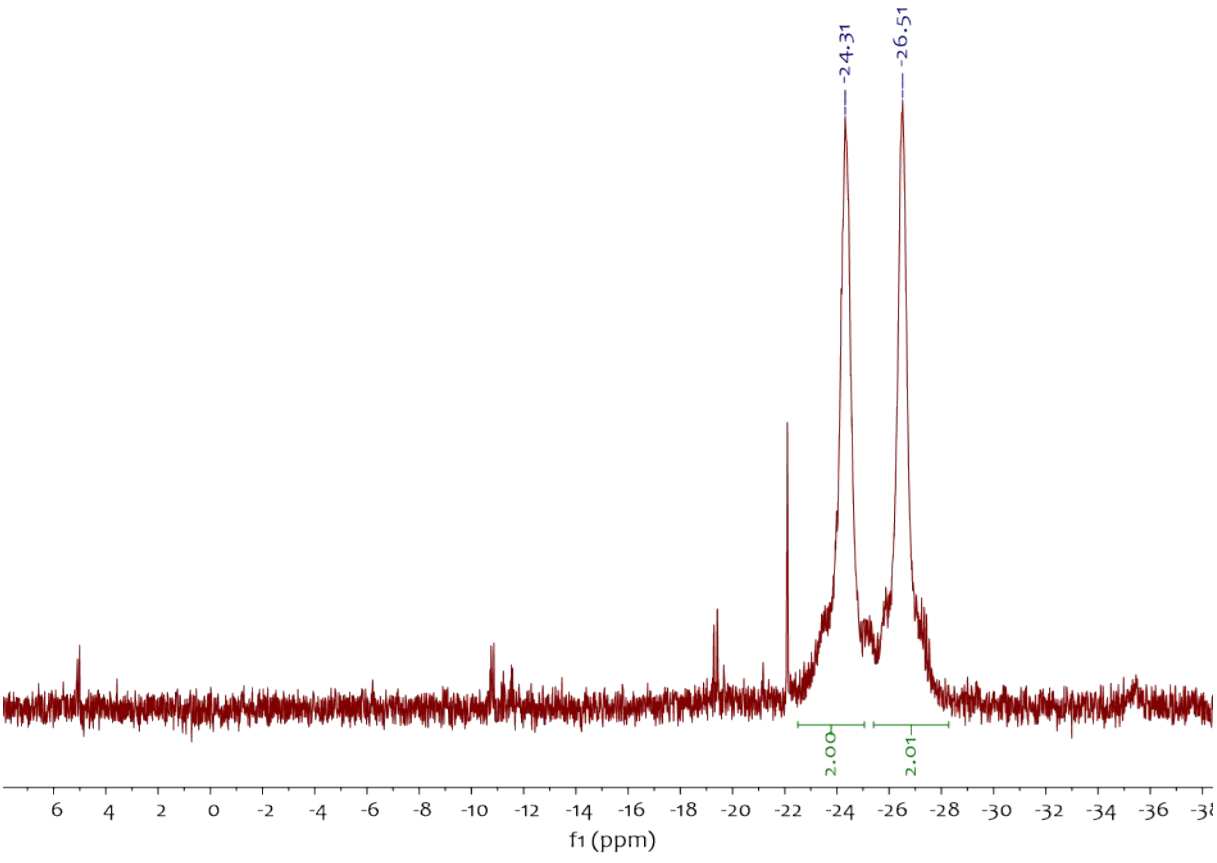

Figure S63. ^{19}F-NMR spectra (376.2 MHz, toluene-d_8, 298K) relating to the reaction of *cis*-[W(PMe$_2$Ph)$_4$(N$_2$)$_2$] + B(C$_6$F$_5$)$_3$ after 30 minutes (bottom) and 2 hours (top) at room temperature.

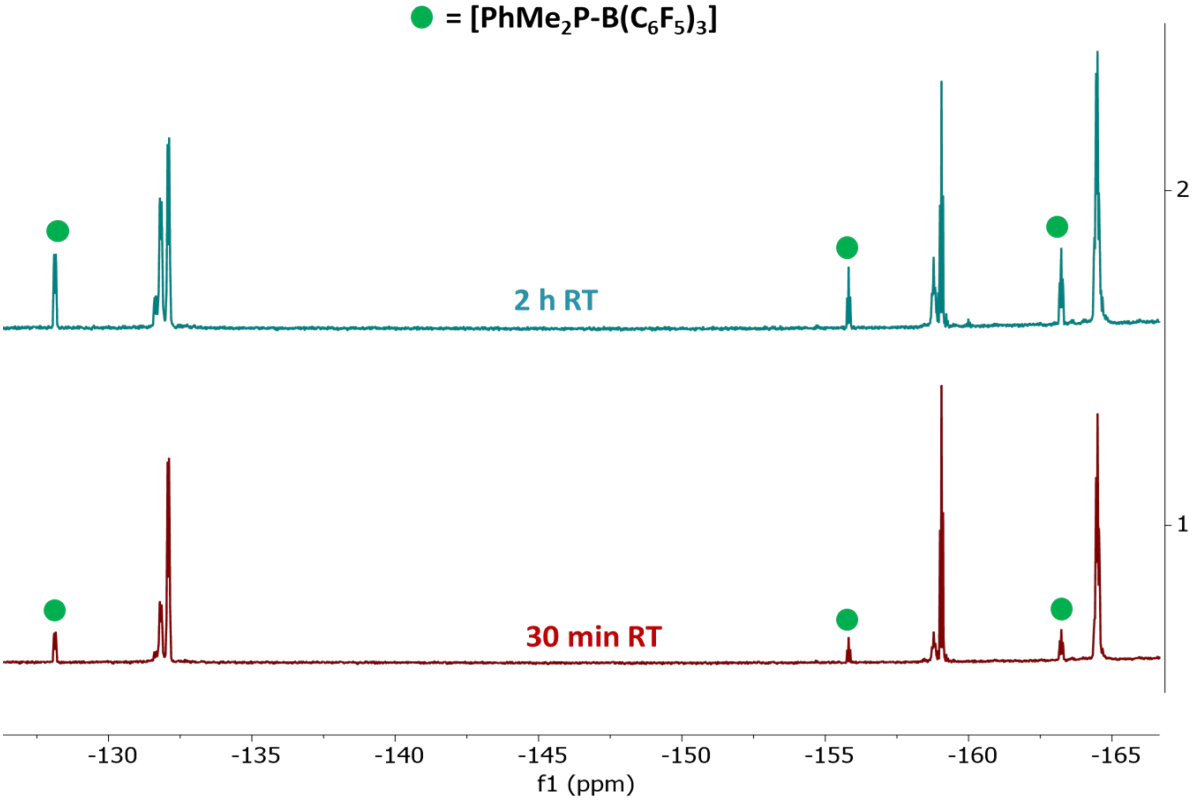

Figure S64. ^{31}P{^{1}H}-NMR spectra (163.2 MHz, toluene-d_8, 298K) relating to the reaction of *cis*-[W(PMe$_2$Ph)$_4$(N$_2$)$_2$] + B(C$_6$F$_5$)$_3$ after 30 minutes (middle) and 2 hours (top) at room temperature. The black line represents the spectrum of *cis*-[W(PMe$_2$Ph)$_4$(N$_2$)$_2$] precursor.

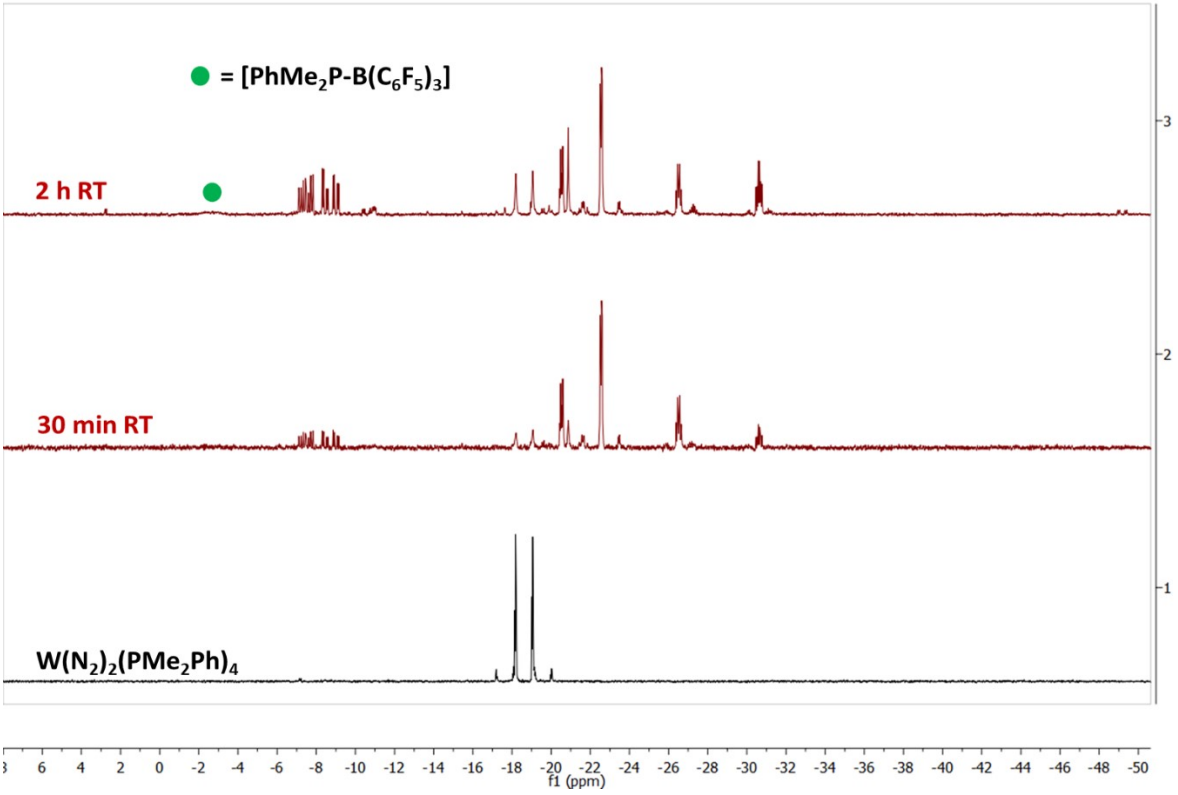

3 IR spectroscopic data

Figure S65. ATR spectrum (298K, under nitrogen) of compound 1_{Al}.

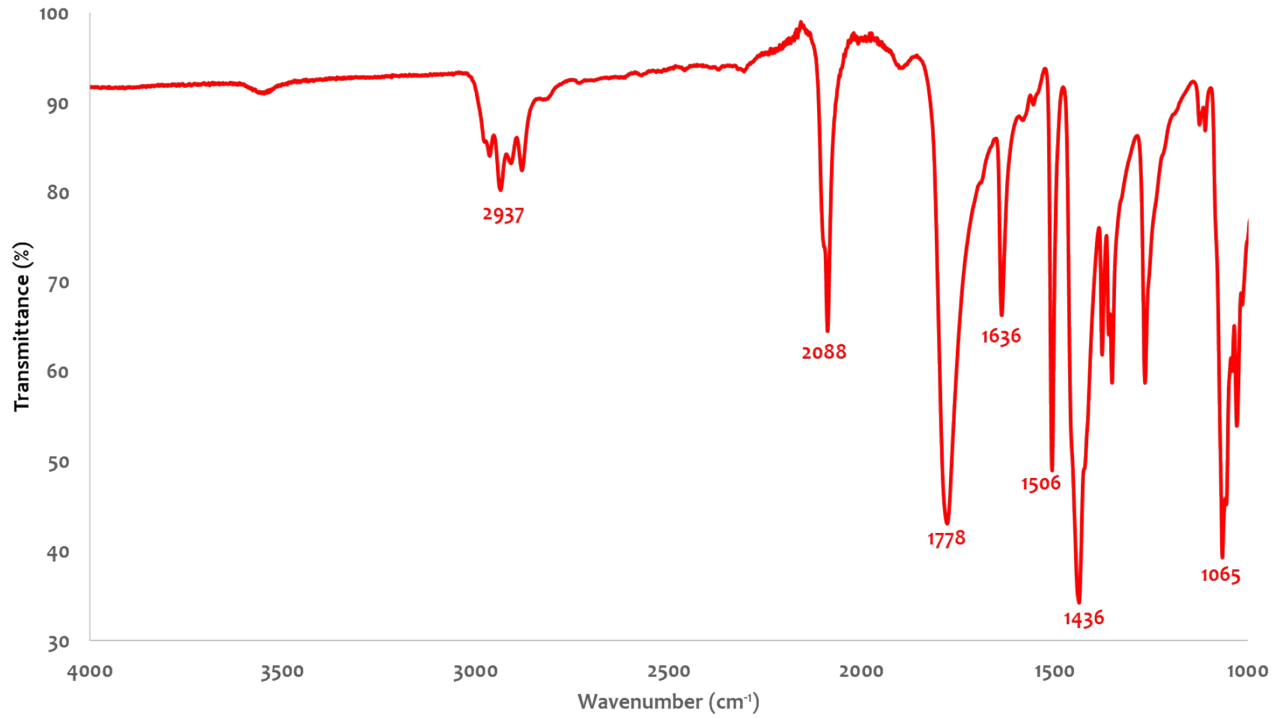

Figure S66. ATR spectrum (298K, under nitrogen) of compound 2_{Al}.

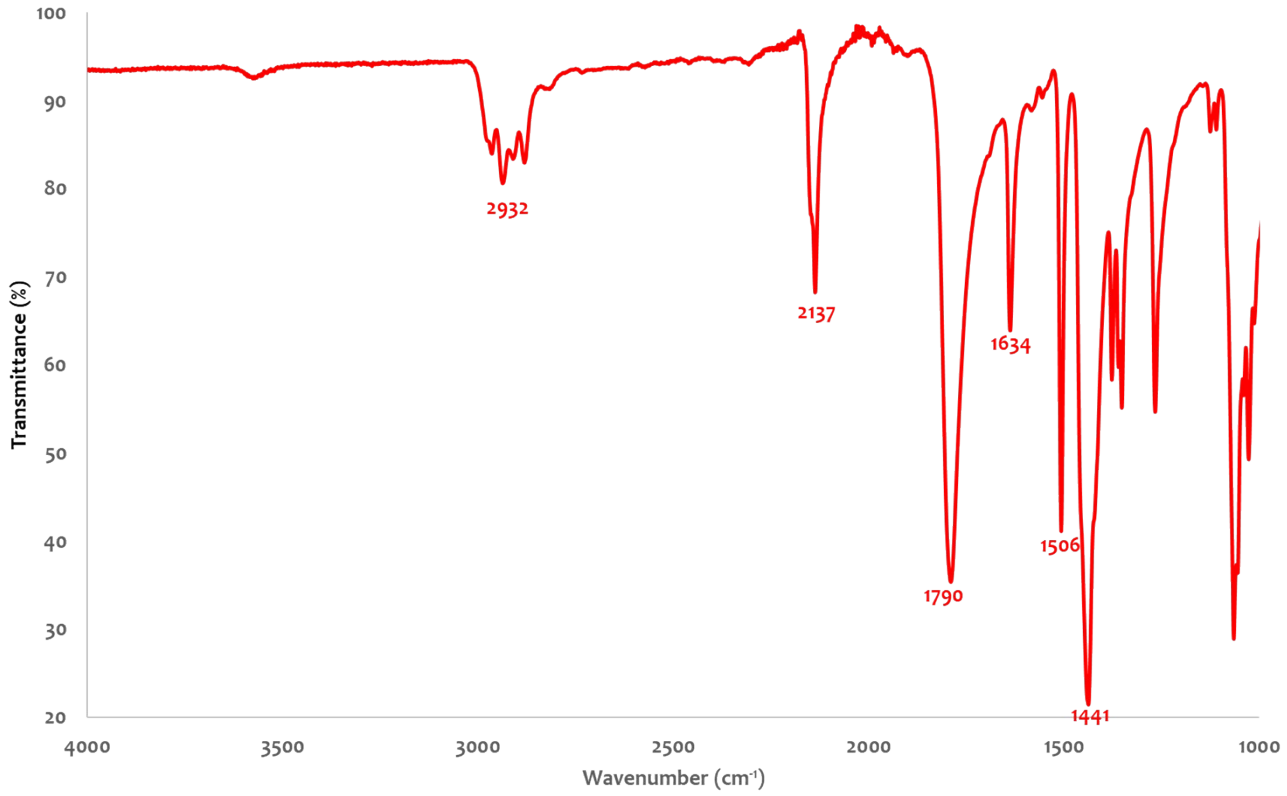

Figure S67. ATR spectrum (298K, under nitrogen) of compound 5_{Al}.

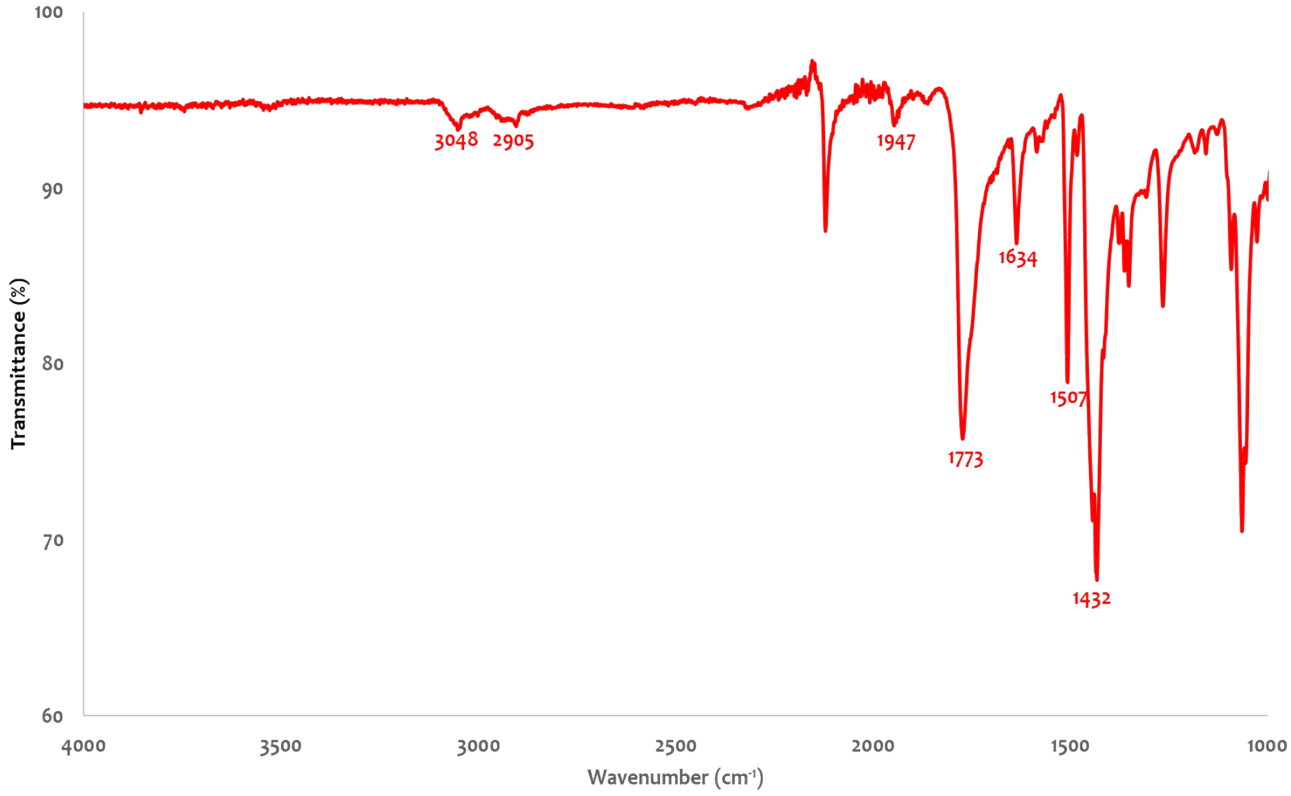

Figure S68. ATR spectrum (298K, under nitrogen) of compound 6_{Al}.

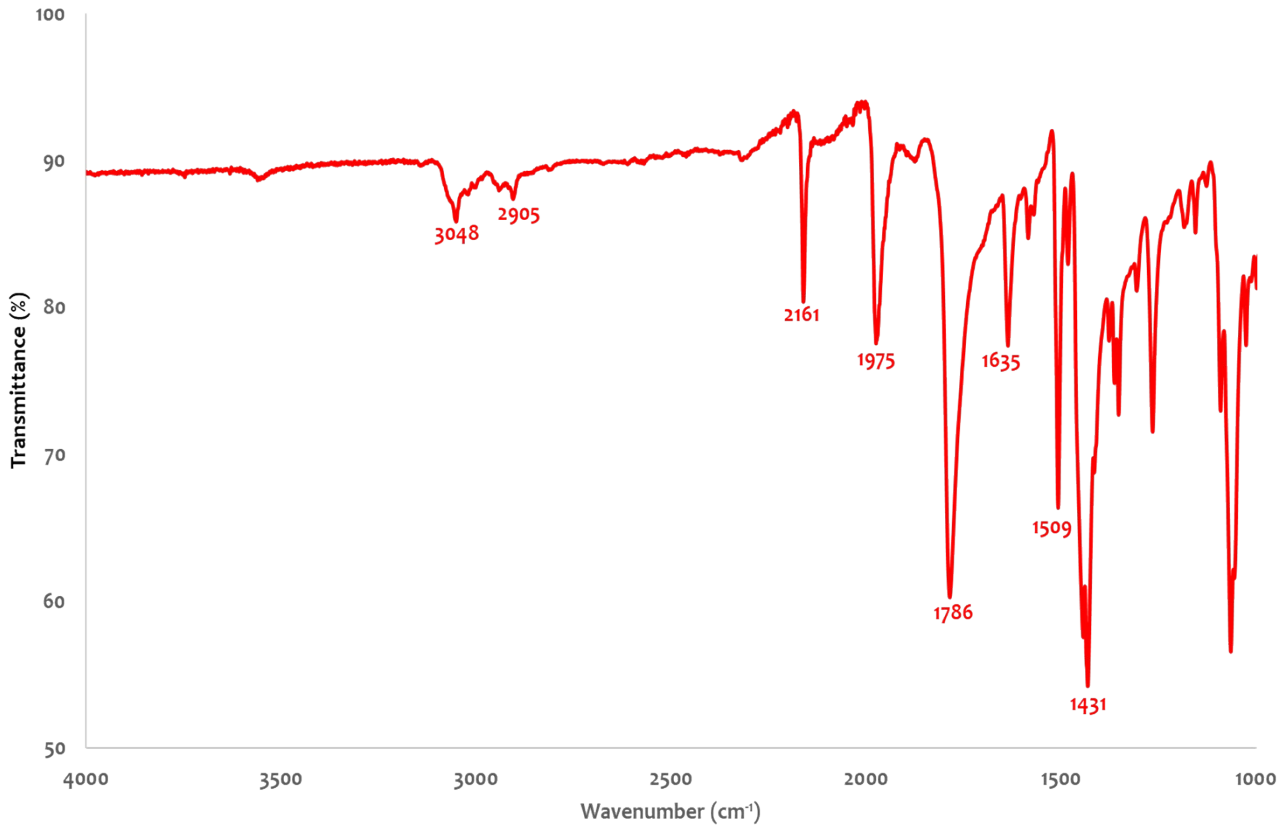

Figure S69. ATR spectrum (298K, under nitrogen) of compound 7_{Al}.

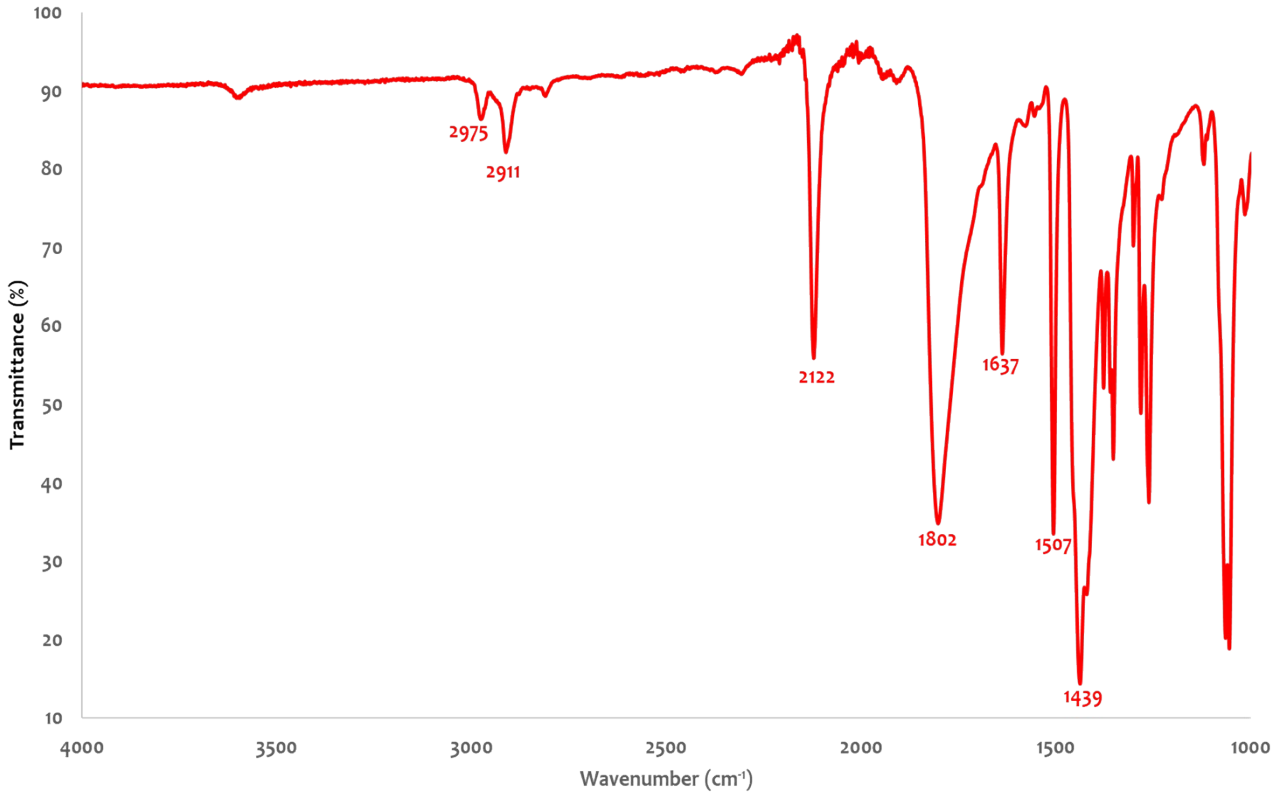

Figure S70. ATR spectrum (298K, under nitrogen) of compound 8_{Al}.

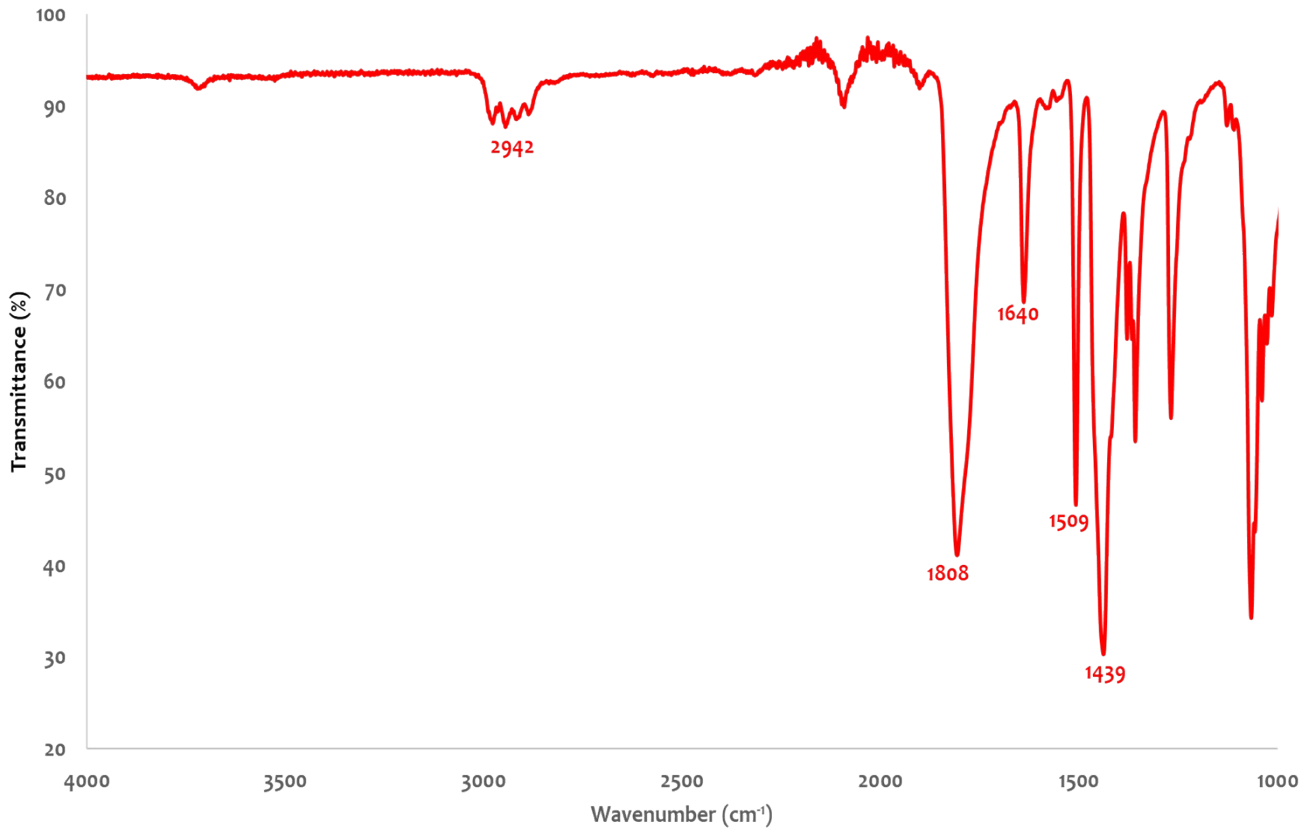

Figure S71. ATR spectrum (298K, under nitrogen) of compound 11_{Al}.

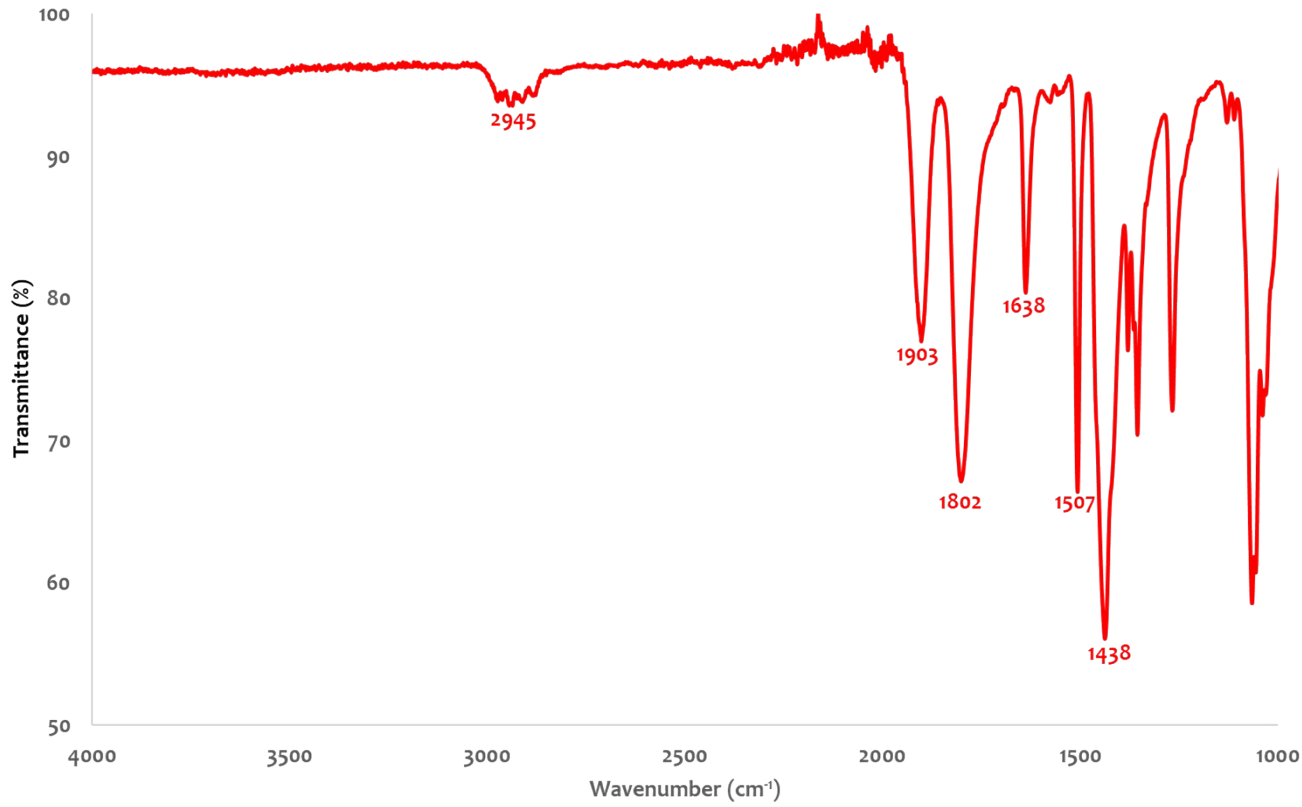

Figure S72. ATR spectrum (298K, under nitrogen) of compound 12_{Al}.

Figure S73. ATR spectrum (298K, under nitrogen) of compound 13_{Al}.

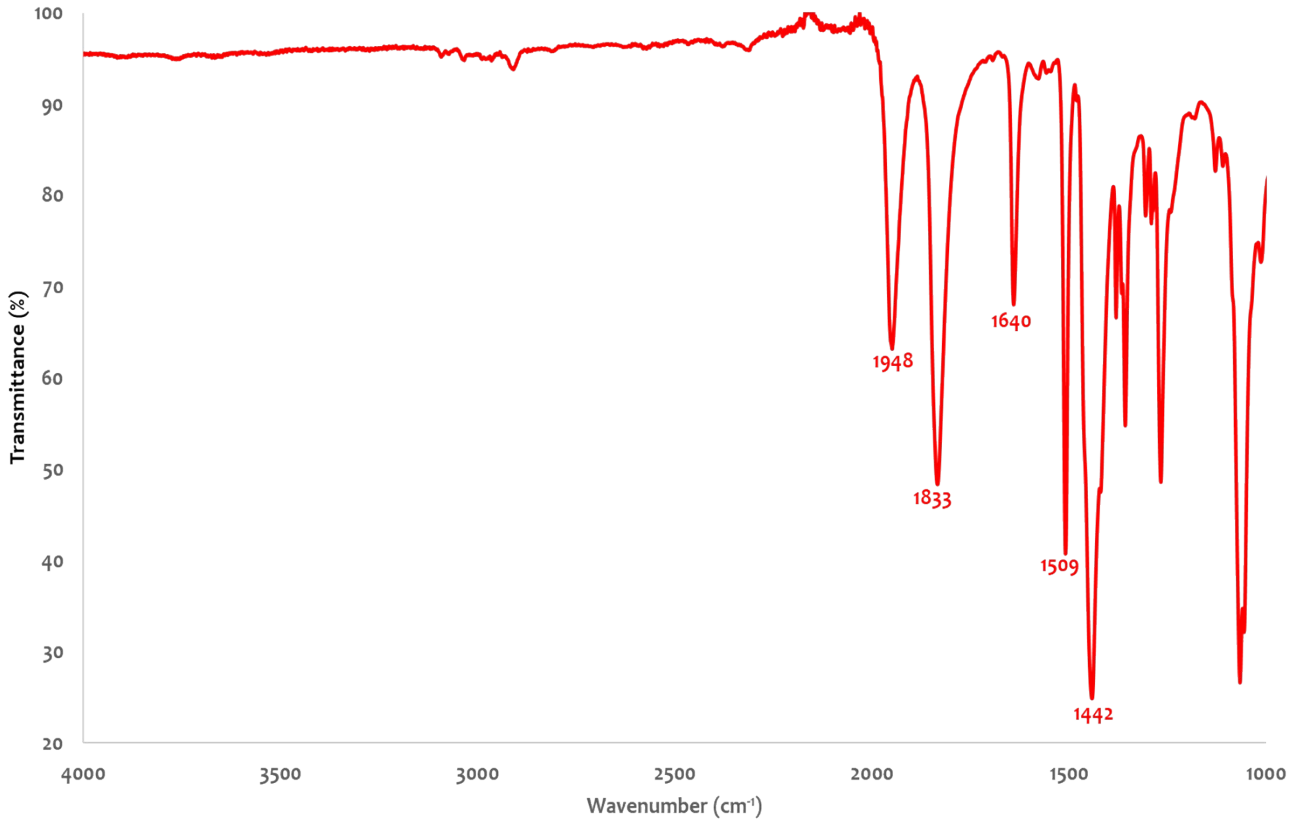

Figure S74. ATR spectrum (298K, under nitrogen) of compound 15_{Al}.

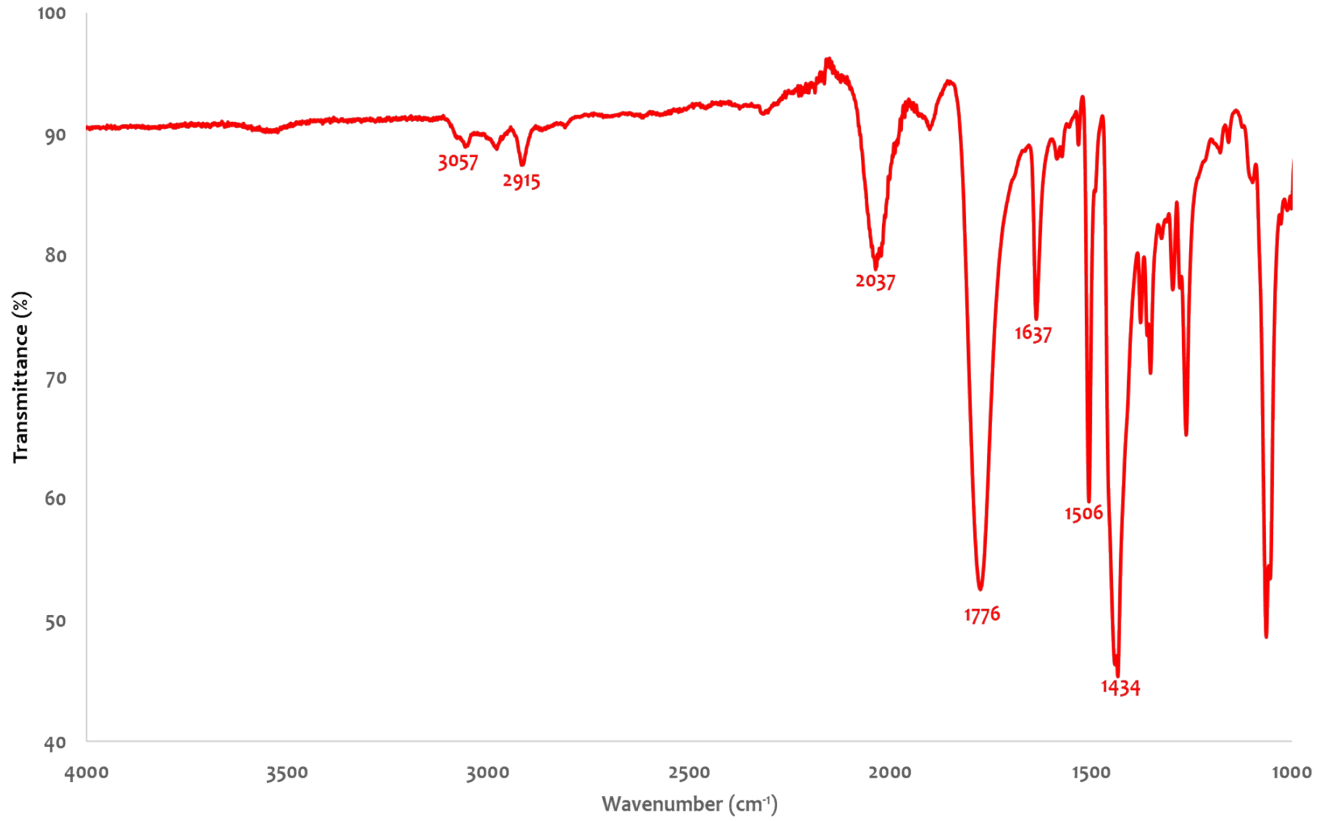

Figure S75. ATR spectrum (298K, under nitrogen) of compound 16_{Al}.

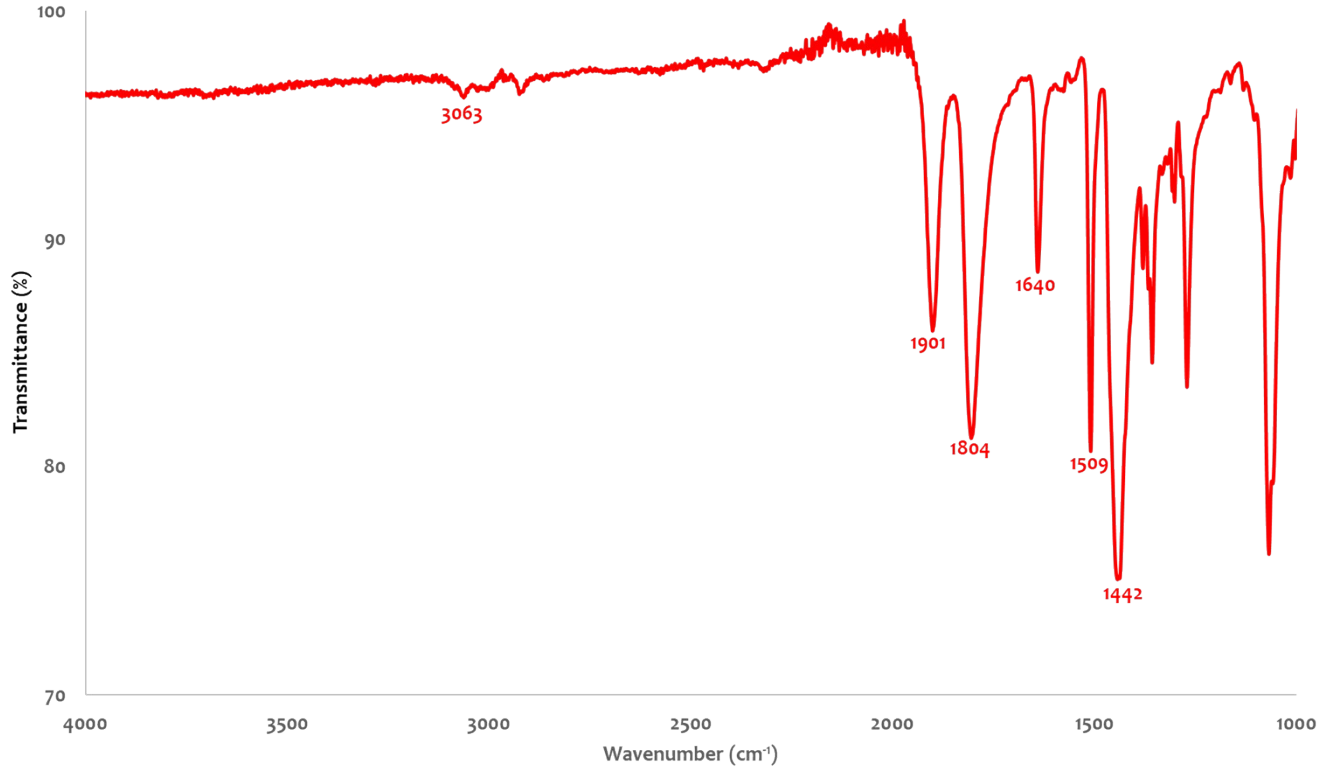

4 UV-vis spectroscopic data

Figure S76. UV-vis spectrum of trans-W(depe)$_2$(N$_2$)$_2$ in benzene at a concentration of 30 µmol/L

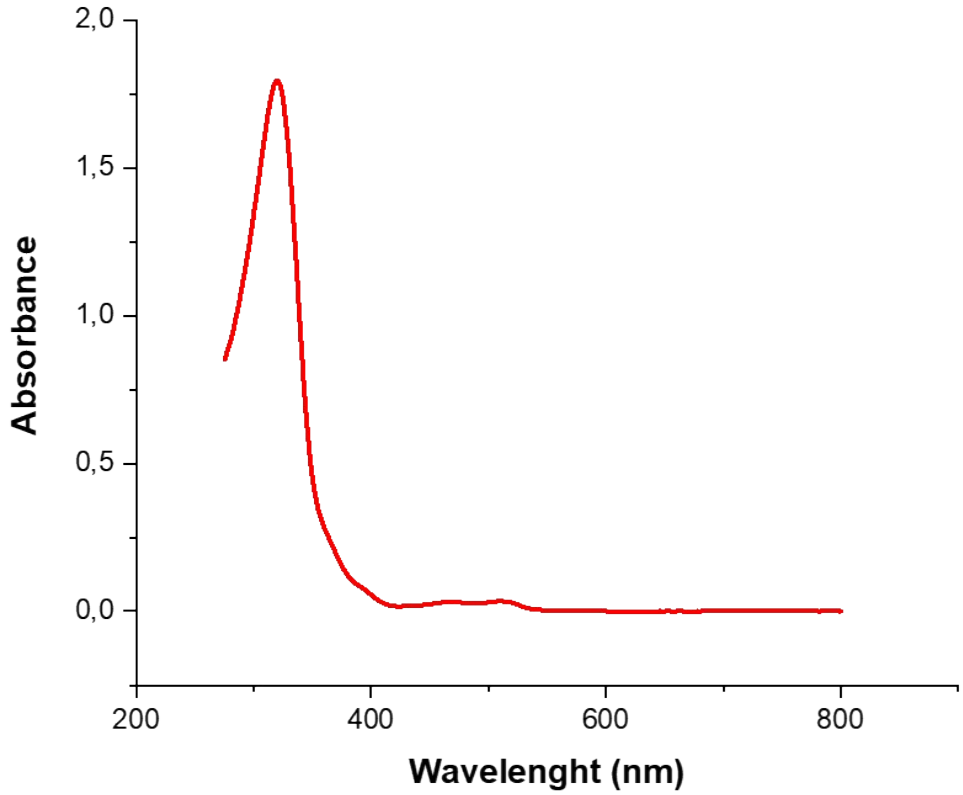

Figure S77. UV-vis spectrum of compound 1$_{Al}$ in benzene at a concentration of 30 µmol/L

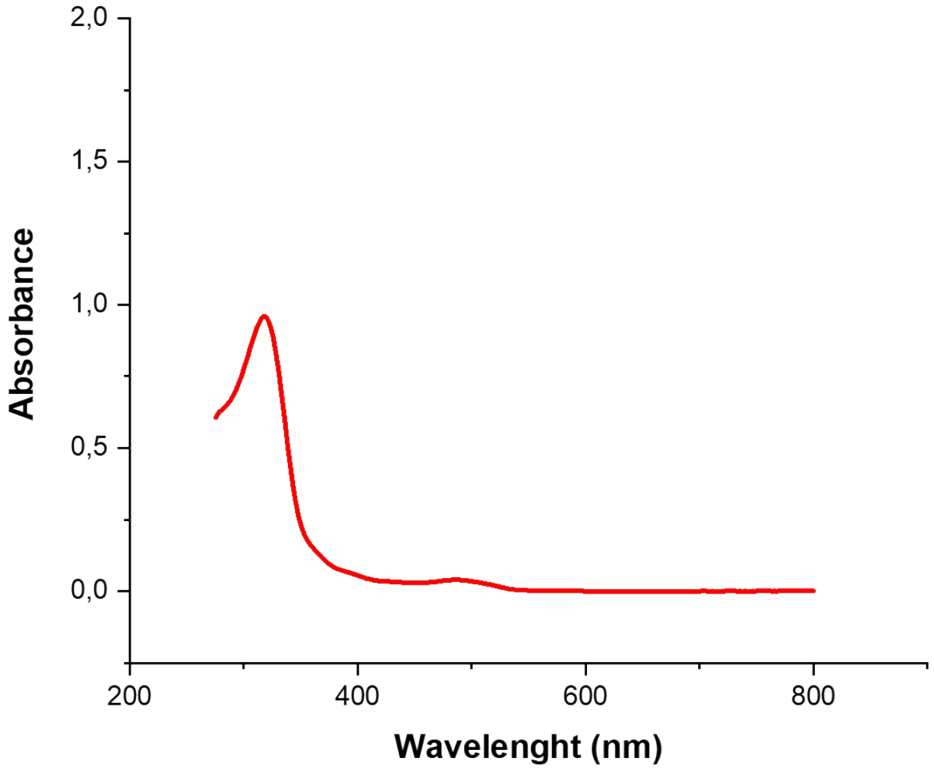

Figure S78. UV-vis spectrum of $Al(C_6F_5)_3$(tol) in benzene at a concentration of 30 µmol/L

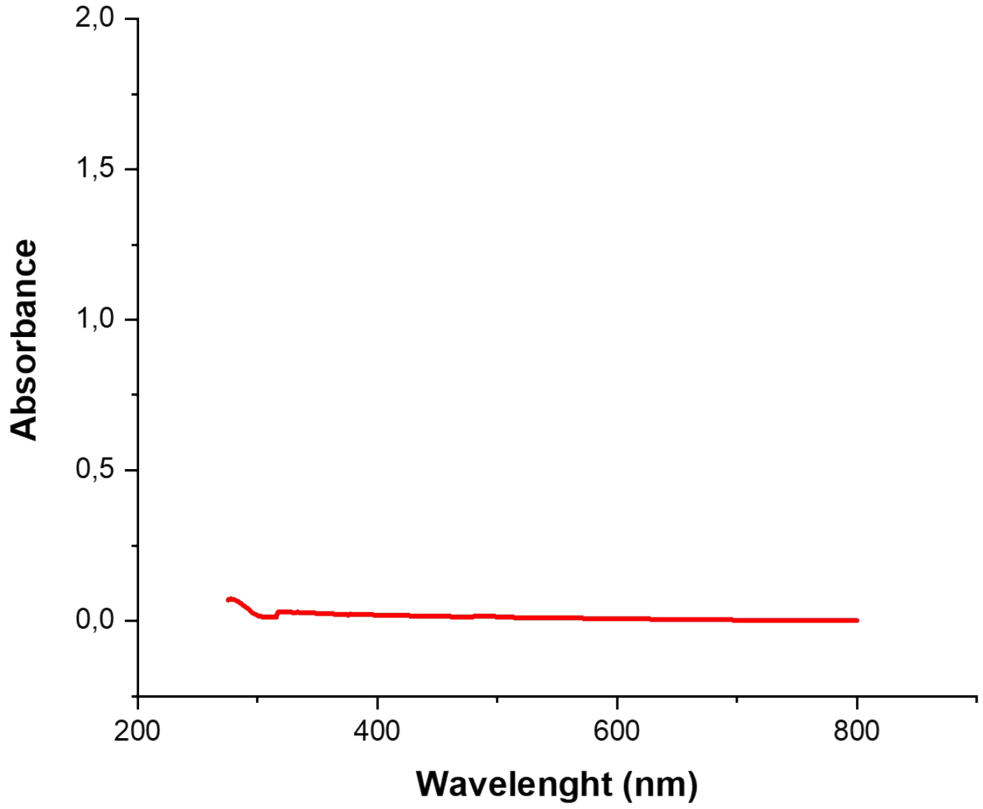

Figure S79. UV-vis spectrum of compound 8_{Al} in benzene at a concentration of 30 µmol/L

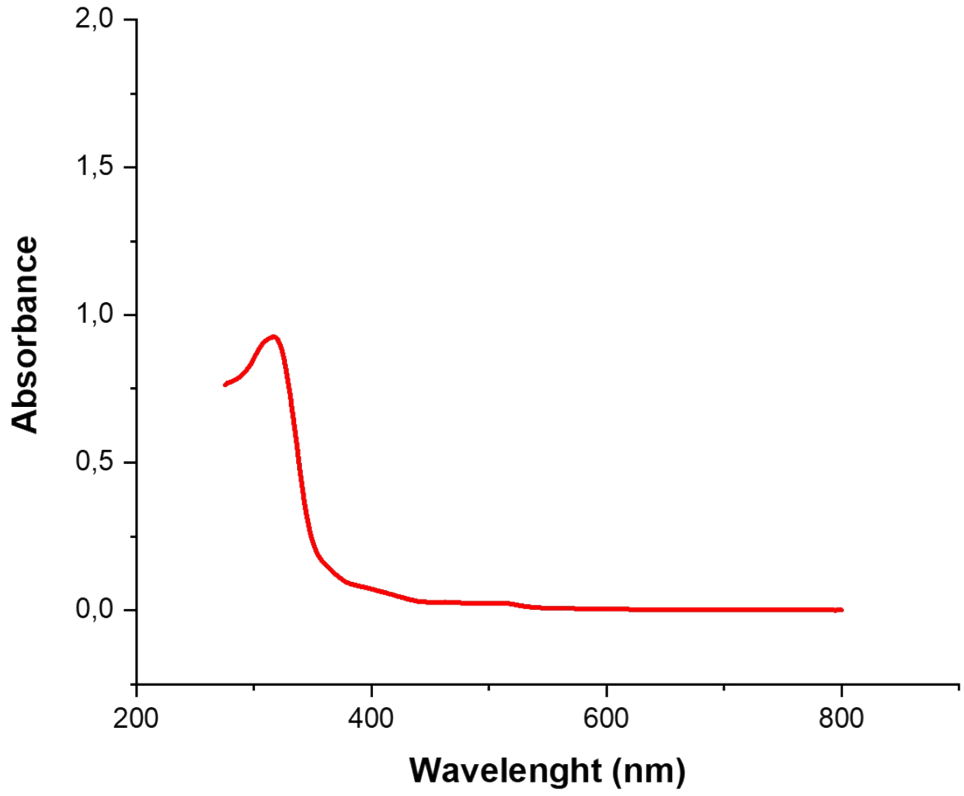

Figure S80. UV-vis spectrum of compound 11_{Al} in benzene at a concentration of 30 µmol/L

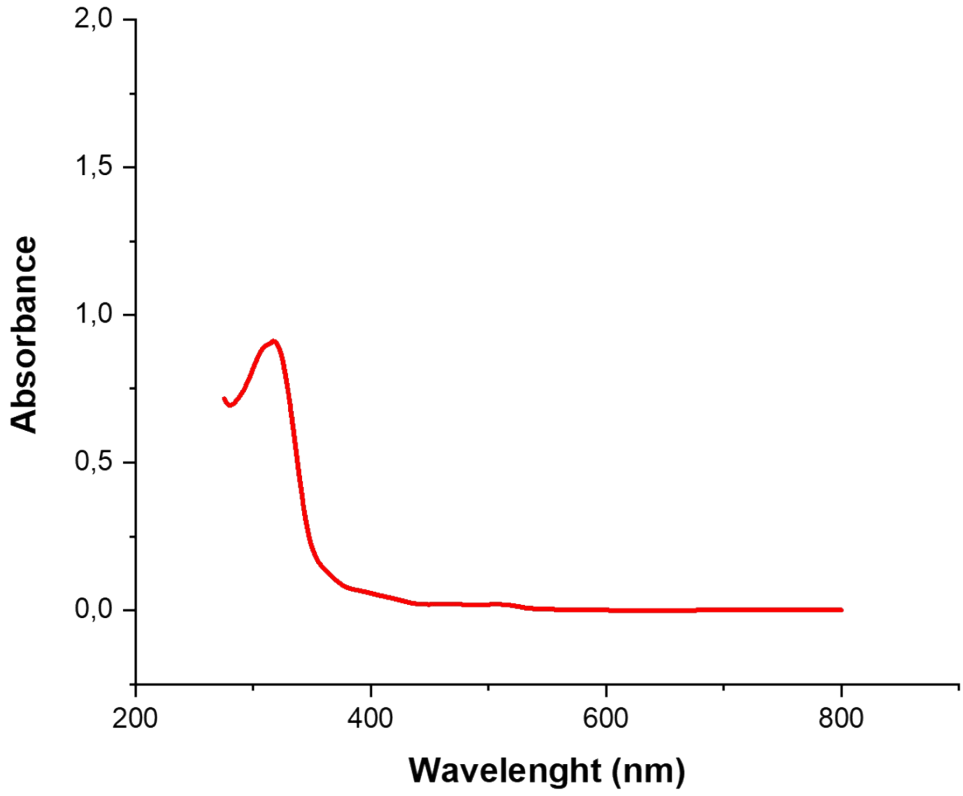

Figure S81. UV-vis spectrum of compound 1_B in benzene at a concentration of 30 µmol/L

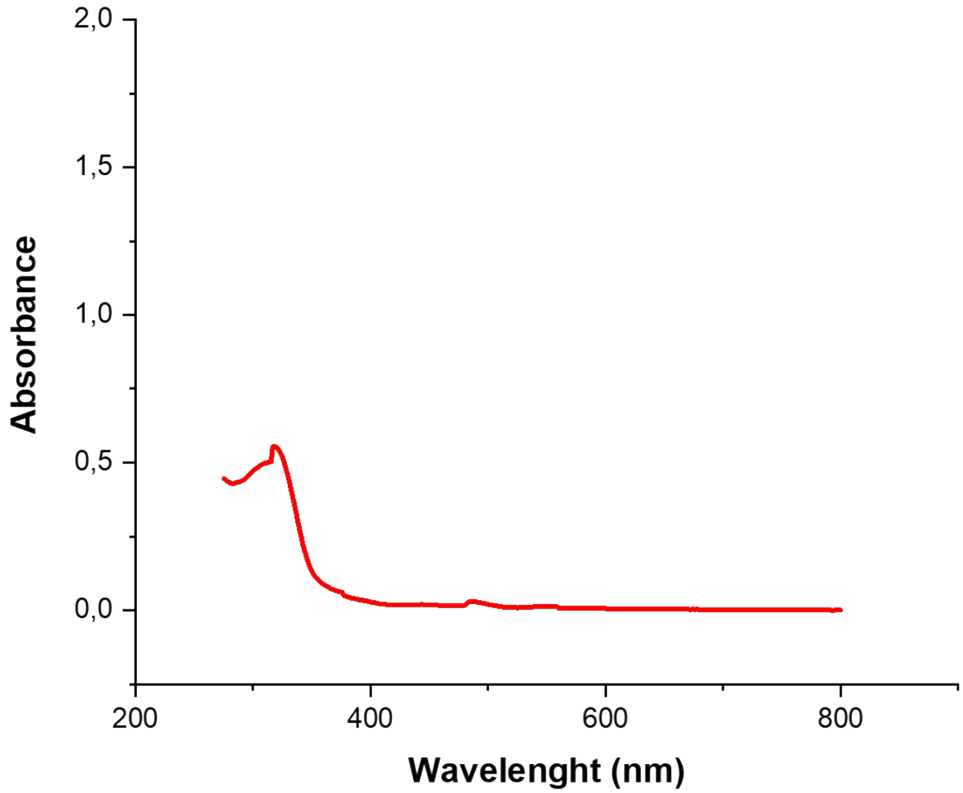

Figure S82. Visible spectrum of trans-$W(depe)_2(N_2)_2$ in benzene at a concentration of 1000 µmol/L

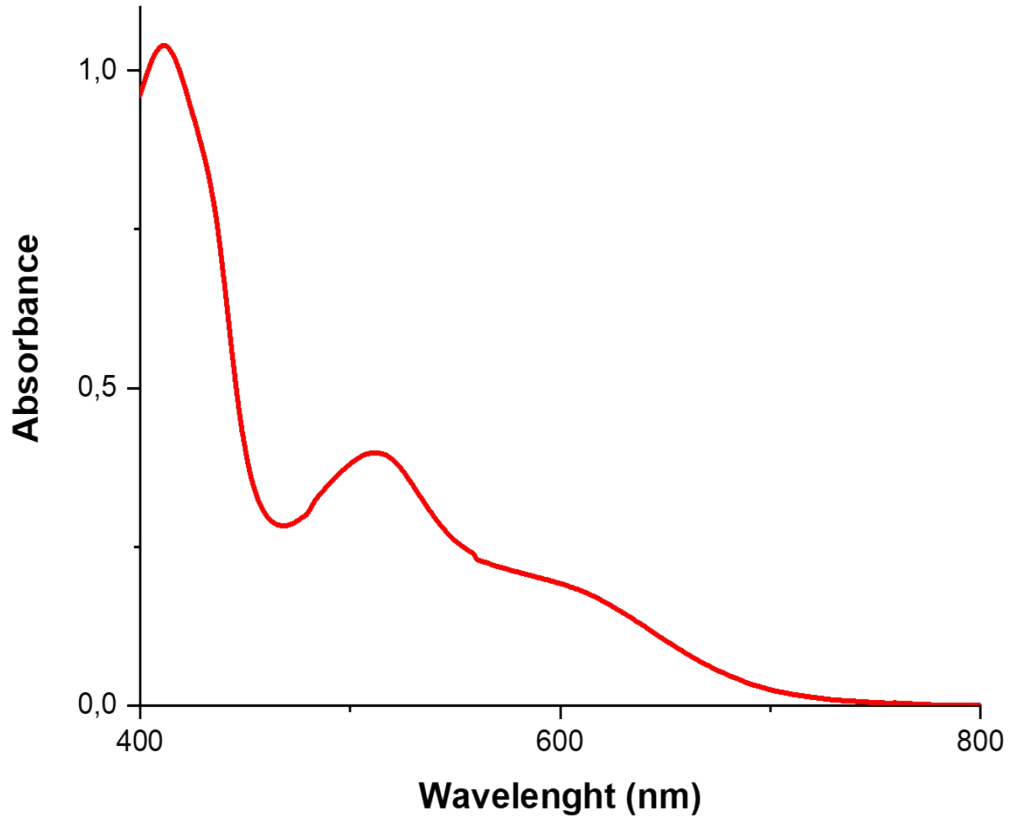

Figure S83. Visible spectrum of compound 1_{Al} in benzene at a concentration of 1000 µmol/L

Figure S84. Visible spectrum of compound 8_{Al} in benzene at a concentration of 1000 µmol/L

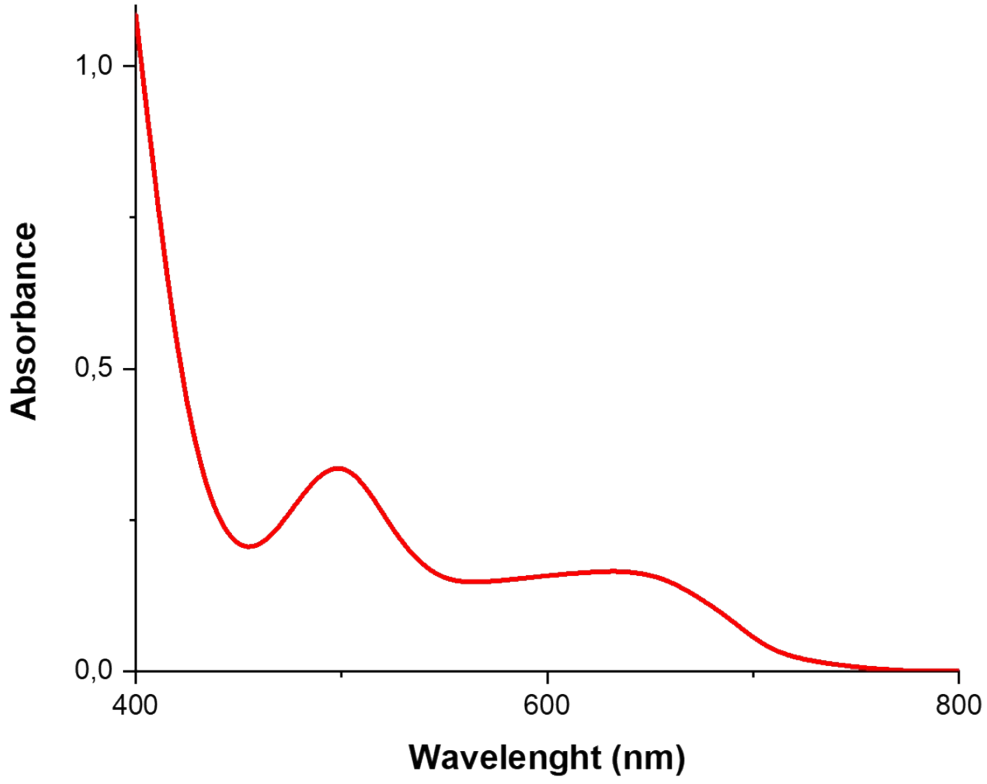

Figure S85. Visible spectrum of compound 11_{Al} in benzene at a concentration of 1000 µmol/L

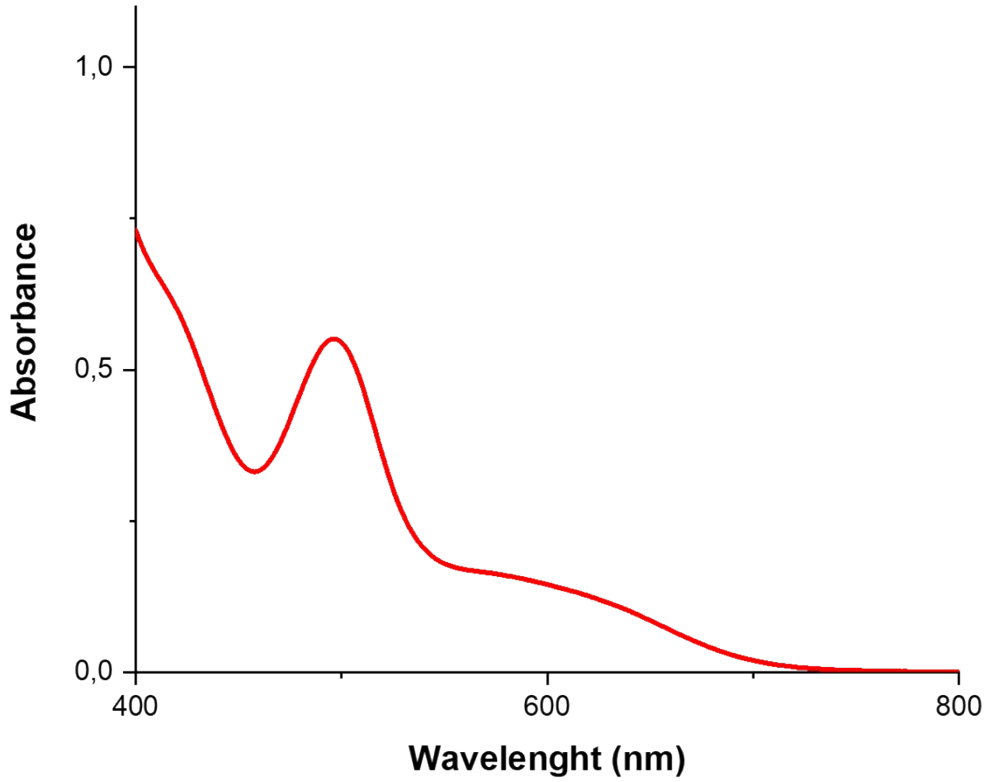

Figure S86. Visible spectrum of compound 1_B in benzene at a concentration of 1000 µmol/L

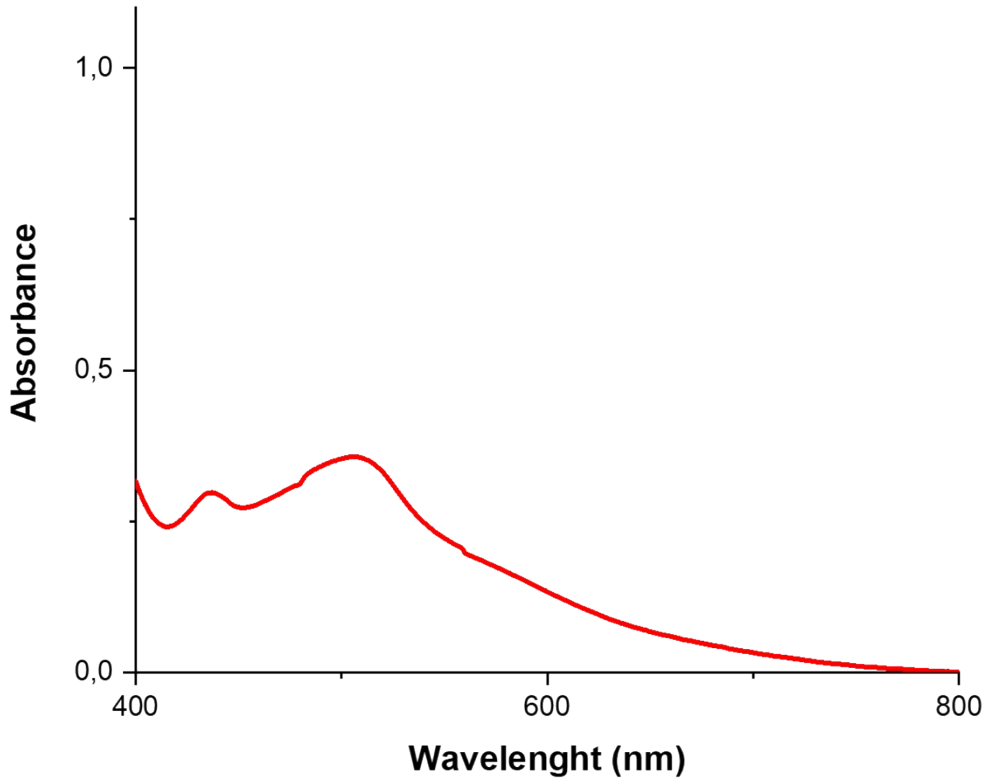
1,0
0,5
0,0
Absorbance
400
600
800
Wavelenght (nm)

5 Crystallographic data

5.1 Data collection and refinement

Data for compounds $\mathbf{1_{Al}}$, $\mathbf{2_{Al}}$, $\mathbf{4_{Al}}$, $\mathbf{6_{Al}}$, $\mathbf{7_{Al}}$, $\mathbf{8_{Al}}$, $\mathbf{11_{Al}}$, $\mathbf{12_{Al}}$, $\mathbf{13_{Al}}$, $\mathbf{16_{Al}}$ were collected at low temperature (100 K) on a XtaLAB Synergy, Dualflex, HyPix diffractometer using a Cu or Mo-Ka radiation (l = 0.71073Å) micro-source and equipped with an Oxford Cryosystems Cryostream Cooler Device. The structures have been solved by Direct Methods and refined by means of least-squares procedures using the SHELXS97[16] program included in the softwares package WinGX version 1.63[17] or with the aid of the software package Crystal[18]. The Atomic Scattering Factors were taken from International tables for X-Ray Crystallography[19]. Hydrogen atoms were placed geometrically and refined using a riding model. All non-hydrogens atoms were anisotropically refined. Drawing of molecules in the following figures were performed with the program Mercury[20] with 30% probability displacement ellipsoids for non-hydrogen atoms. The crystal structures have been deposited at the Cambridge Crystallographic Data Centre and allocated the deposition numbers CCDC 2346952–2346961.

5.2 XRD data

Table S1. XRD data for compounds $\mathbf{1_{Al}}$, $\mathbf{2_{Al}}$, and $\mathbf{4_{Al}}$.

Compound	$\mathbf{1_{Al}}$	$\mathbf{2_{Al}}$	$\mathbf{4_{Al}}$
Formula	$C_{38}H_{48}AlF_{15}N_4P_4W$	$C_{38}H_{48}AlF_{15}MoN_4P_4$	$C_{140}H_{96}Al_2F_{30}Mo_2N_4P_8$
cryst syst	Triclinic	Triclinic	Monoclinic
space group	P-1	P-1	P 1 21/c 1
volume (Å^3)	4624.3 (3) Å^3	4626.84 (19)	15884.8(5)
a (Å)	12.1087 (5) Å	12.0871 (4)	39.6401(7)
b (Å)	16.7894 (6)	16.7971 (3)	13.8830(2)
c (Å)	23.7857 (7)	23.8312 (4)	31.1016(5)
α (deg)	87.462 (3)	87.584 (2)°	90
β (deg)	85.545 (4)°	85.376 (3)	111.864(2)
γ (deg)	73.630 (4)°	73.657 (2)	90
Z	4	4	4
Formula weight (g/mol)	1180.51	1092.61	2897.91
density (g cm^{-3})	1.696	1.569	1.212
Absorption Coeff. (mm^{-1})	6.98	4.66	2.845
F(000)	2344	2216	5856
θ_{max} (°)	65.1	65.1	76.974
no. refined reflections	9354	15754	/
no. refined restrains	7	0	/
no. refined parameters	1135	1151	/
wR(F^2)	0.184	0.179	/
R[F^2 > 2σ(F^2)]	0.085	0.066	/

Table S2. XRD data for compounds 5_{Al}, 6_{Al}, and 7_{Al}

Compound	5_{Al}	6_{Al}	7_{Al}
Formula	$C_{39}H_{48}AlF_{15}O_2P_4W \cdot 2(C_7H_8)$	$C_{70}H_{48}AlF_{15}MoN_4P_4$	$C_{30}H_{32}AlCrF_{15}N_4P_4$
cryst syst	Monoclinic	Triclinic	Triclinic
space group	$P2_1/n$	P-1	P-1
volume (Å^3)	5581.0 (3)	3290.37 (6)	1963.24 (6)
a (Å)	13.8441 (4)	14.6308 (1)	10.01668 (16)
b (Å)	11.8025 (3)	15.5072 (1)	12.25253(19)
c (Å)	34.6152 (8)	15.9055 (2)	17.2703(3)
α (deg)	90	77.247 (1)	79.3130(13)
β (deg)	99.341 (2)	69.209 (1)	88.9694(13)
γ (deg)	90	85.109 (1)	70.6686(14)
Z	4	2	2
Formula weight (g/mol)	1352.75	1476.96	936.45
density (g cm^{-3})	1.610	1.491	1.584
Absorption Coeff. (mm^{-1})	5.87	3.45	5.09
F(000)	2720	1492	944
θ_{max} (°)	65.1	79.9	80.8
no. refined reflections	9502	14137	8441
no. refined restrains	0	0	0
no. refined parameters	714	856	496
wR(F^2)	0.094	0.111	0.114
R[$F^2 > 2\sigma(F^2)$]	0.039	0.038	0.038

Table S3. XRD data for compounds 8_{Al}, 11_{Al}, and 12_{Al}

Compound	8_{Al}	11_{Al}	12_{Al}
Formula	$C_{56}H_{48}Al_2F_{30}N_4P_4W \cdot C_7H_8$	$C_{56}H_{48}Al_2F_{30}N_4P_4W \cdot 2(C_6H_6)$	$C_{56}H_{48}Al_2F_{30}MoN_4P_4 \cdot 2(C_6H_6)$
cryst syst	Triclinic	Triclinic	Triclinic
space group	P-1	P-1	P-1
volume (Å^3)	3800.84(5)	7378.43(18)	7385.21(13)
a (Å)	13.91510(10)	12.2122(2)	12.20110(10)
b (Å)	14.04580(10)	24.4664(3)	24.5110(3)
c (Å)	20.98840(10)	25.0551(3)	25.0556(2)
α (deg)	79.92	92.0780(10)	92.0680(10)
β (deg)	80.39	99.059(2)	99.1110(10)
γ (deg)	71.4090(10)	92.5410(10)	92.3970(10)
Z	2	4	4
Formula weight (g/mol)	1800.80	1864.88	1776.98
density (g cm^{-3})	1.574	1.679	1.598
Absorption Coeff. (mm^{-1})	4.87	5.04	3.59
F(000)	1784	3704	3576
θ_{max} (°)	80.4	80.4	80.7
no. refined reflections	15873	31656	31217
no. refined restrains	0	0	0
no. refined parameters	946	1963	1963

wR(F^2)	0.070	0.149	0.180
R[$F^2 > 2\sigma(F^2)$]	0.026	0.060	0.070

Table S4. XRD data for compounds 13_{Al}, and 16_{Al}

Compound	**13_{Al}**	**16_{Al}**
Formula	$C_{56}H_{48}Al_2F_{30}N_4P_4Cr \cdot C_6H_6$	$C_{68}H_{44}Al_2F_{30}N_4P_4W \cdot C_7H_8$
cryst syst	Monoclinic	Triclinic
space group	$P2_1/n$	P-1
volume (Å^3)	12369.65(19)	4114.84(8)
a (Å)	20.2615(2)	13.44705(13)
b (Å)	25.2623(2)	13.61546(15)
c (Å)	24.4599(2)	24.0453(2)
α (deg)	90	75.1197(9)
β (deg)	98.8840(10)	82.0640(9)
γ (deg)	90	76.0014(9)
Z	8	2
Formula weight (g/mol)	1542.73	1940.91
density (g cm^{-3})	1.657	1.566
Absorption Coeff. (mm^{-1})	4.00	4.55
F(000)	6160	1920
θ_{max} (°)	80.7	80.1
no. refined reflections	21083	17491
no. refined restrains	18	0
no. refined parameters	1729	1046
wR(F^2)	0.232	0.121
R[$F^2 > 2\sigma(F^2)$]	0.082	0.046

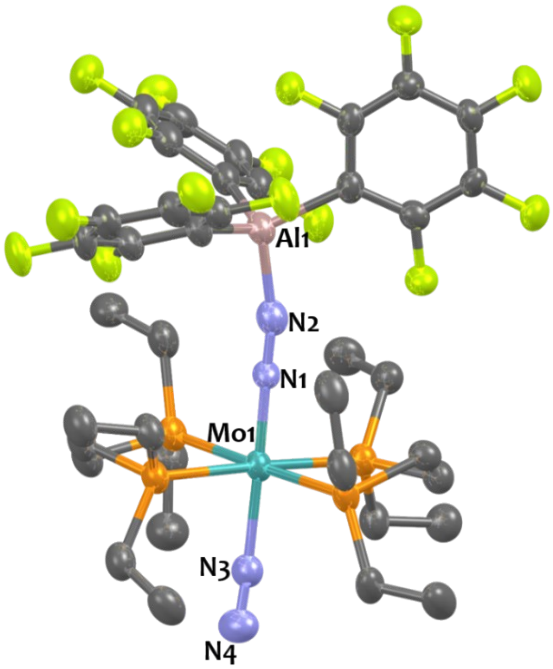

Figure S87. Solid-state structures of $\mathbf{2}_{Al}$. Ellipsoids are represented with 30% probability. Hydrogen atoms have been omitted for clarity. Two independent molecules were found in the asymmetric unit (Z'=2) but one of them has been omitted for clarity. Selected bond distances (Å) and angles (°) have been averaged between both independent molecules: Al1-N2 1.841(65), Mo1-N1 1.869(0), Mo1-N3 2.127(6), N1-N2 1.168(25), N3-N4 1.102(8), Mo1-N1-N2 179.0(1), Mo-N3-N4 176.1(6), Al1-N1-N2

167.5(5).

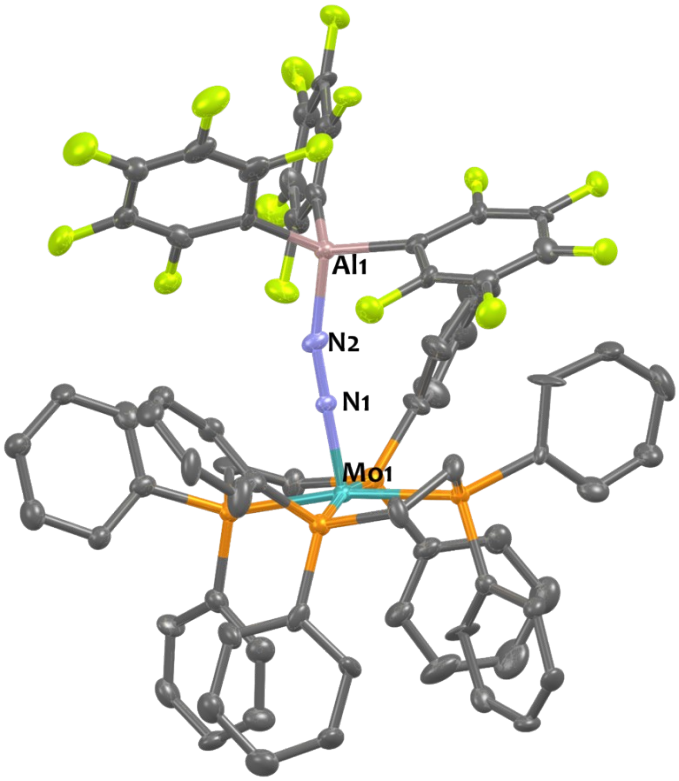

Figure S88. Solid-state structures of $\mathbf{4}_{Al}$. Ellipsoids are represented with 30% probability. Hydrogen atoms have been omitted for clarity.

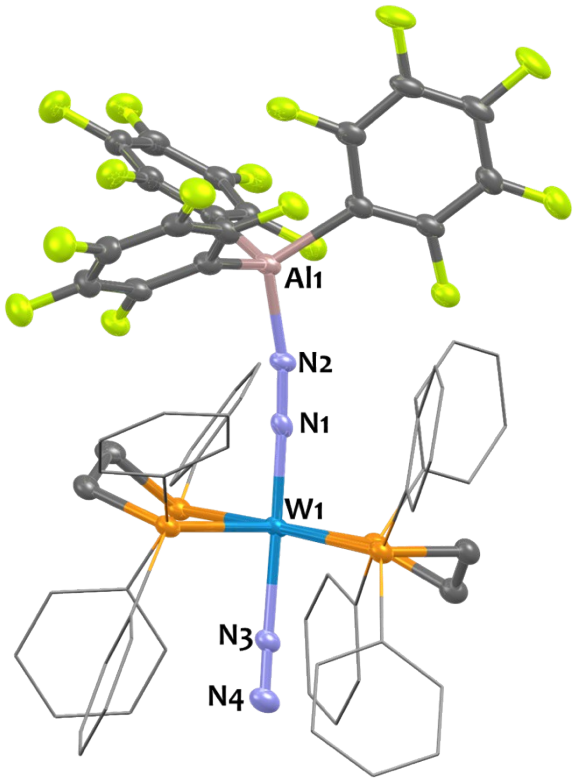

Figure S89. Solid-state structure of $\mathbf{5}_{Al}$. Ellipsoids are represented with 30% probability. Hydrogen atoms have been omitted for clarity. Phenyl rings are plotted with a wireframe style for clarity. Selected bond distances (Å) and angles (°): Al1-N2 1.864(5), W1-N1 1.885(4), W1-N3 2.108(4), N1-N2

1.180(6), N4-N3 1.089(7), N3-W1 -N1 175.39(18), W1-N1-N2 177.2(4), W1-N3-N4 178.0(4), Al1 -N2-N1 169.3(4).

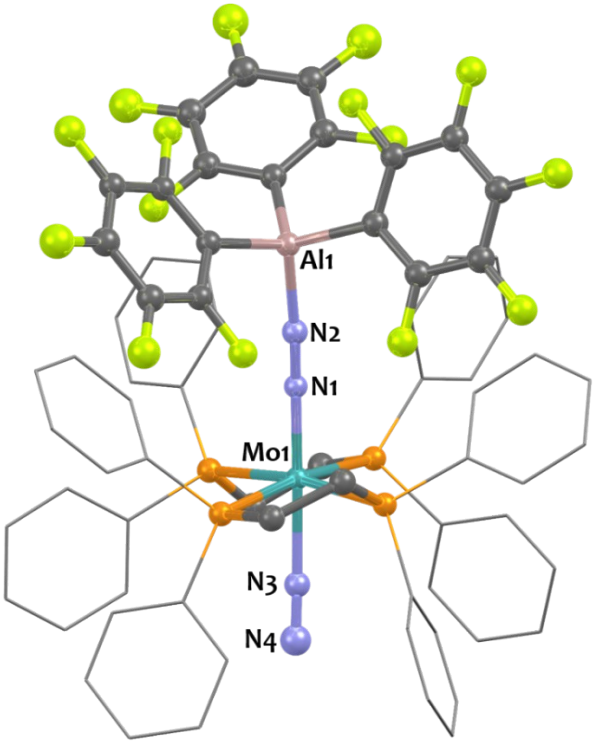

Figure S90. Solid-state structure of $\mathbf{6}_{Al}$. Ellipsoids are represented with 30% probability. Hydrogen atoms have been omitted for clarity. Phenyl rings are plotted with a wireframe style for clarity. Selected bond distances (Å) and angles (°): Al1-N2 1.876(2), Mo1-N1 1.8937(17), Mo1-N3 2.1394(19), N1-N2 1.174(3), N3-N4 1.094(3), Mo1-N1-N2 175.19(7), Mo-N3-N4 178.4(2), Al1-N1-N2 176.59(18).

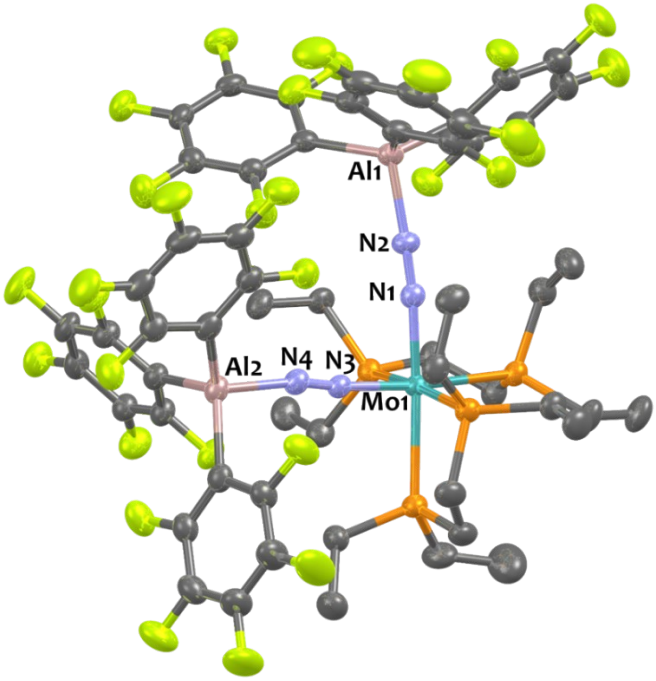

Figure S91. Solid-state structure of $\mathbf{10}_{Al}$**.** Ellipsoids are represented with 30% probability. Hydrogen atoms have been omitted for clarity. Two independent molecules were found in the asymmetric unit (Z'=2) but one of them has been omitted for clarity. Selected bond distances (Å) and angles (°) have been averaged between both independent molecules: Al1-N2 1.891(9), Al2-N4 1.906(9), Mo1-N1

1.909(9), Mo1-N3 1.921(4), N1-N2 1.147(5), N3-N4 1.137(5), Mo1-N1-N2 176.8(4) , Mo-N3-N4 174.8(3), N1-Mo1-N3 88.5(9), Al1-N2-N1 173.9(4), Al2-N4-N3 170.6(8).

6 DFT calculations

6.1 Computational details

Density Functional Theory[21] calculations were performed with the ORCA 5[22–24] suite of programs. Geometry optimizations and numerical frequency calculations were performed with the functional combining the exchange energy approximation by Becke[25] and correlation by Perdew[26] (BP86) in combination with the balanced polarized triple-ζ basis set from the Ahlrichs family[27] (def2-TZVP) for all atoms. The resolution of the identity integral method,[28] with the appropriate auxiliary basis (def2/J), was used in order to lower the computational cost. Grimme's DFT-D4[29] was included to account for dispersion interactions. Solvent effects were considered using the conductor-like polarizable continuum model (CPCM)[30] for toluene. One explicit solvent molecule (toluene) was included in all calculations. Counterions and other species commonly found in solution are not explicitly included. TD-DFT calculations were employed with the same setup, except for the functional as the range-corrected CAM-B3LYP[31] was used. The criteria used for the geometry optimizations were the default for ORCA (ΔE < 5e-6, RMS gradient ≈ 1e-4, MAX gradient ≈ 3e-4, RMS step < 2e-3, MAX step < 4e-3) and TightSCF for the SCF convergence (ΔE < 1e-8, $\Delta dens_{RMS}$ < 5e-9, Δdens < 1e-7, DIIS error < 1e-5, TolG = 1e-5, TolX = 1e-5).
All the computational data have been uploaded (https://iochem.udg.edu/browse/handle/100/5299) onto the ioChem-BD[32] platform (www.iochem-bd.org) to facilitate data exchange and dissemination, according to the FAIR[33] principles of OpenData sharing.

6.2 Computational model assessment

Table S5. Comparison between experiment and computationally obtained selected distances (metal-proximal nitrogen, nitrogen-nitrogen and distal nitrogen-Lewis acid), N-N-Lewis acid angle, and N-N stretching vibrational mode of the 1:1 adducts. Distances in Å, angles in degrees and vibrational modes in cm^{-1}.

	Complex (1:1)	Experiment	DFT	δ	%δ
M-N_1	Al	1.855	1.907	0.052	3
	B	1.909	1.920	0.011	6
N_1-N_2	Al	1.204	1.174	-0.030	2
	B	1.181	1.177	-0.004	3
N_2-LA	Al	1.817	1.870	0.053	3
	B	1.549	1.556	0.007	5
N_1-N_2-LA	Al	168.4	170.4	2	1
	B	148.4	148.4	0	0

ν_{N-N}	Al	1778	1864	86	5
	B	1767	1846	79	4

Table S6. Comparison between experiment and computationally obtained selected distances (nitrogen-nitrogen and distal nitrogen-Lewis acid), angles (N-N-Lewis acid), and symmetrical and asymmetrical N-N stretching vibrational modes of the AlCF Lewis Acid 2:1 adducts. Distances in Å, angles in degrees and vibrational modes in cm^{-1}.

	Complex (2:1)	Experimental	DFT	δ	%δ
N-N-LA_1	*cis*	168.7	173.6	4.9	3
	trans	175.2	161.5	-13.7	8
N-N-LA_2	*cis*	175.8	173.7	-2.1	2
	trans	168.6	171.4	2.8	2
N_1-N_2	*cis*	1.157	1.165	0.008	0.7
	trans	1.114	1.159	0.045	4
N_2-N_3	*cis*	1.145	1.164	0.019	2
	trans	1.113	1.158	0.045	4
N_2-LA_1	*cis*	1.894	1.896	0.002	0.1
	trans	1.919	1.909	-0.010	0.5
N_4-LA_2	*cis*	1.902	1.885	-0.017	0.9
	trans	1.927	1.904	-0.023	1
ν_{sN-N}	*cis*	1903	1959	56	3
	trans	- (low intensity)	1987	-	-
ν_{asN-N}	*cis*	1802	1873	71	4
	trans	1808	1880	72	4

Table S7. Discriminated energy contributions to the Gibbs energies of relevant species, in Eh.

	W	WACF	WBCF	$W(ACF)_{2cis}$	$W(ACF)_{2trans}$	$W(BCF)_{2cis}$	$W(BCF)_{2trans}$
$E_{Electronic}$	-2443.6353	-5142.3582	-4924.6997	-7841.0736	-7841.0686	-7405.7639	-7405.7599
$E_{Thermal}$	-2442.9445	-5141.3546	-4923.6923	-7839.7573	-7839.7538	-7404.4406	-7404.4380
Enthalpy	-2442.9435	-5141.3536	-4923.6913	-7839.7564	-7839.7528	-7404.4396	-7404.4371

Entropy	0.1121	0.1911	0.1855	0.2699	0.2688	0.2616	0.2585
E_{Gibbs}	**-2443.0556**	**-5141.5448**	**-4923.8768**	**-7840.0263**	**-7840.0216**	**-7404.7012**	**-7404.6956**

Table S8. Electronic (ΔE) and *entropy* (ΔS) terms, *and* total *Gibbs energy* (Δ*G*) *of reactions for* the subsequent binding of one and two Lewis acids, ACF or BCF, in Eh.

		W + LA ✂ W-LA	W + 2 LA ✂ W-$(LA)_{2trans}$
AlCF	ΔE	-0.0589	-0.1054
	ΔS	0.0301	0.0602
	ΔG	-0.0288	-0.0453
BCF	ΔE	-0.0444	-0.0847
	ΔS	0.0348	0.0678
	ΔG	**-0.0096**	**-0.0168**

6.3 Molecular Orbital diagrams

Figure S92. MO diagram for the bare W complex. HOMO and LUMO orbital energies represented in orange.

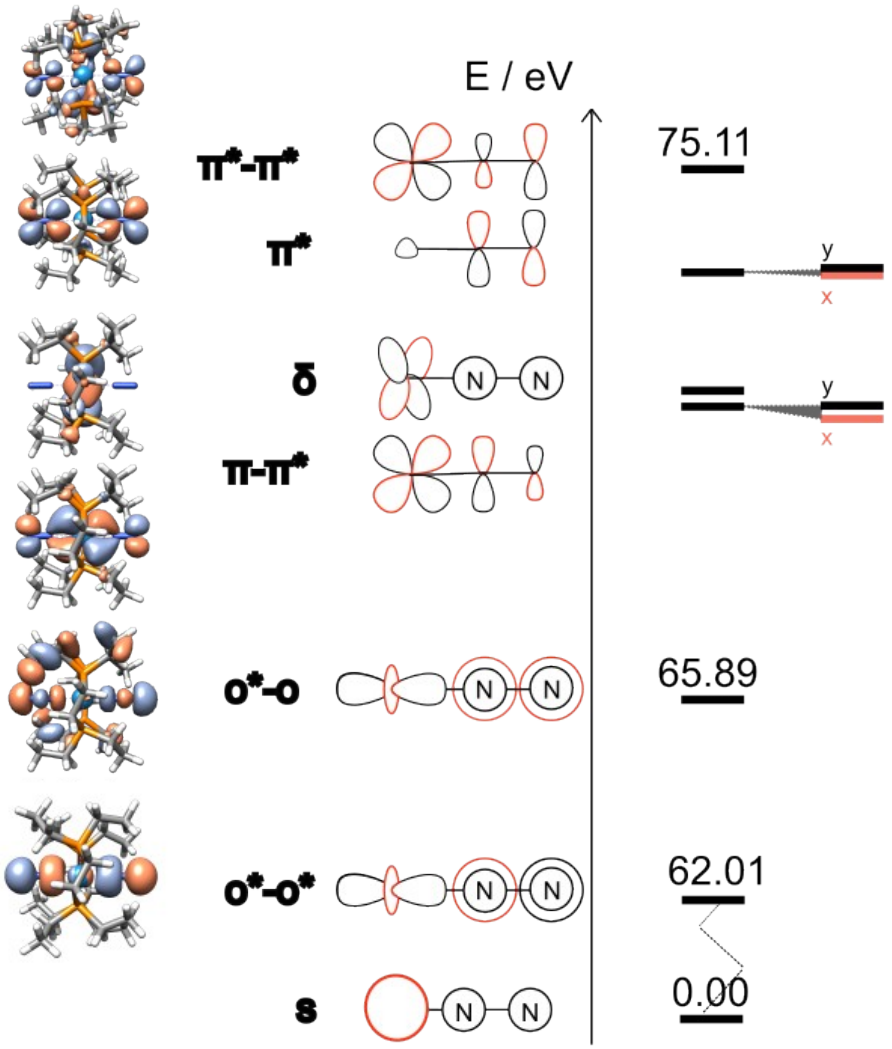

Figure S93. π-π* (HOMO-1 & HOMO-2 average) energy relative to the tungsten s orbital for the two LA 1:1 adducts (center) and modified structures with the opposing N=N-LA angle (left and right). The N=N-LA angles of W-Al_1 and W-B_1 are 172° and 148°, respectively.

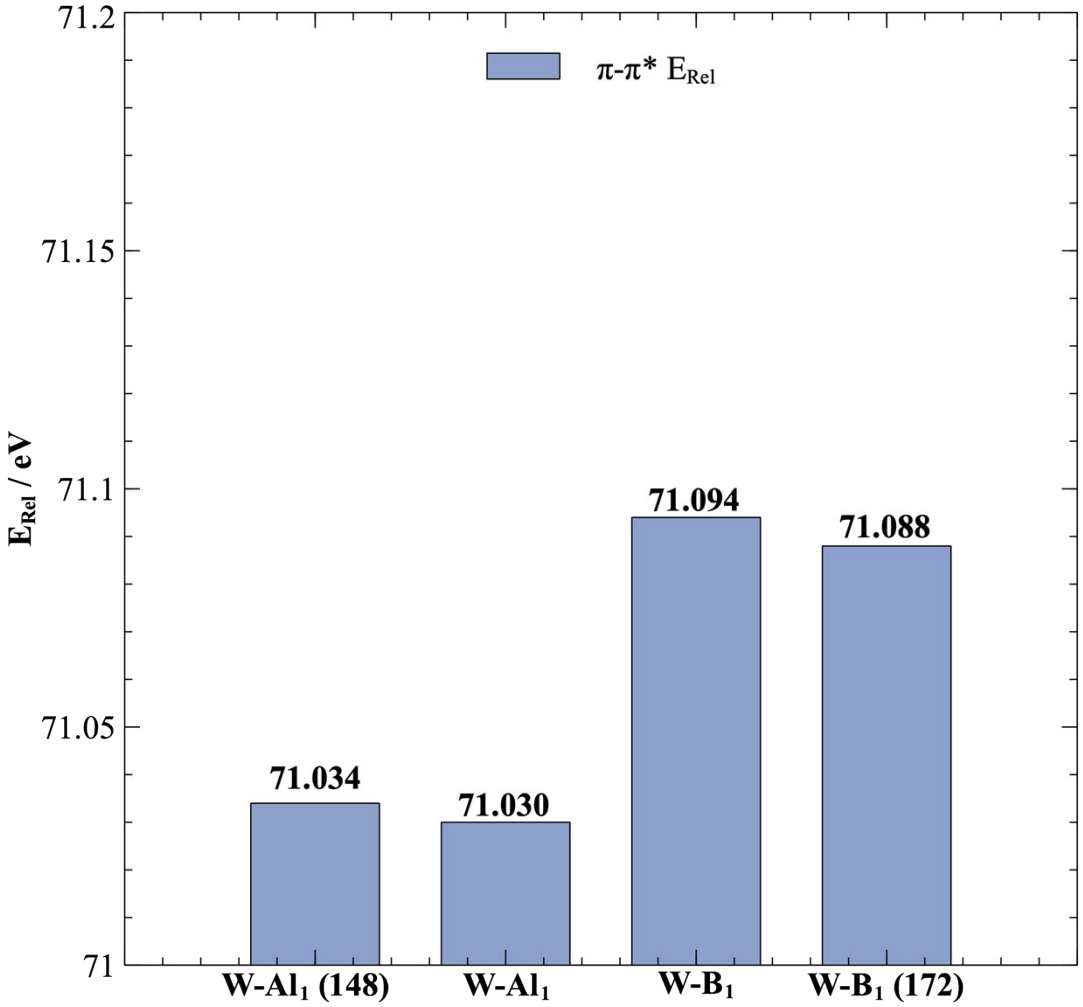

6.4 Electronic excitations

Figure S94. TD-DFT calculated electronic excitations for the first 9 states of the bare W complex (top) and simulated experimental spectrum (Gaussian broadening, FWHM = 40nm - bottom). Intensities scaled to match experiment. Numbers represent the wavelength of the excitation.

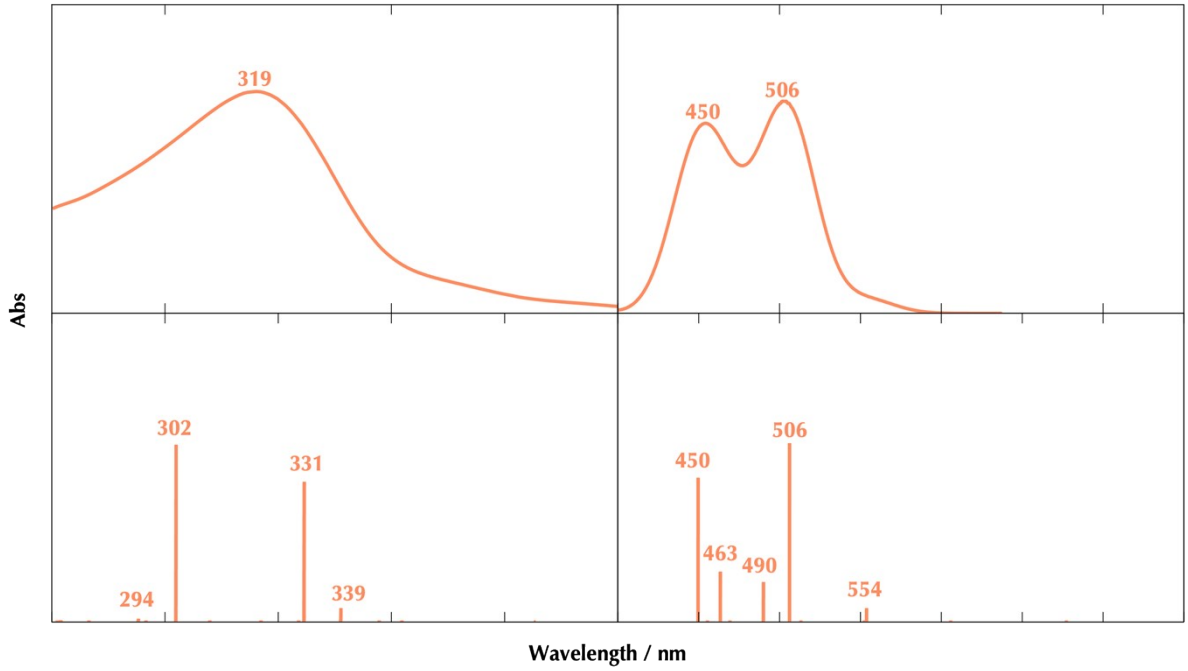

Figure S95. Difference densities (orange to purple) for the excitations of the associated wavelength.

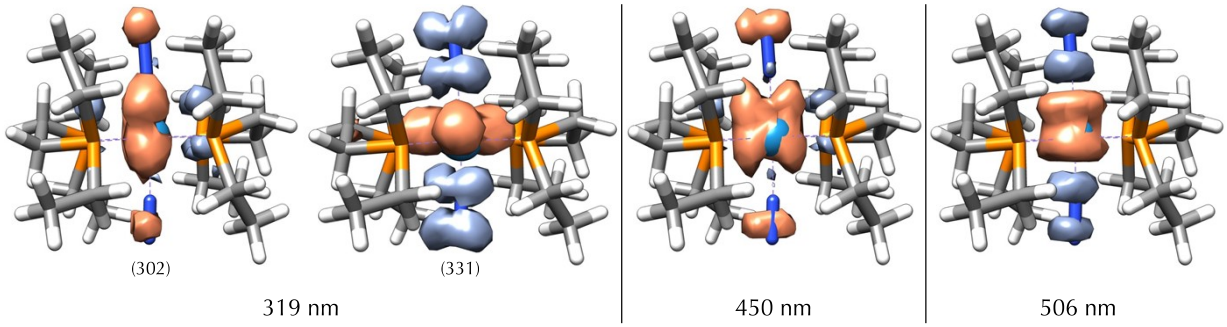

Figure S96. Natural Transition Orbitals (NTOs) for the 319 nm band (left) and the 506 nm peak (right). Transition occurs from bottom (translucent) orbital to the top one.

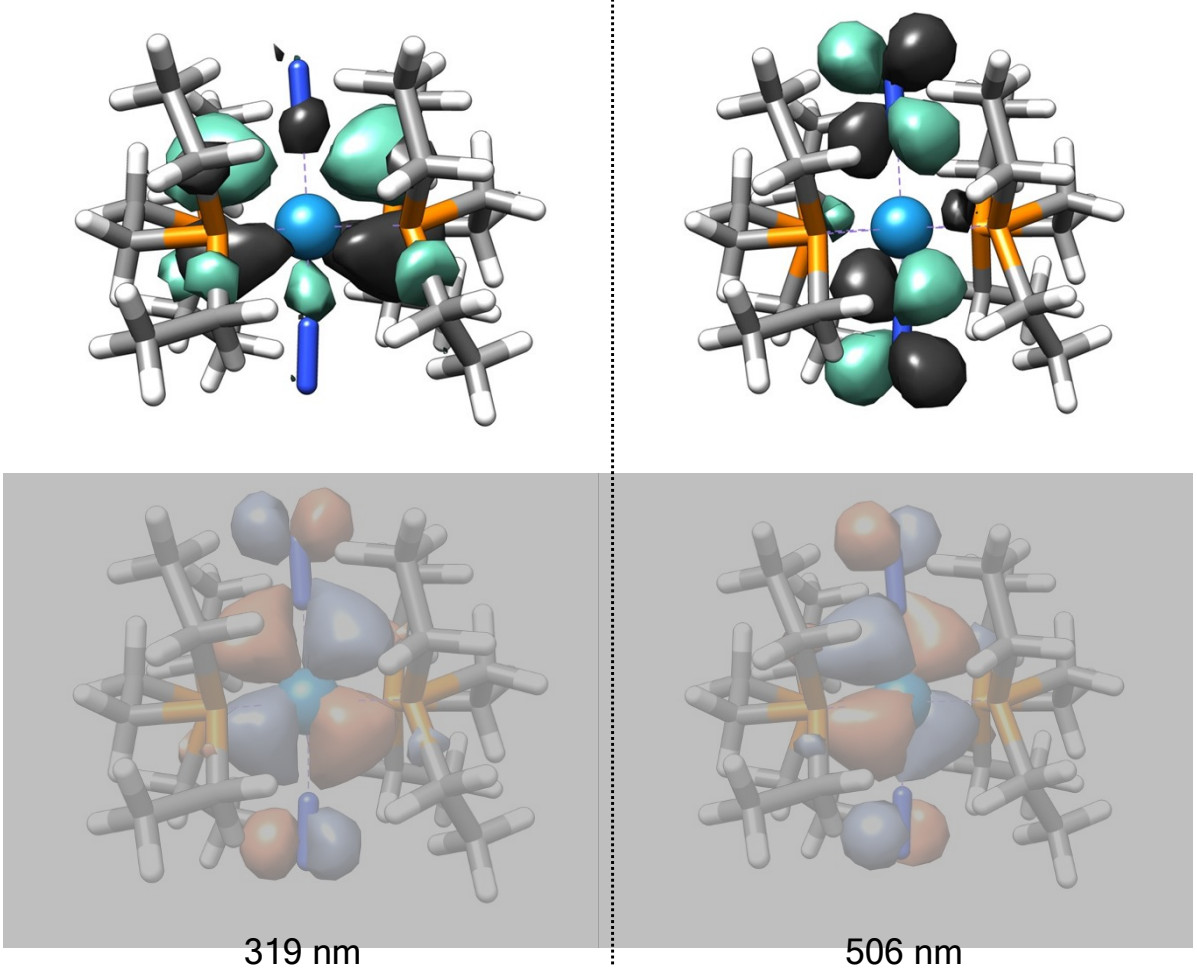

Figure S97. Computational (CAM-B3LYP) absorption spectra of trans-[W(depe)$_2$(N$_2$)$_2$] (W, grey line), trans-[W(depe)$_2$(N$_2$)(μ-N$_2$-Al(C$_6$F$_5$)$_3$] (W-Al, crimson line), trans-[W(depe)$_2${(μ-N$_2$-Al(C$_6$F$_5$)$_3$}$_2$] (trans-W-Al$_2$, dotted crimson line), cis-[W(depe)$_2${(μ-N$_2$-Al(C$_6$F$_5$)$_3$}$_2$] (cis-W-Al$_2$, dashed crimson line), and trans-[W(depe)$_2$(N$_2$)(μ-N$_2$-B(C$_6$F$_5$)$_3$] (W-B, red line) from 600 to 1000 nm.

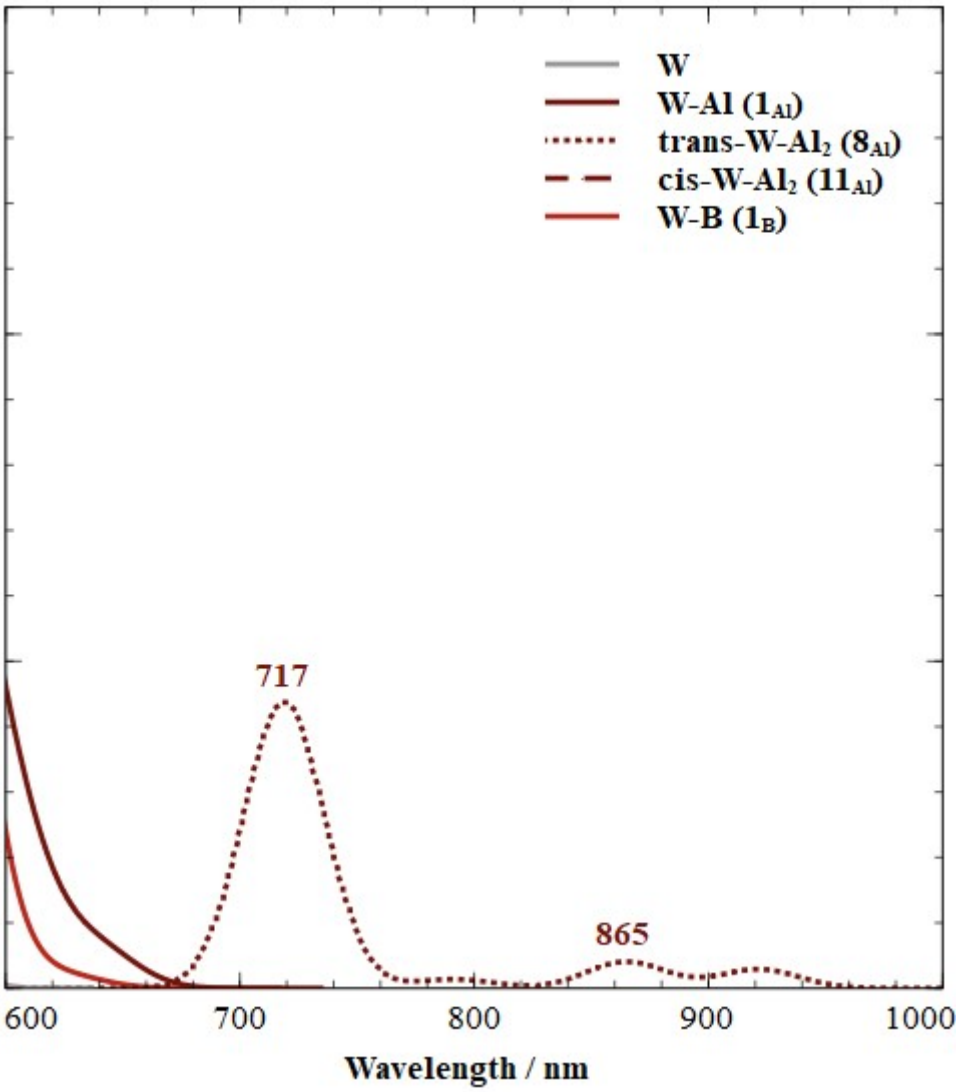

7 References

(1) George, T. A.; Noble, M. E. A Direct One-Step Preparation of Bis(Dinitrogen) Complexes of Molybdenum(0) from Molybdenum(V) Chloride. *Inorg. Chem.* **1978**, *17* (6), 1678–1679. https://doi.org/10.1021/ic50184a065.

(2) Dilworth, J. R.; Richards, R. L.; Chen, G. J.-J.; Mcdonald, J. W. The Synthesis of Molybdenum and Tungsten Dinitrogen Complexes. In *Inorganic Syntheses*; John Wiley & Sons, Ltd, 1990; pp 33–43. https://doi.org/10.1002/9780470132593.ch7.

(3) Poli, R.; Mui, H. D. True Nature of Trihalotris(Tetrahydrofuran)Molybdenum(III), MoX3(THF)3 (X = Cl, Br, I). A Paramagnetic Proton NMR Study. *J. Am. Chem. Soc.* **1990**, *112* (6), 2446–2448. https://doi.org/10.1021/ja00162a070.

(4) Stoffelbach, F.; Saurenz, D.; Poli, R. Improved Preparations of Molybdenum Coordination Compounds from Tetrachlorobis(Diethyl Ether)Molybdenum(IV). *Eur. J. Inorg. Chem.* **2001**, *2001* (10), 2699–2703. https://doi.org/10.1002/1099-0682(200109)2001:10<2699::AID-EJIC2699>3.0.CO;2-S.

(5) Filippou, A. C.; Schnakenburg, G.; Philippopoulos, A. I.; Weidemann, N. Ge2 Trapped by Triple Bonds between Two Metal Centers: The Germylidyne Complexes Trans,Trans-[Cl(Depe)2M[Triple Chemical Bond]Ge--Ge[Triple Chemical Bond]M(Depe)2Cl] (M=Mo, W) and Bonding Analyses of the M[Triple Chemical Bond]Ge--Ge[Triple Chemical Bond]M Chain. *Angew Chem Int Ed Engl* **2005**, *44* (37), 5979–5985. https://doi.org/10.1002/anie.200501968.

(6) Simonneau, A.; Turrel, R.; Vendier, L.; Etienne, M. Group 6 Transition-Metal/Boron Frustrated Lewis Pair Templates Activate N_2 and Allow Its Facile Borylation and Silylation. *Angew. Chem. Int. Ed.* **2017**, *56* (40), 12268–12272. https://doi.org/10.1002/anie.201706226.

(7) Specklin, D.; Coffinet, A.; Vendier, L.; del Rosal, I.; Dinoi, C.; Simonneau, A. Synthesis, Characterization, and Comparative Theoretical Investigation of Dinitrogen-Bridged Group 6-Gold Heterobimetallic Complexes. *Inorg. Chem.* **2021**, *60* (8), 5545–5562. https://doi.org/10.1021/acs.inorgchem.0c03271.

(8) Zolnhofer, E. M.; Opalade, A. A.; Jackson, T. A.; Heinemann, F. W.; Meyer, K.; Krzystek, J.; Ozarowski, A.; Telser, J. Electronic Structure and Magnetic Properties of a Low-Spin Cr^{II} Complex: *Trans*-[$CrCl_2(Dmpe)_2$] (Dmpe = 1,2-Bis(Dimethylphosphino)Ethane). *Inorg. Chem.* **2021**, *60* (23), 17865–17877. https://doi.org/10.1021/acs.inorgchem.1c02471.

(9) Girolami, G. S.; Wilkinson, G.; Galas, A. M. R.; Thornton-Pett, M.; Hursthouse, M. B. Synthesis and Properties of the Divalent 1,2-Bis(Dimethylphosphino)Ethane (Dmpe) Complexes MCl2(Dmpe)2 and MMe2(Dmpe)2(M = Ti, V, Cr, Mn, or Fe). X-Ray Crystal Structures of MCl2(Dmpe)2(M = Ti, V, or

Cr), MnBr2(Dmpe)2, TiMe1.3Cl0.7(Dmpe)2, and CrMe2(Dmpe)2. *J. Chem. Soc., Dalton Trans.* **1985**, No. 7, 1339. https://doi.org/10.1039/dt9850001339.

(10) Kendall, A. J.; Johnson, S. I.; Bullock, R. M.; Mock, M. T. Catalytic Silylation of N_2 and Synthesis of NH_3 and N_2H_4 by Net Hydrogen Atom Transfer Reactions Using a Chromium P_4 Macrocycle. *J. Am. Chem. Soc.* **2018**, *140* (7), 2528–2536. https://doi.org/10.1021/jacs.7b11132.

(11) Salt, J. E.; Girolami, G. S.; Wilkinson, G.; Motevalli, M.; Thornton-Pett, M.; Hursthouse, M. B. Synthesis and Characterisation of 1,2-Bis(Dimethylphosphino)Ethane (Dmpe) Complexes of Chromium-(0) and -(IV): X-Ray Crystal Structures of Trans-Cr(N2)2(Dmpe)2, Cis-Cr(CO)2(Dmpe)2, Cr(C2Ph2)2(Dmpe), and CrH4(Dmpe)2. *J. Chem. Soc., Dalton Trans.* **1985**, No. 4, 685. https://doi.org/10.1039/dt9850000685.

(12) Berben, L. A.; Kozimor, S. A. Dinitrogen and Acetylide Complexes of Low-Valent Chromium. *Inorg. Chem.* **2008**, *47* (11), 4639–4647. https://doi.org/10.1021/ic702275g.

(13) Feng, S.; Roof, G. R.; Chen, E. Y.-X. Tantalum(V)-Based Metallocene, Half-Metallocene, and Non-Metallocene Complexes as Ethylene−1-Octene Copolymerization and Methyl Methacrylate Polymerization Catalysts. *Organometallics* **2002**, *21* (5), 832–839. https://doi.org/10.1021/om010702c.

(14) Harris, R. K.; Becker, E. D.; Cabral de Menezes, S. M.; Granger, P.; Hoffman, R. E.; Zilm, K. W. Further Conventions for NMR Shielding and Chemical Shifts (IUPAC Recommendations 2008). *Pure Appl. Chem.* **2008**, *80* (1), 59–84. https://doi.org/10.1351/pac200880010059.

(15) Xu, T.; Chen, E. Y.-X. Probing Site Cooperativity of Frustrated Phosphine/Borane Lewis Pairs by a Polymerization Study. *J. Am. Chem. Soc.* **2014**, *136* (5), 1774–1777. https://doi.org/10.1021/ja412445n.

(16) Sheldrick, G. Institut Fur Anorganische Chemie Der Universitat, Tammanstrasse 4, D-3400 Gottingen. **1998**.

(17) Farrugia, L. J. *WinGX* Suite for Small-Molecule Single-Crystal Crystallography. *J Appl Crystallogr* **1999**, *32* (4), 837–838. https://doi.org/10.1107/S0021889899006020.

(18) Betteridge, P. W.; Carruthers, J. R.; Cooper, R. I.; Prout, K.; Watkin, D. J. *CRYSTALS* Version 12: Software for Guided Crystal Structure Analysis. *J Appl Crystallogr* **2003**, *36* (6), 1487–1487. https://doi.org/10.1107/S0021889803021800.

(19) Schmitz, W. International Tables for X-Ray Crystallography, Vol. IV (Ergänzungsband). Herausgegeben von Der International Union of Crystallography. The Kynoch Press, Birmingham, England, 1974, 366 Seiten Einschließlich Tabellen Und Sachwortverzeichnis. *Kristall und Technik* **1975**, *10* (11), K120–K120. https://doi.org/10.1002/crat.19750101116.

(20) Macrae, C. F.; Sovago, I.; Cottrell, S. J.; Galek, P. T. A.; McCabe, P.; Pidcock, E.; Platings, M.; Shields, G. P.; Stevens, J. S.; Towler, M.; Wood, P. A. Mercury 4.0: From Visualization to Analysis, Design

and Prediction. *J Appl Crystallogr* **2020**, *53* (Pt 1), 226–235. https://doi.org/10.1107/S1600576719014092.

(21) Fukui, K.; Pullman, B. *Horizons of Quantum Chemistry: Proceedings of the Third International Congress of Quantum Chemistry Held at Kyoto, Japan, October 29 - November 3, 1979*; Springer Netherlands: Dordrecht, 1980; Vol. 3.

(22) Neese, F. The ORCA Program System. *WIREs Comput Mol Sci* **2012**, *2* (1), 73–78. https://doi.org/10.1002/wcms.81.

(23) Neese, F. Software Update: The ORCA Program System—Version 5.0. *WIREs Comput Mol Sci* **2022**, *12* (5), e1606. https://doi.org/10.1002/wcms.1606.

(24) Neese, F.; Wennmohs, F.; Becker, U.; Riplinger, C. The ORCA Quantum Chemistry Program Package. *The Journal of Chemical Physics* **2020**, *152* (22), 224108. https://doi.org/10.1063/5.0004608.

(25) Becke, A. D. Density-Functional Exchange-Energy Approximation with Correct Asymptotic Behavior. *Phys. Rev. A* **1988**, *38* (6), 3098–3100. https://doi.org/10.1103/PhysRevA.38.3098.

(26) Perdew, J. P. Density-Functional Approximation for the Correlation Energy of the Inhomogeneous Electron Gas. *Phys. Rev. B* **1986**, *33* (12), 8822–8824. https://doi.org/10.1103/PhysRevB.33.8822.

(27) Weigend, F.; Ahlrichs, R. Balanced Basis Sets of Split Valence, Triple Zeta Valence and Quadruple Zeta Valence Quality for H to Rn: Design and Assessment of Accuracy. *Phys. Chem. Chem. Phys.* **2005**, *7* (18), 3297. https://doi.org/10.1039/b508541a.

(28) Kendall, R. A.; Früchtl, H. A. The Impact of the Resolution of the Identity Approximate Integral Method on Modern Ab Initio Algorithm Development. *Theoretical Chemistry Accounts: Theory, Computation, and Modeling (Theoretica Chimica Acta)* **1997**, *97* (1–4), 158–163. https://doi.org/10.1007/s002140050249.

(29) Caldeweyher, E.; Bannwarth, C.; Grimme, S. Extension of the D3 Dispersion Coefficient Model. *The Journal of Chemical Physics* **2017**, *147* (3), 034112. https://doi.org/10.1063/1.4993215.

(30) Barone, V.; Cossi, M. Quantum Calculation of Molecular Energies and Energy Gradients in Solution by a Conductor Solvent Model. *J. Phys. Chem. A* **1998**, *102* (11), 1995–2001. https://doi.org/10.1021/jp9716997.

(31) Yanai, T.; Tew, D. P.; Handy, N. C. A New Hybrid Exchange–Correlation Functional Using the Coulomb-Attenuating Method (CAM-B3LYP). *Chemical Physics Letters* **2004**, *393* (1–3), 51–57. https://doi.org/10.1016/j.cplett.2004.06.011.

(32) Álvarez-Moreno, M.; De Graaf, C.; López, N.; Maseras, F.; Poblet, J. M.; Bo, C. Managing the Computational Chemistry Big Data Problem: The **ioChem-BD** Platform. *J. Chem. Inf. Model.* **2015**, *55* (1), 95–103. https://doi.org/10.1021/ci500593j.

(33) Wilkinson, M. D.; Dumontier, M.; Aalbersberg, Ij. J.; Appleton, G.; Axton, M.; Baak, A.;

Blomberg, N.; Boiten, J.-W.; Da Silva Santos, L. B.; Bourne, P. E.; Bouwman, J.; Brookes, A. J.; Clark, T.; Crosas, M.; Dillo, I.; Dumon, O.; Edmunds, S.; Evelo, C. T.; Finkers, R.; Gonzalez-Beltran, A.; Gray, A. J. G.; Groth, P.; Goble, C.; Grethe, J. S.; Heringa, J.; 'T Hoen, P. A. C.; Hooft, R.; Kuhn, T.; Kok, R.; Kok, J.; Lusher, S. J.; Martone, M. E.; Mons, A.; Packer, A. L.; Persson, B.; Rocca-Serra, P.; Roos, M.; Van Schaik, R.; Sansone, S.-A.; Schultes, E.; Sengstag, T.; Slater, T.; Strawn, G.; Swertz, M. A.; Thompson, M.; Van Der Lei, J.; Van Mulligen, E.; Velterop, J.; Waagmeester, A.; Wittenburg, P.; Wolstencroft, K.; Zhao, J.; Mons, B. The FAIR Guiding Principles for Scientific Data Management and Stewardship. *Sci Data* **2016**, *3* (1), 160018. https://doi.org/10.1038/sdata.2016.18.